Ragnhild Åkre Reite

Fluoroethylene and H$_2$O as Additives in Electrolytes Based on Lithium bis(fluorosulfonyl)imide with Silicon Anodes

Master's thesis

◘ NTNU
Norwegian University of
Science and Technology

Ragnhild Åkre Reite

Fluoroethylene and H$_2$O as Additives in Electrolytes Based on Lithium bis(fluorosulfonyl)imide with Silicon Anodes

NTNU

Norwegian University of
Science and Technology

Preface

This master thesis is a part of the ongoing research project "Norwegian Giga Battery Factories", NorGiBatF. The project includes the research partners SINTEF, Technical University of Braunschweig and Institute for Energy Technology (IFE) and the industrial partners Freyr, Beyonder, Norsirk, Nordic Mining and Norsk Hydro. The project was carried out at the Department of Materials Science and Engineering (IMA) at NTNU.

I would first and foremost like to express my gratitude to my supervisor Ann Mari Svensson for wonderful guidance, quick feedback and assistance whenever needed throughout the semester. I want to thank to my co-supervisor Philipp Schweigart for great help both in and outside of the lab, and for quick and informative responses to every question I might have had. Thank you to Camilla Lian for helping me do the XRD analysis on the silicon powders. Additionally, I want to thank the laboratory engineers at IMA for training in the use of laboratory equipment and for always being available for assistance. Thanks to the battery group for good discussions and feedback throughout my project.

I want to thank my family for the continued support throughout these five years. Thank you to my classmates for creating a fun working environment and for much needed breaks, and an extra shout-out to Mellomlagring and to my lunch buddies. It turns out that chemists aren't all that scary after all. A special thanks to my classmates Emilie Bjønnes and Mari Hognestad for invaluable discussions and help in the lab, and to Marthe Nybrodahl for always being available to answer questions about anything related to powder characterisation.

Lastly, I want to thank ReSiTec for providing silicon powder for the silicon anodes used in this project, and for the use of NanoLab, The Research Council of Norway is acknowledged for the support to the Norwegian Micro- and Nano-Fabrication Facility, NorFab, project number 295864.

Ragnhild Åkre Reite
Trondheim
10th June 2022

Abstract

The effect of fluoroethylene carbonate (FEC) and 1000 ppm H_2O as additives in an electrolyte based on lithium bis(fluorosulfonyl)imide (LiFSI) on silicon anodes, was studied with respect to cycling performance, Coulombic efficiency, lithiation/delithiation potentials and electrode resistance. FEC has been shown to enhance the cycling performance of silicon anodes by improving the solid electrolyte interface (SEI) formed on the anode, possibly due to formation of LiF in the inner layer of the SEI, or flexible and passivating polycarbonates in the outer layer. It has been reported that 1000 ppm H_2O showed the same enhancing properties as FEC on the cycling performance of a $LiNi_{0,3}Mn_{0,3}Co_{0,3}O_2$/silicon cell. Hence, the aim of this thesis was to investigate if H_2O could replace FEC as an additive in battery electrolytes.

Electrolytes with ethylene carbonate (EC)/dimethyl carbonate (DMC) (1:1 mass ratio) and LiFSI salt were prepared with either no additive, FEC, H_2O or both FEC and H_2O. Silicon anodes with 75 wt.% of either amorphous or crystalline silicon powder were combined with one of the electrolytes and lithium foil as counter electrode in a coin cell, or $LiFePO_4$ (LFP) cathode in a PAT-cell. The cells were subjected to electrochemical testing and post mortem characterisation using scanning electron microscope and Fourier-transform infrared spectroscopy.

The results showed that FEC drastically improved the cycling performance of the silicon anodes, both with and without additional H_2O, possibly due to increased amounts of polycarbonates from the addition of FEC, forming a stable, flexible and passivating SEI. The addition of FEC also reduced the total electrode resistance. H_2O as the only additive resulted in lower capacities and increased resistance compared to no additives. The anodes paired with electrolytes with FEC obtained lower Coulombic efficiencies compared to the electrolytes with no additives or just H_2O after 100 cycles, possibly due to higher capacities, thus larger volume expansions. No difference in lithiation/delithiation potentials were observed with the different additives. To conclude, H_2O can not replace FEC as an additive, as FEC is required to form a stable SEI, but the silicon anodes can tolerate 1000 ppm H_2O in a LiFSI-based electrolyte.

Sammendrag

Effekten av fluoretylenkarbonat (FEC) og 1000 ppm H_2O som tilsetningsstoffer i en elektrolytt basert på litium bis(fluorsulfonyl)imid (LiFSI) på silisiumanoder, ble studert med hensyn på syklingsevne, Coulombisk effektivitet, litierings/delitierings potensialer og motstand i elektroden. Det har blitt vist at tilsats av FEC forbedrer syklingsevnen til silisiumanoder ved å danne et mer stabilt "solid electrolyte interface" (SEI) på anoden, muligens grunnet økte mengder LiF i det indre laget av SEI, eller fleksible og passiverende polykarbonater i det ytre laget. Det har blitt rapportert at 1000 ppm H_2O, i likehet med FEC, førte til forbedring av syklingsevnen til en $LiNi_{0,3}Mn_{0,3}Co_{0,3}O_2$/silisium celle. Derfor var målet med denne oppgaven å undersøke om H_2O kunne erstatte FEC som tilsetningsstoff i batterielektrolytter.

Elektrolytter med etylenkarbonat (EC)/dimetylkarbonat (DMC) (1:1 masseforhold) og LiFSI-salt ble fremstilt og tilsatt enten ingen tilsetningsstoffer, FEC, H_2O eller både FEC og H_2O. Silisiumanoder med 75 vekt.% av enten amorft eller krystallinsk silisiumpulver ble kombinert med en av elektrolyttene og litium metall som motelektrode i en knappecelle, eller en $LiFePO_4$ (LFP) katode i en PAT-celle. Elektrokjemiske tester og post mortem karakterisering, ved bruk av elektronmikroskop og Fourier-transform infrarød spektroskopi, ble utført på cellene.

Resultatene viste at FEC forbedret syklingsevnen til silisiumanodene, både med og uten tilsatt H_2O, muligens på grunn av økte mengder polykarbonater fra reduksjon av FEC, og dannet et stabilt, fleksibelt og passiverende SEI. Tilsetning av FEC reduserte også den totale motstanden i elektroden. H_2O som eneste tilsetningsstoff resulterte i lavere kapasitet og økt motstand sammenlignet med ingen tilsetningsstoffer. Anodene syklet med FEC i elektrolytten oppnådde lavere Coulombisk effektivitet sammenlignet med elektrolyttene uten tilsetningsstoffer, eller kun H_2O etter 100 sykler, muligens på grunn av høyere kapasitet, dermed større volumendringer. Det ble ikke observert noen forskjell i litierings/delitierings-potensialene med de forskjellige tilsetningsstoffene. For å konkludere, H_2O kan ikke erstatte FEC som et tilsetningsstoff, ettersom FEC kreves for å danne et stabilt SEI, men silisiumanodene tåler 1000 ppm H_2O i en LiFSI-basert elektrolytt.

Contents

List of Figures

List of Tables

List of Abbreviations

Term	Description
LIB	Lithium-ion battery
SEI	Solid electrolyte interface
$LiPF_6$	Lithium hexafluorophosphate
LiFSI	Lithium bis(fluorosulfonyl)imide
FEC	Fluoroethylene carbonate
LFP	$LiFePO_4$
SEM	Scanning electron microscope
FTIR	Fourier-transform infrared spectroscopy
ICL	Irreversible capacity loss
LUMO	Lowest unoccupied molecular orbital
HOMO	Highest occupied molecular orbital
CEI	Cathode-electrolyte interface
EC	Ethylene carbonate
DMC	Dimethyl carbonate
VC	Vinylene carbonate
EIS	Electrochemical Impedance Spectroscopy
XRD	X-ray diffraction
PSD	Particle size distribution
EDS	Energy-dispersive x-ray spectroscopy
IR	Infrared
ATR	Attenuated total reflectance

1 Introduction

1.1 Motivation

In 2022, the word on everyone's lips when talking about the green energy transition, is batteries. Batteries allows electricity to replace fossil fuel in the automotive industry and allows storage of green energy. A lot of research has gone into developing batteries that can store more energy, that can be fast-charged and that can provide large amounts of energy at once. However, the production of batteries is very energy consuming, so in order to properly accelerate the green energy transition, the energy consumption related to battery production must be decreased. Hence, research on alternative and less energy demanding production methods and battery chemistries is just as important as increasing the battery cell performance. Trace amounts of H_2O in the cell will cause detrimental side reactions that reduce the performance of the battery. Hence, the batteries are produced in dry rooms to ensure very low moisture levels in the cell. However, dry rooms and drying battery components are some of the most energy consuming parts of the battery production.[1] Therefore, by developing a battery cell that can tolerate a higher water content, the energy consumption related to battery production can be reduced.

Lithium ion batteries (LIBs) dominate the battery market today. The most used active material for the anode in conventional batteries is graphite.[2] However, silicon has been proposed as a promising material due to the very high theoretical capacity. But due to the high capacity combined with the alloying mechanism of silicon upon lithiation, silicon experience large volume changes during insertion and desertion of the lithium ions. These volume changes will cause cracking of the passivating solid electrolyte interface (SEI) layer that is formed between the electrolyte and anode, exposing the anode to more electrolyte. The result is a thick and non-uniform SEI layer that traps more lithium ions and reduce the performance of the battery. The cracking of the SEI layer has been especially problematic when the most conventionally used lithium salt, lithium hexafluorophosphate ($LiPF_6$), is used in the electrolyte. $LiPF_6$ will also react with trace amounts of water in the electrolyte and form HF, which will cause detrimental side reactions on the silicon anode. Due to these issues, the lithium salt lithium bis(fluorosulfonyl)imide (LiFSI) has been proposed to replace $LiPF_6$, as LiFSI has shown to create a more flexible and homogeneous SEI layer on silicon anodes, and the non hydrolysing properties prevents the formation of HF when in contact with H_2O. Hence, replacing $LiPF_6$ with LiFSI could both improve the performance of silicon anodes, which can increase the energy density in a battery compared to when graphite anodes are used, and help reduce energy consumption related to battery production if a LiFSI-based electrolyte can tolerate more water.

Additives have been used in electrolytes to help enhance battery performance. Fluoroethylene carbonate (FEC) is an additive believed to create an SEI layer that is passivating and helps suppress the expansion of the silicon anode. However FEC is costly compared to other components in the electrolyte. Young et al.[3] claimed that adding 1000 ppm H_2O to a $LiPF_6$-based electrolyte showed similar enhancing effects as FEC on the cycling performance of a cell with a silicon anode and a $LiNi_{0,3}Mn_{0,3}Co_{0,3}O_2$ cathode.[3] Hence, if the lithium salt LiFSI prevents detrimental side reactions with trace amounts of water in the electrolyte, H_2O could be a cheaper alternative as an additive in battery electrolytes.

1.2   Aim and scope

This master project is a part of the NorGiBatF project. The aim of this master thesis is to investigate the effect of FEC and H_2O as additives on the cycling performance, Coulombic efficiency, lithiation/delithiation potentials and total resistance of silicon anodes, to find out if H_2O might be a cheaper alternative to FEC. Four different electrolytes will be used in this project; one with just LiFSI and no additive, one with FEC, one with H_2O and finally one electrolyte with FEC and H_2O as additives. The electrolytes are combined with anodes containing 75 wt.% of micron sized silicon powder, recycled from the cutting process of silicon wafers for the solar industry, provided by ReSiTeC. The silicon anodes and electrolytes are assembled in coin cells with lithium metal as counter electrode and PAT-cells with LFP ($LiFePO_4$) as counter electrode. Electrochemical testing and post mortem characterisation using a scanning electron microscope (SEM) and Fourier-transform infrared spectroscopy (FTIR) analysis will be performed.

2 Theory

2.1 Fundamentals of Li-ion batteries

2.1.1 Working principles

A Li-ion battery (LIB) is a device used to store electrical energy. A battery transforms chemical energy to electrical energy by redox reactions, i.e. reactions where one species is reduced and the other is oxidized resulting in a transfer of electrons. Electrical energy can be utilized as the electrons are conducted in the external circuit.

The components of a battery are shown in figure 2.1. A battery consists of two electrodes, a cathode and an anode, which are connected to current collectors that ensures electrical contact between the electrodes and the external contact. An electrolyte connects the anode and cathode, and transfers ions. A porous separator soaked in the electrolyte is ionically conducting, but electrically insulating. During discharge, an oxidation occurs at the anode and a reduction at the cathode. The opposite reaction occurs during charging of a rechargeable battery where the redox reactions are reversed. Hence both electrodes will be the anode (and cathode) during a full charge/discharge cycle. However, in the field of batteries, by convention, the electrode where the oxidation occurs during discharge is always termed the anode and the electrode where the reduction occurs is termed the cathode.

The LIB was first demonstrated in the 1970's, but it wasn't until 1991 that Sony Corporation commercialised the LIB. The first LIB used metallic lithium as the negative electrode, but this resulted in stability issues related to dendrite formation. Therefore, Sony replaced lithium metal with a coke anode, and used a $LiCoO_2$ cathode. Today, graphite is the most conventionally used anode material for LIBs, with 98% of the market share as of October 2020.[2] The cathode in a LIB is a lithium-oxide material.

LIBs dominate the battery market today as they display superior properties compared to other rechargeable battery chemistries, like lead-acid, nickel-metal hydride and nickel-cadmium batteries, such as high energy density, high operating voltage and long cycle life.[4]

During charging of a LIB, an oxidation of the lithium oxide occurs at the cathode. Li^+ delithiates and is transported through the ionically conducting electrolyte to the anode where the Li-ions are intercalated into the anode structure and recombined with the electrons that are forced through the external circuit. Then, during discharge, the lithium in the anode is oxidised and the ions are transported back towards the cathode where they are recombined with the electrons. This back and forth motion of the Li-ions between the electrodes has given rise to the name "rocking-chair batteries". Figure 2.2 shows the charging mechanism
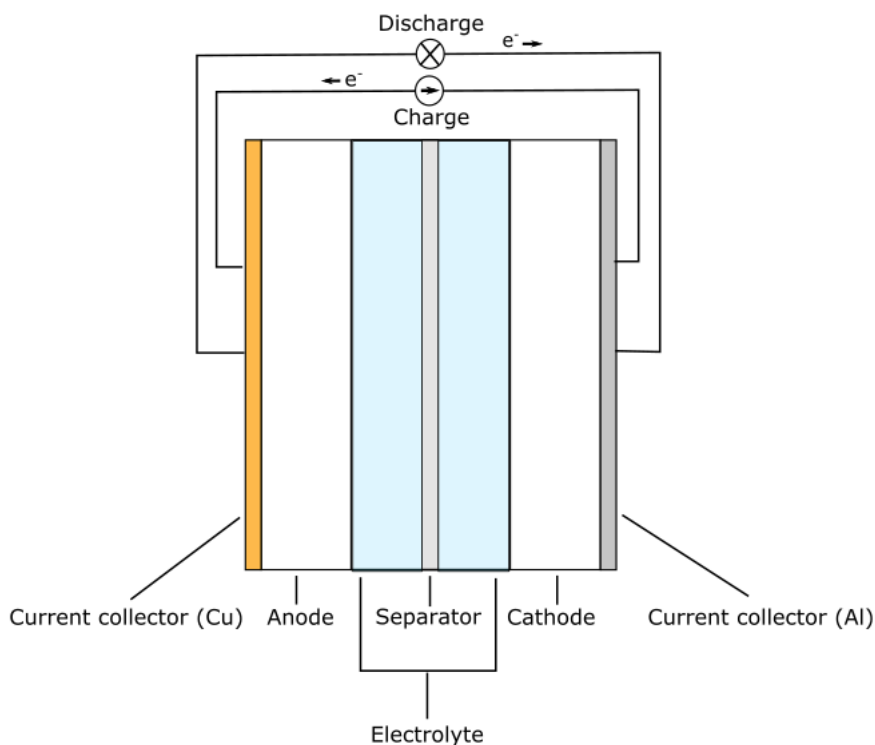
Figure 2.1: A schematic drawing of the main components in a battery; two electrodes, current collectors, electrolyte and separator.

in a LIB.

2.1.2   Terminology

Some terms of importance when discussing LIBs will be explained in this section.

- The **Charge transferred**, $Q(t)$, during a given time period, Δt, per unit weight with the discharge current, I, is given as

$$Q(t)\ (\text{Ah/kg}) = \int_0^{\Delta t} \frac{I}{m} dt \tag{2.1}$$

- **Open circuit voltage**, V_{oc}

  The potential between the electrodes when no charge or discharge current is applied is the open circuit voltage, and is determined by the electrochemical potential of the anode and the cathode, μ_a and μ_c respectively, and the elementary charge, e.

$$V_{oc}\ (\text{V}) = \frac{\mu_a - \mu_c}{e} \tag{2.2}$$
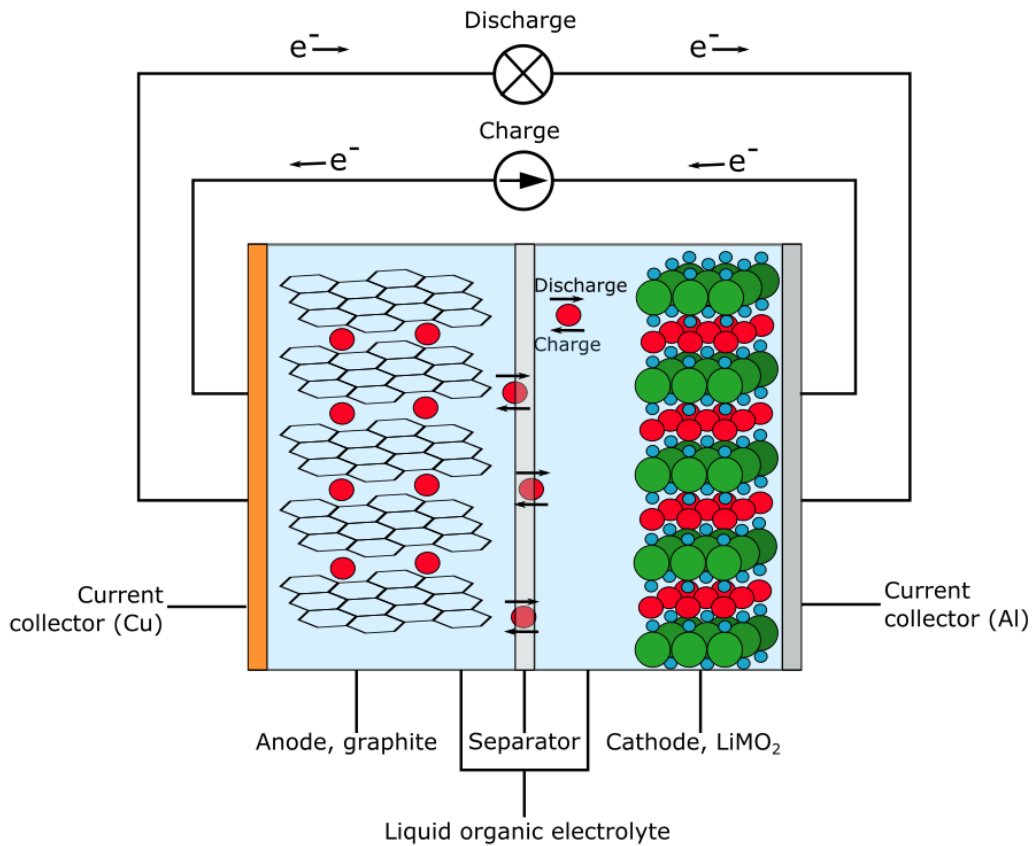
Figure 2.2: A schematic drawing of a Li-ion battery. The electrons and Li-ions move back and forth between the two electrodes depending on whether the battery is charging or discharging. During discharge, the ions are deintercalated from the anode and move through the electrolyte and recombine with the electrons at the cathode.

- **Theoretical specific capacity**, C_{sp}

  The capacity is often expressed as charge stored in the cathode or anode per unit mass of active electrode material (mAh/g), and this term is called the specific capacity. The theoretical specific capacity is determined by the electrons transferred in the redox reaction, n, the molar weight of the active electrode material, M, and Faraday's constant, F.

$$C_{sp} \text{ (mAh/g)} = \frac{nF}{M} \tag{2.3}$$

- **Energy**, E

  The energy stored in the cell can be described by the potential in the cell, V, when a charge, q, is moved between the electrodes over a given time, t.

$$E \text{ (Wh)} = \int_0^Q V(q)dq \approx Q \cdot V(t) \tag{2.4}$$

Energy density

In battery technology, the energy density is a term often used to describe the energy stored per volume (volumetric energy density (Wh/L)) or per mass (gravimetric energy density (Wh/g)).

$$\text{Energy density (Wh/g)} = E/m \tag{2.5}$$

- **C-rate**

  The C-rate describes the discharge and charge current, I_{dis} and I_{ch}, applied to the cell to charge/discharge the cell during a given time period. For instance, 1C is a measure of the current required to discharge/charge the cell in 1 hour, and is dependent on the mass of the active material, m, and the specific capacity of the electrode, C. 0,5C is the current required to discharge/charge the cell in 2 hours, and 2C is the current required to discharge/charge the cell in 30 minutes.

$$1C = C \cdot m \tag{2.6}$$

- **Power**, P

  The output power, P, is based on the discharge current, I_{dis}, and the output potential, V_{dis}, and is a measure of how much energy is released per unit time for a given discharge current. The power can also be expressed as the output energy for a given time

  $$P \text{ (W)} = I_{dis}V_{dis} = \frac{E}{dt} \tag{2.7}$$

  Power density

  Just as for energy density, power density is a term often used in relation to batteries to describe the output power per unit mass of the device (W/g).

  $$\text{Power density (W/g)} = P/m \tag{2.8}$$

- **Discharge (output) potential and charge potential**, V_{dis} and V_{ch}

  Internal resistance in the cell will affect the discharge and charge potential by causing a polarisation, $\eta = I_{dis}R$ or $\eta = I_{ch}R$ respectively, that will reduce the output voltage from the open circuit voltage and increase the required charge voltage with respect to the V_{oc}.

  $$\begin{aligned} V_{dis} \text{ (V)} &= V_{oc} - \eta(q, I_{dis}) \\ V_{ch} \text{ (V)} &= V_{oc} + \eta(q, I_{ch}) \end{aligned} \tag{2.9}$$

- **Coulombic efficiency**, CE

  The Coulombic efficiency is a measure of how much of the charge passed during charging of the battery can be released during discharge. For a single cycle, the Coulombic efficiency is the ratio of the charge passed during discharge to the charge passed during charge.

  $$CE \text{ (\%)} = \frac{Q_{dis}}{Q_{ch}} \cdot 100\% \tag{2.10}$$

- **Irreversible capacity loss**, ICL

  In a LIB, the irreversible capacity loss corresponds to the fractions of Li ions that are not delithiated during discharge. Hence, the irreversible capacity loss is related to the CE.

$$ICL \ (\%) = 100\% - CE = \frac{Q_{ch} - Q_{dis}}{Q_{ch}} \cdot 100\% \tag{2.11}$$

- **Cycle life**

  The cycle life of an energy storage device is the number of cycles the cell will sustain before being considered dead, which is when the capacity reaches 80% of it's initial capacity.[5] LIBs typically display a cycle life of <1000 cycles.[6]

2.2   Electrode materials

The battery as an energy storage unit can be divided into two groups of application; stationary and mobile energy storage. As for the stationary batteries, the most important factor is the cost per energy unit. As the battery is stationary, the mass and volume is not as important as for a mobile battery. In addition, the safety aspect is important, but external safety systems can be integrated instead of developing more expensive and safer battery chemistries. However, for the mobile batteries, energy density is more important. Hence, battery chemistry with high energy density is developed to minimize the weight of the device. Regarding safety, it is imperative to develop safer batteries rather than integrating safety systems that add on to the weight of the device.[7] Hence, the choice of electrode materials is largely dependent on the intended use of the battery, but there are several common factors of importance for the electrode materials. Abundance, low cost and ethical production methods are important for commercialisation of the electrodes in addition to properties like high capacity, open circuit voltage, reversability, low polarisation and cycling stability.

The anode should hold the lithium ions in the highest possible energy state and hold as many ions as possible in the smallest amount of space and mass. When the ion moves back to the cathode during discharge, it needs to be in a much lower energy state than in the anode to ensure that it is thermodynamically favorable for the ions to move from anode to cathode, and for the electrons to move in an external circuit to perform work. As shown in equation 2.2, a larger difference between the energy states of the ions when in the anode and in the cathode gives a higher open circuit voltage, which again will result in higher energy density.[7]

2.2.1   Cathode materials

Cathode materials for LIBs display a lower specific capacity than the anode materials. Hence, the energy density for LIBs is limited by the cathode. Therefore, one important challenge of the cathode materials for LIBs is to obtain a specific capacity that is as large

as possible, in addition to a high operating voltage. Numerous different cathode chemistries are used in LIBs, but in this thesis, only the most common will be briefly discussed. Table 2.1 shows an overview of the chemistries discussed with their specific capacity and operating voltage.[8]

The layered chalcogenide LTS ($LiTiS_2$) display a high gravimetric energy density and long cycle life, hence it has been studied widely, and Exxon eventually commercialised the cathode material in the 1970s.[9,8]

LCO ($LiCoO_2$) is a layered oxide and was introduced by Goodenough in 1980[10] and commercialised by SONY. Today, this chemistry is still widely used in LIBs due to its high specific gravimetric energy density, high discharge voltage, low self-discharge and good cyclability. However, the disadvantages with the LCO cathode material are the ethical concerns and high cost of Co, in addition to low thermal stability.[8]

LNO ($LiNiO_2$) display the same structure as LCO and similar specific capacity. LNO has a high energy density and is a cheaper alternative compared to Co-based chemistries. However, Ni^{2+} tend to substitute the Li^+ cites during delithiation, blocking the diffusion paths of Li-ions. Partial substitution of Ni^{2+} with Co^{2+} has been shown to reduce the cationic disorder.[8]

LMO ($LiMnO_2$) is a promising cathode material due to Mn being much cheaper than Co and Ni. LMO has a layered structure, but during lithium extraction the structure tends to change into a spinel structure, which reduces the cycling properties. In addition, Mn tends to leach out of the LMO cathode during cycling, destabilising the SEI layer on the anode. Hence, the poor cyclability of LMO cathodes has hindered the material from being widely commercialised.[8]

NMC ($LiNi_xCo_yMn_zO_2$) is a widely used cathode material in the battery market due to its high reversible specific capacity, high operating voltage and good cycling properties. The most commonly used NCM composition is $LiNi_{0,3}Co_{0,3}Mn_{0,3}O_2$.[8] The NMC cathode dominates the market of high energy cathodes.

The final cathode material that will be briefly introduced is the polyanion compound LFP ($LiFePO_4$). In this class of cathode materials, the polyanions XO_4^{3-} (X = S, Si, P, As, W, Mo) occupy lattice positions and stabilise the structure and increasing the redox potential. As for LFP, the material with olivine structure has good thermal stability and high power capability. LFP has a low cost and display a stable operating potential, but the disadvantage is that the operating potential is quite low compared to other cathode chemistries.[8] Due to the stable operating potential, LFP cathodes are often used in research as a counter electrode when anodes or electrolytes are being studied.

Table 2.1: Overview of specific capacity and average voltage of some of the different cathode chemistries. Recreated from[8]

Cathode	Compound	Theoretic specific capacity [mAh/g]	Operating voltage [V]
LTS	$LiTiS_2$	225	1,9
LCO	$LiCoO_2$	274	3,8
LNO	$LiNiO_2$	275	3,8
LMO	$LiMnO_2$	285	3,3
NMC	$LiNi_{0,3}Co_{0,3}Mn_{0,3}O_2$	280	3,7
LFP	$LiFePO_4$	170	3,4

2.2.2 Anode materials

In earlier studies of LIBs, one believed that the excellent rechargeable characteristics of LIBs was due to the reversible recycling of Li^+. However, it has been shown that there are several losses related to the lithiation/delithiation process. One of the major losses in a LIB is caused by the formation of a solid electrolyte interface between the anode and the electrolyte.[11] The most used electrolytes in LIBs are organic electrolytes with oxidation potentials at 4,7 V vs. Li/Li^+ and reduction potentials at 1,0 V vs. Li/Li^+, while the lithiation occurs at lower potentials. Hence, the electrolyte in LIBs are not thermodynamically stable at the operating voltage of the battery. As a result, the electrolyte will decompose at the anode interface and form a solid electrolyte interface (SEI) layer. The SEI layer consists of decomposition of the organic solvents, the lithium salt, lithium ions and impurities. The SEI layer is mainly formed during the first cycle, often called the SEI formation cycle. The layer is electronically insulating and ionically conducting, hence when the SEI is complete, it should be stable and passivates the anode surface, only allowing Li^+ to pass through.[12] Therefore, the performance of the anode, and thus the battery cell, is highly affected by the formation of an SEI layer.

As mentioned, the purpose of an anode material is to hold the lithium ion at a high energy state and to store as many ions as possible in the smallest amount of mass possible. Thus, the optimal anode material for LIBs would be lithium metal, with its highest possible energy state and highest capacity compared to other anode materials. However, as lithium metal experience issues with dendrite formation that can propagate through the separator causing safety issues and short circuiting, other anode materials has been developed. The anode materials are classified according to how the lithium ions interacts with the anode material. The three different groups of materials are intercalation, conversion and alloying materials.

The insertion and desertion of Li^+ into the interlayer spacing in a layered material is the

lithiation/delithiation mechanism in an intercalation anode material. There are no structural changes to the structure of the host material when ions are inserted besides an increase in the interlayer spacing.[7] Graphite is a layered material with weak van der Waals forces between the basal planes which allows for intercalation of Li-ions in between the layers.[13] Graphite has been used as anode material in LIBs since 1991, and is the most used anode material in conventional LIBs today. The low lithiation/delithiation potential results in a high cell potential which, in addition to the high capacity of 372 mAh/g, gives high energy density. One drawback with the intercalation type anode materials is the limited power density due to slow kinetics of the intercalation process.

The conversion materials involves a structural change of the anode material upon lithiation. Electrochemical reactions between the ions and anode material results in new chemical species that are structurally different to the initial anode material.[7] Transition-metal oxides, sulfides and phosphates are conversion type anode materials. Conversion type anodes experience issues like cycling and rate instability, voltage hysteresis between charging and discharging, which reduce the energy efficiency, high ICL and low Coulombic efficiency.[14]

The alloying type materials experience structural changes like the conversion materials. However, the alloying materials form a lithium alloy with the anode upon lithiation. Alloying materials typically have a low delithiation potential, making them a suitable choice as anode material. However, as the anode material undergoes the alloying process, the anode experience volume changes. Si, Sn and Sb are the most studied alloying materials, and Si for instance, experiences volume changes of $\sim$300%. The volume changes leads to cracking of the SEI layer, loss of inter particle contact and loss of electric contact with the current collector.[7] The cracking of the SEI layer results in electrolyte decomposition, trapping of lithium ions and increasing cell impedance. Hence, alloying materials usually suffer from short cycle life, especially at high mass loading and low Coulombic efficiency.[8] Alloying materials are often used in a composite with carbon materials to control the expansion and increase conductivity.[7]

2.3   Silicon as anode material

Silicon is a promising anode material due to its non-toxicity, high abundance, low cost, low lithiation/delithiation potential and very high theoretical specific capacity of 3579 mAh/g at room temperature. The low lithiation/delithiation potentials contribute to a high operating voltage, which in combination with the high capacity cathode, can increase the energy density by 15-20% compared to conventional graphite electrodes.[15] However, silicon anodes experience large volume changes upon lithiation and delithiation ($\sim$300% at $Li_{3.5}Si$). This cause high internal stress, pulverisation of the anode, continuous formation of the SEI layer and loss of electrical contact between the active material and the current collector, which

eventually will cause capacity fade and reduce cycling performance.[16] The semiconductor properties of silicon, results in poor electronic and ionic conductive properties. Thus, a silicon anode is made with additives like carbon black to ensure conductive paths in the anode.

Due to the large volume expansion of the silicon anode upon lithiation, the SEI layer will crack and expose the anode to the electrolyte again. This results in a continuous SEI formation, decomposing of the electrolyte and trapping of Li^+, reducing the Coulombic efficiency, capacity and cycling performance of the battery. Hence, it is an advantage that the SEI layer formed on the silicon anode is flexible and homogeneous in order to avoid a thick SEI layer. This is highly controlled by the composition of the electrolyte.

The crystallinity of the silicon anode material affects the lithiation potential in the initial cycle. If the anode is made from crystalline silicon, the lithiation follows the irreversible reaction

$$c - \text{Si} \; + \; x\text{Li}^+ \; \rightarrow \; a - \text{Li}_x\text{Si} \tag{2.12}$$
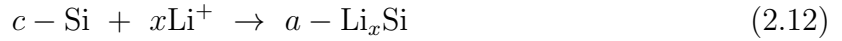
The reaction occurs at 0,10 V vs. Li/Li^+ during the very first cycle, forming amorphous silicon. If the anode is made from amorphous silicon, the lithiation will occur at 0,25-0,30 V and 0,10 V vs. Li/Li^+, corresponding to the following reactions.

$$a - \text{Si} \; + \; 2\text{Li}^+ \; \rightarrow \; a - \text{Li}_{2,0}\text{Si}$$
$$\text{Li}_{2,0}\text{Si} \; + \; 1,5\text{Li}^+ \; \rightarrow \; \text{Li}_{3,5}\text{Si} \tag{2.13}$$
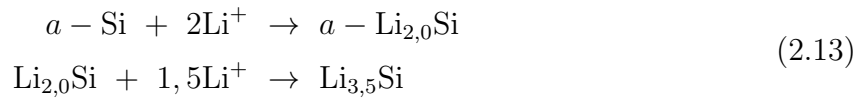
The lithiation/delithiation potentials will show up as plateaus in the potential profile of the anode. If the silicon is cycled at potentials below 50 mV, crystalline $c - \text{Li}_{3,75}\text{Si}$ is formed. Further decrease in potential gives $c - \text{Li}_{4,4}\text{Si}$ which gives the specific capacity of 4200 mAh/g.[12] However, there are several reasons why this crystalline phase is unfavorable. New intermetallic phases might form upon lithiation leading to inhomogeneous volume changes. This might cause cracking and pulverisation of the active material, which reduce the cycling performance. While the amorphous Si experience homogeneous volume expansion.[17] In addition, the delithiation of the crystalline $c - \text{Li}_{3,75}\text{Si}$ occurs at 0,43 V, hence it requires a larger overpotential for delithiation than the delithiation of the amorphous phase, $a - \text{Li}_{3,75}\text{Si} \rightarrow a - \text{Li}_{2,0}\text{Si}$ at 0,27-0,30 V.

$$c - \text{Li}_{3,75}\text{Si} \; \rightarrow \; a - \text{Li}_{1,1}\text{Si} \; + \; 2,65\text{Li}^+ \qquad 0,43 \; V$$
$$a - \text{Li}_{3,75}\text{Si} \; \rightarrow \; a - \text{Li}_{2,0}\text{Si} \; + \; 1,75\text{Li}^+ \qquad 0,27 - 0,30 \; V \tag{2.14}$$
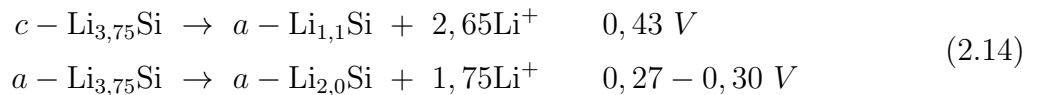
Due to the unfavorable cycling performance of the silicon anode when the crystalline phase $c - \text{Li}_{3,75}\text{Si}$ is formed, a cut-off voltage at 50 mV vs. Li/Li^+ is used for silicon anodes.

2.4 Electrolyte

In a review article from 2016, Q. Li et al. constructed a list of minimal criteria that an ideal electrolyte should meet.[18]

1. Good ionic conductor and electronic insulator to facilitate a simple transport of Li^+ and low self-discharge.

2. Wide electrochemical stability window to minimize the electrolyte degradation

3. Be inert towards cell components like separator, cell packaging materials and current collectors

4. Be thermally stable such that both boiling and melting temperature for the liquid electrolyte is outside the operating temperatures of the cell

5. Low environmental hazard

6. Based on suitable chemistries with abundant elements and synthesis methods with as low environmental impact as possible

7. As low cost as possible regarding materials and production

As one of the five main components in a battery, the electrolyte contributes to determining the properties of the cell, like the cycling performance and energy density. This is mainly related to the formation and physical properties of the SEI layer, which highly depends on the nature of the electrolyte.[18] The electrochemical stability window is the energy gap between the lowest unoccupied and highest occupied molecular orbital (LUMO and HOMO respectively) of the liquid electrolyte (or the gap between the bottom of the conduction and top of the valence band for a solid electrolyte). Figure 2.3 shows the electrochemical stability window, with the electrochemical stability window being larger than the difference between the electrochemical potentials of the electrodes. If the LUMO is at a lower potential than the electrochemical potential of the anode, μ_a, the electrolyte will be reduced rather than the anode. Reduction reaction continues until the anode is blocked by the passivating SEI layer. Similarly, if the HOMO is at a higher potential than the electrochemical potential of the cathode, μ_c, the electrolyte will be oxidised rather than the cathode, until the reaction is blocked by a cathode-electrolyte interface (CEI) layer. Hence, in order to obtain a large V_{oc}, not only must the difference in electrochemical potential of the anode and cathode be large, but the electrolyte must be constructed in a way that will ensure a large electrochemical stability window.[19]
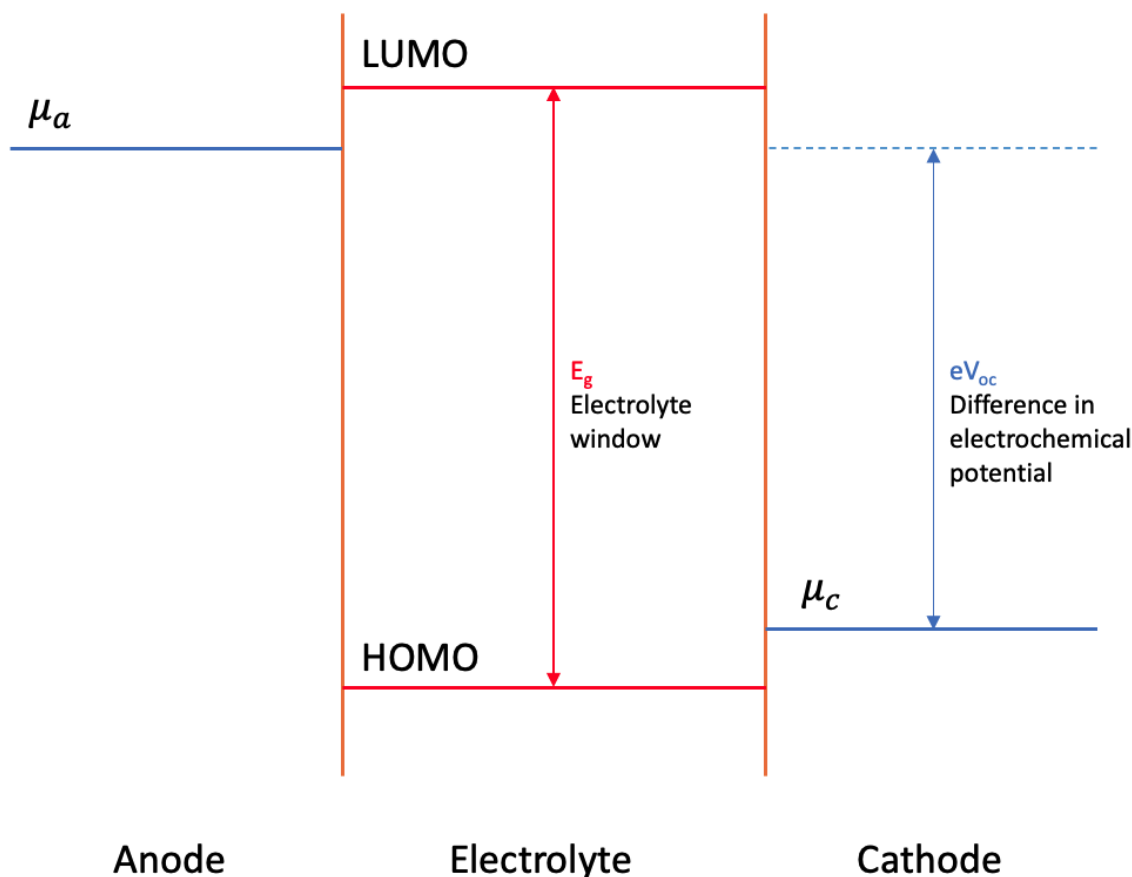
Figure 2.3: The electrochemical stability window of the electrolyte. The LUMO should be at a higher potential than the electrochemical potential of the anode, and the HOMO must be at a lower potential than the electrochemical potential of the cathode. The figure is recreated from.[19]

2.4.1   Electrolyte components

Electrolytes are classified in to four groups; aqueous electrolytes, ionic liquid electrolytes, inorganic solid state electrolytes and organic electrolytes. The organic electrolytes are the most common group used in LIBs, hence this is the group that will be discussed further in this thesis.

Organic electrolytes consists of lithium salt dissolved in an organic solvent or solvent mixture. According to Xu K. et al.,[20] the most common requirements for the solvents in an organic electrolyte in conventional LIBs are as follows:

1. Have a high dielectric constant, which will enable the solvents to dissolve the salts to a sufficient concentration

2. Have a low viscosity to enable a good and facile transport of the ions

3. Be inert to all cell components, in particular the charged surface of the electrodes

during operation of the cell

4. Have a low melting point and high boiling point to ensure that the electrolyte stays liquid within the operating temperature range.

5. Be safe, non toxic and have a low cost

As stated in the first requirement, the solvent must be able to dissolve sufficient amounts of lithium salts. Hence, organic compounds with polar groups like carbonyl (C=O), nitrile (C≡N), sulfonyl (S=O) and ethers (−O−) are suitable. However, solvents commonly used in LIBs usually fall under the category of ethers or esthers.[20] The most common solvents in electrolytes for LIBs are ethylene carbonate, EC, dimethyl carbonate, DMC, diethyl carbonate, DEC, polypropylene carbonate, PC, and ethyl methyl carbonate, EMC.[18] All of these groups have an esther-linkage polar group. The solvents used in this thesis are EC and DMC, whose structure can be seen in figure 2.4.

(a) (b)
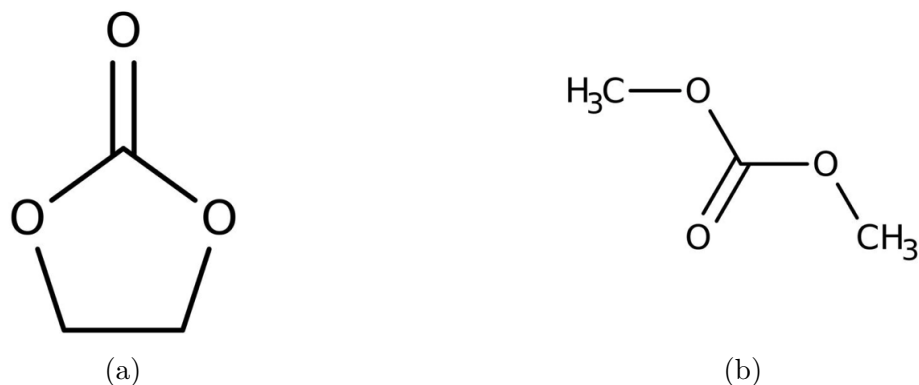
Figure 2.4: Molecular structure of the organic compounds (a) ethylene carbonate (EC) (b) dimethyl carbonate (DMC) used as solvents in electrolytes for LIBs.

EC is, as seen in figure 2.4a, a cyclic carbonate. EC has a high dielectric constant, allowing for high solvation of lithium salts, and high anodic stability on the cathodic surface. In addition, EC was found to form the protective SEI layer on the anode, preventing electrolyte decomposition once formed. However, EC has a high melting temperature (∼36°C). The high melting temperature can be suppressed when the solute is dissolved in EC and if EC is mixed with a co-solvent. Linear carbonates differ from EC by having low boiling point, low viscosity and low dielectric constant. DMC is an example of a linear carbonate (as seen in figure 2.4b) and can mix homogeneously with EC. This combination can help suppress the high melting temperature of EC and also benefit from the low viscosity of DMC, the high dielectric constant and high anodic stability on the cathode of EC. In addition, the combination of EC and DMC has shown to have a large electrochemical stability window. Thus, EC and DMC solvent mixture is widely used in the electrolytes of LIBs today.

In order to provide lithium ions for the LIB, a lithium salt is added to the electrolyte. Xu K. et al.[20] states that the solute in electrolytes for LIBs should meet the following minimal criteria:[20]

1. The salt must be able to dissolve completely in the solvent. The ions, especially Li^+ must be able to move with high mobility in the solvent.

2. The anion must be non toxic and inert towards the solvents, in addition to being stable against oxidative reactions at the cathode.

3. Both the cation (Li^+) and anion must be inert to other cell parts like the separator, current collector and battery package.

Because of the small ionic radius of the lithium ion, most simple lithium salts such as halides (LiX where X = Cl and F) and oxides (Li_2O) does not meet the solubility requirements of a lithium salt in an electrolyte. Hence, most lithium salts used in electrolytes for LIBs are based on complex anions. These complex anions are composed of a simple anion core that is stabilised by a Lewis acid agent. One example of this type of anion is the PF_6^- that is composed of the F^- anion core complexed by PF_5.[20] This anion belongs to the lithium salt $LiPF_6$, which is the most used lithium salt for conventional batteries with a graphite anode and 3-4 V cathode. Other lithium salts that may be used are $LiAsF_6$, $LiClO_4$, $LiBF_4$ and LiTFSI.[21] In addition, the lithium salt LiFSI, has shown promising performance with silicon anodes and will be discussed further in section 2.4.2.

Finally, to further improve the performance of an electrolyte for LIBs and modify targeted functions, additives can be added at small concentrations. Due to the large volume changes in a silicon anode, the electrolyte additives used with silicon anodes must form an SEI layer with a good flexibility and mechanical strength and prevent continuous SEI formation. The most commonly used additives in electrolytes for silicon anodes are fluoroethylene carbonate (FEC) and vinylene carbonate (VC).[22] VC is mostly used to increase the Coulombic efficiency and thermal stability in graphite anodes, but has sometimes been used for silicon anodes as well.[23] FEC will be discussed further in section 2.4.3.

2.4.2   LiFSI

The lithium salt $LiPF_6$ is conventionally used in LIBs, due to its good ionic conductivity, reasonable solubility and thermal and electrochemical stability. However, $LiPF_6$ reacts with trace amounts of water in the electrolyte and form HF which will etch away the SiO_2-layer on the surface of Si anodes.[24] More details on the side reactions of H_2O at the anode will

$$F_3C-\overset{\overset{\displaystyle O}{\|}}{\underset{\underset{\displaystyle O}{\|}}{S}}-\overset{\overset{}{}}{\underset{\underset{\displaystyle Li}{|}}{N}}-\overset{\overset{\displaystyle O}{\|}}{\underset{\underset{\displaystyle O}{\|}}{S}}-CF_3$$
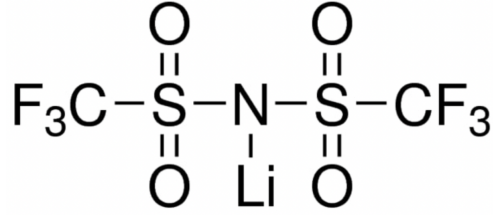
Figure 2.5: The molecular structure of the lithium salt, LiFSI, used in electrolytes for LIBs.

be given in section 2.4.4. The oxidation layer, SiO_2, is a passivating layer that acts as a ceramic stabiliser that will help constrain the volume changes of the anode in addition to forming a stable interface between the electrolyte and the anode. When HF etches away the SiO_2 layer, a reactive Si-H surface remains, which again will cause agglomeration of the Si particles that become susceptible to pulverisation and loss of electrical contact.[25]

Hence, to improve the performance of silicon anodes, the lithium salt LiFSI has been proposed as a promising alternative as LiFSI does not form HF. In addition, LiFSI shows a high ionic conductivity and a better thermal stability than $LiPF_6$. The structure of LiFSI is shown in figure 2.5

Silicon experience large volume changes during lithiation and delithiation, which cause cracking of the SEI layer. Hence, it is important that the electrolyte used in the battery forms a flexible SEI layer on the anode. When the lithium salt $LiPF_6$ is used, the SEI layer shows a "mosaic" and bilayer structure. The inner layer is a dense inorganic layer that, for silicon anodes, is again divided into two layers. The inner layer of the inorganic layer consists of the passivating SiO_2 layer, in addition to lithiated compunds of SiO_2, like Li_xSiO_y, Li_xSi and Li_2O. The outer part of the inorganic layer consists of decomposed compounds from the electrolyte, mostly LiF. The outermost layer is a softer organic layer consisting of decomposed solvent carbonate molecules. Asheim et al.[25] showed that when $LiPF_6$ is replaced with LiFSI, the SEI layer becomes thinner, more flexible and homogeneous. The inner inorganic layer of the SEI layer becomes more dominant with LiFSI salt, as the reduction of LiFSI occurs at higher potentials than the organic solvent components, and also at comparatively higher potentials than other known electrolyte chemistries.[25,26] Hence, the SEI layer formed with LiFSI has more of a bilayer structure, as opposed to for $LiPF_6$ where the SEI is composed of a mixture of the organic and inorganic compounds in a mosaic structure to a larger extent.[25] The surface morphology of the SEI layer formed by LiFSI-based electrolytes appears more granular[12] than the SEI layer formed by $LiPF_6$-based electrolytes, which appears thicker and more continuous.[27]

Jafta et al.[26] suggests that the reduction product SO_2 can be formed directly from the reduction of LiFSI. The pairing of two SO_2 molecules with lithium ions could further result

in the reduction products Li_2S and Li_2O according to the following reactions.[26]

$$2SO_2 \; + \; 2e^- \; + \; 2Li^+ \; \rightarrow \; Li_2S_2O_4$$
$$Li_2S_2O_4 \; + \; 6e^- \; + \; 6Li^+ \; \rightarrow \; 2Li_2S \; + \; 4Li_2O \qquad (2.15)$$
$$Li_2S_2O_4 \; + \; 4e^- \; + \; 4Li^+ \; \rightarrow \; Li_2SO_3 \; + \; Li_2S \; + \; Li_2O$$
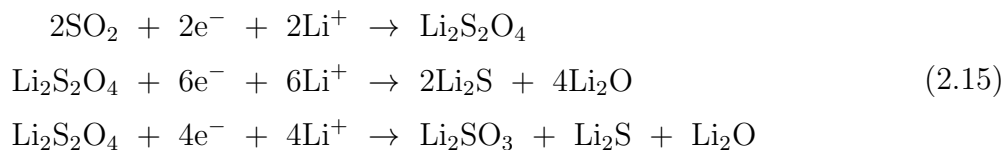
Li_2O is mostly formed in the inner part of the SEI layer and will therefore give less signal using characterisation techniques like X-ray photoelectron spectroscopy (XPS). However, it has been shown to appear with small intensity when LiFSI-based electrolytes has been used, confirming that a thinner and more inorganic SEI layer is formed with LiFSI salt.[28]

Asheim et al.[25] performed electrochemical testing of silicon anodes containing 60 wt.% silicon, with LiFSI-based electrolyte. The silicon anodes were made from micron-sized silicon particles, Silgrain®e-Si 400, battery grade silicon from Elkem. The electrolyte used was 1M LiFSI in a EC:PC:DMC (1:1:3 wt.%) solvent mixture, with 1 wt.% VC and 5 wt.% FEC. The anodes were used in half-cell coin cells and galvanostatically cycled between 0,05V - 1V for 500 cycles. The initial capacity of the cells were approximately 2700 mAh/g. After 100 cycles the capacity was reduced to approximately 1500 mAh/g.[25] Rogstad et al.[16] used the same silicon powder as Asheim to make anodes with 73,2 wt.% Si combined with an electrolyte with 0,74 M LiFSI in EC:DMC (1:2 wt.%) solvent mixture with 1 wt.% VC and 5 wt.% FEC. The anodes were cycled galvanostatically for 100 cycles with an initial capacity of approximately 3000 mAh/g. After 100 cycles, the capacity had decreased to approximately 750 mAh/g.[16]

2.4.3 FEC as an additive

As mentioned, FEC is an additive that is added to improve the SEI layer, hence to improve the performance of the battery. The structure of FEC is shown in figure 2.6. Uchida et al.[29] tested the effect of FEC as an additive in a $LiPF_6$-based electrolyte with micron-sized silicon in 2015. They concluded that the addition of 10 wt.% FEC drastically improved the cyclability of the silicon anode.[29] FEC is reduced at a higher potential (1,47 V) than the EC/DMC solvent mixture.[23]

The SEI layer formed with FEC as an additive is composed of a larger amount of LiF that covers the Si surface and effectively suppresses the expansion of the anode. In addition, the SEI layer formed with FEC shows a very low resistance and low impedance.[29,25] The reason for the reduced impedance is not yet clear, but one possible explanation proved by Jaumann et al.[23] could be that the LiF nanocrystals in the SEI layer combined with Li_2CO_3 cause high Li^+ conductivity. The formation of crystalline LiF and Li_2CO_3 phases cause the grain boundaries to become pathways for the Li^+, while the LiF itself is a bad conductor of Li^+.[23]
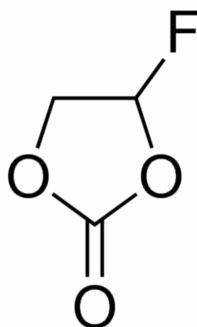
Figure 2.6: Molecular structure of the organic compound FEC, used as additive in electrolytes for LIBs.

However, the LiF nanocrystals has also shown to reduce the flexibility of the SEI layer, hence causing cracks during the volume changes. But oppositely, it has been shown by Wang et al.,[30] by the use of density function theory (DFT) calculations, that the ductility of the SEI layer increase when Li_xSi is bound to LiF compared to being bound to Li_2O.[30] Although, the results by Wang is based on a highly ideal system. Thus, the effect of LiF and Li_2O could be different in a real system. The SEI layer formed with FEC is a dense and compact layer with passivating properties that prevents molecules from reaching the Si surface. This results in less parasitic reactions, hence reduced ICL. The inner layer of the inorganic layer of the SEI is enriched with LiF.[25] Other suggested reasons for the improved performance with FEC is that FEC facilitate polymerisation and cross-linking of polymer chains that results in an elastic coating that can withstand the stress caused by the volume expansion during lithiation.[31] In addition, the polycarbonates will form a passivating organic layer in the SEI, as the inorganic layer is not passivating in itself. Etacheri et al.[32] suggested that the main reason for improved stability observed with the additive FEC is due to the facilitation of decomposition products like polycarbonates.[32,25] Hence, the improvement on the cycling abilities of Si-alloys when adding FEC can be due to both the formation of an inorganic layer that is Li_2CO_3- and LiF-rich, and to the formation of organic polymers in the bilayered SEI layer. There are still disagreements in the literature whether it is the inorganic or the organic decomposition products that contributes to the increased performance of anodes when FEC is used as an additive.

Schroder et al.[33] and Jauman et al.[23] tested the effect of FEC in an electrolyte with EC/DMC (1:1) solvent mixture and 1 M $LiPF_6$ and 10 wt.% FEC. Schroder et al.[33] tested the effect of FEC on amorphous nano-silicon. The initial capacity obtained in the first cycle was approximately 3800 mAh/g for the electrolyte without additives and 3600 mAh/g with the addition of FEC. The stability of the anodes were much higher with FEC in the electrolyte with approximately 17% capacity reduction after 100 cycles, compared to 68% reduction for the electrolyte without additives.[33] Similarly, Jaumann et al.[23] tested the same electrolyte mixture on a nanostructured silicon/carbon composite anode. The stability increased with

the addition of FEC, as the capacity of the anodes cycled without additives displayed a capacity reduction of 90%, while the reduction was 35% with FEC as an additive.[23] Etacheri et al.[32] did electrochemical testing of micro-silicon anodes with an electrolyte with EC/DMC (1:1) solvent mixture and 1 M $LiPF_6$ and 3 wt.% FEC. The stability of the micro-silicon anodes increased as well with the addition of FEC. A 55% capacity reduction was observed for the anodes cycled without additives after 50 cycles, while a 30% capacity reduction was observed with FEC in the electrolyte.[32]

However, there are also drawbacks to using FEC as an additive in battery electrolytes. FEC is continuously consumed during cycling and large amounts are therefore required to obtain a long cycle life. In addition, FEC is costly compared to other conventional electrolyte components.[33]

2.4.4 Water in the electrolyte

As mentioned, $LiPF_6$ is the most used lithium salt for LIB electrolytes. However, one major disadvantage of $LiPF_6$ is its sensitivity towards H_2O. Due to an unstable P-F bond, H_2O will react with the salt and form POF_3 and HF. The HF will react with the silicon on the surface of the anode and create new H_2O molecules. The water will again react with the salt and form additional HF that reacts with the silicon surface. This feedback process will continue until the SiO_2 layer on the Si surface is consumed, leaving the surface susceptible to pulverisation and loss of electrical contact.[24] The HF will also etch away other species on the surface, like Li_2O. This was shown by Philippe et al.[34]

However, Han et al.[35] investigated the effect of adding H_2O to a LiFSI-based electrolyte. The results showed no HF formation, suggesting that the FSI^--ion does not hydrolyse like the PF_6^--ion does.[35] Hence, in addition to forming a better SEI-layer, LiFSI might increase the performance of Si anodes by not hydrolysing to form HF.

The water-splitting reaction

$$H_2O \; + \; e^- \; \rightarrow \; \frac{1}{2}H_2 \; + \; OH^- \tag{2.16}$$

occurs at the standard reduction potential of 0,83 V, which corresponds to 2,21 V vs. Li/Li^+. The silicon anodes are usually lithiated down to 50 mV vs. Li/Li^+. Hence, as a large overpotential is applied, the splitting of H_2O according to reaction 2.16 is inevitable. OH^- reacts with EC in the solvent mixture forming CO_2.

$$OH^- \; + \; EC \; \rightarrow \; alkyl \; di-alcoholates \; + \; CO_2 \tag{2.17}$$

Thus, the OH^--ion formed from the water splitting cause ring breaking of the EC molecule,

forming polycarbonates that forms the passivating organic layer in the SEI layer. As a result of the water in the electrolyte, gas formation will occur in the cell. Observation of CO_2 indicates that the formation of polycarbonates has occured. Gas formation in a battery cell could cause cell swelling, which would be a detrimental effect of the addition of water.

Young et al.[3] used an NMC cathode in combination with a silicon-alloy anode in a full-cell configuration with a $LiPF_6$-based electrolyte, to investigate the effects of adding water to the electrolyte. Young stated that CO_2 shows the similar improvements on the cycling abilities of silicon-alloy containing anodes as FEC.[3,36] However, the solubility of CO_2 is low in the battery electrolyte and it is in practice difficult to supply enough CO_2 to the battery. Hence, the in situ gas formation of CO_2 from H_2O in the electrolyte might be utilised to enhance the cycling ability, therefore being a beneficial effect rather than a detrimental effect of the addition of water. The alkyl di-alcoholates will react further with EC and form more CO_2. As a result, Young et al.[3] claims that the trace amounts of water added to the electrolyte will provide continuous CO_2 formation that shows the same SEI-stabilising effects as FEC.[3]

CO_2-formation at the cathode may also occur. For $LiCoO_2$-cathodes, the amount CO_2 generated is minimal, but for cathodes with Mn or Ni, the formation is considerably larger.[3] Gasteiger et al.[37] proposed that the CO_2-generation at the cathode is a result of oxygen release as the NMC cathode is decomposed. O_2 reacts with EC and produce CO_2 and CO according to the following reaction:

$$EC \; + \; 2O_2 \; \rightarrow \; 2CO_2 \; + \; CO \; + \; 2H_2O \tag{2.18}$$
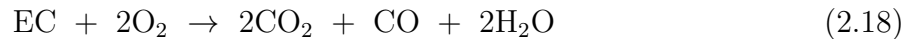
The H_2O produced will lead to further CO_2-production at the anode.[37]

The reasons for the beneficial effects of CO_2 in the electrolyte on the cycling abilities of silicon anodes is still not clear. However, Young et al.[3] claims that CO_2 reacts with the Li ions to form Li_2CO_3, which can, together with LiF, form conductive paths at the grain boundaries for Li^+.[3] However, without FEC in the electrolyte, the source of F is smaller seeing as it can only originate from LiFSI. Li_2CO_3 is formed according to the following reaction:[3]

$$2CO_2 \; + \; 2e^- \; + \; 2Li^+ \; \rightarrow \; Li_2CO_3 \; + \; CO \tag{2.19}$$
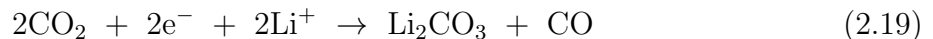
Other reduction products that can be found in the SEI layer is LiOH and Li_2O. The origin of Li_2O in the SEI layer is according to Eshetu et al.[28] arguable. However, several reactions have been reported, including the following reaction with trace amounts of water in the electrolyte.

$$H_2O \; + \; Li^+ \; + \; e^- \; \rightarrow \; LiOH \; + \; \frac{1}{2}H_2 \tag{2.20}$$

$$\text{LiOH} \ + \ \text{Li}^+ \ + \ \text{e}^- \ \rightarrow \ \text{Li}_2\text{O} \ + \ \frac{1}{2}\text{H}_2 \tag{2.21}$$
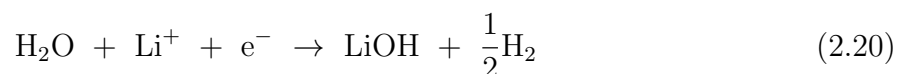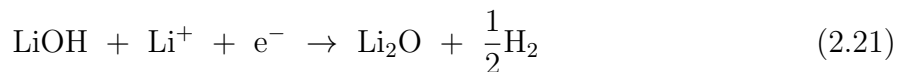
Hence, according to reaction 2.20 and 2.21, an increased amount of Li_2O would be expected with increased amounts of water in the electrolyte.[28]

2.5 Characterisation methods

A brief introduction to the different characterisation methods used in this thesis is presented in this section. X-ray diffraction, BET and particle size distribution analysis are characterisation techniques used on powders used as active material in the electrodes. Galvanostatic cycling and electrochemical impedance spectroscopy are used to characterise the performance of the battery cell. Finally, SEM and FTIR analysis are used for post mortem characterisation of the electrodes after cycling.

2.5.1 X-ray diffraction

Diffraction is the phenomenon when electromagnetic radiation is scattered by a periodic array like atoms in a crystal structure, leading to constructive and destructive interference. As the wavelength of X-rays are similar to the distance between atoms, X-rays can be used to characterise the crystallinity of materials. The scattered x-rays will produce a diffraction pattern that gives information of the arrangement of the atoms in the crystal. Amorphous materials, however, does not have long-range order of periodic arrays, thus will not produce the same diffraction pattern.[38] A diffraction pattern of an amorphous material is characterised by the larger bumps over a larger range of 2θ values rather than the peaks found in a diffraction pattern of a crystalline material. In addition, a material can be semi-crystalline. This material can be recognised from the typical amorphous baseline with additional peaks from the areas with long-range order of periodic arrays.

The geometry of the diffracted beams are described by Bragg's law and express information about the nature of the crystal structure. Bragg's law is given by

$$2d_{hkl}\sin\theta = n\lambda \tag{2.22}$$

where d_{hkl} is the distance between the atomic planes in the crystal, λ is the wavelength of the incident beam and 2θ is the diffraction angle, the angle between the incident beam and the diffracted beam.[39]

An X-ray diffaction (XRD) analysis can give information about the phases in the powder, and the crystallographic structure of the phases, quantification of crystalline compounds,

orientation and texture of the crystalline phases, and strain and crystallite size.[39]

A diffraction pattern is called a diffractogram, where the intensity of the diffracted beams is plotted against 2θ.

2.5.2   BET analysis

The BET analysis is an analysis used to determine the average surface area of the particles in a powder. This is performed by nitrogen adsoption/desorption isotherms measured at 77 K.[40] The surface area is calculated using the BET-equation.

$$\frac{P/P_0}{V(1 - P/P_0)} = \frac{1}{V_m C} + \frac{C - 1}{C} \frac{P/P_0}{V_m} \tag{2.23}$$

V is the volume of the gas adsorbed at the pressure P at the absolute temperature T, P_0 is the vapour pressure of the nitrogen gas at T. V_m is the volume of adsorbed gas that would saturate the surface if the adsorption was limited to a monolayer. C is a constant. $\frac{P/P_0}{V(1-P/P_0)}$ is plotted against $\frac{P}{P_0}$ which gives a straight line, with the slope being $\frac{C-1}{C}$ and the intercept being $\frac{1}{V_m C}$. The slope and intercept is used to find V_m and C, which again is used to find the average surface area of the particles.[41]

2.5.3   Particle size distribution

The particle size distribution can be analysed by the use of laser diffraction analysis. The powder is dispersed in an appropriate liquid to prevent agglomerates from forming. Adding surfactants or sonicating the sample bath are techniques that can be used to prevent agglomeration. The sample bath with the suspended particles are fed through the flow cell at a constant rate by a liquid pump to keep the particles suspended, or the suspension is agitated by a stir bar. The suspension is pumped through the PSD analyser and pass through a laser beam. The diffraction of the laser beam caused by the particles is used to determine the particle size. The Mie theory, which is based on the Maxwell equations, is used to calculate the particle size. The Mie theory gives a solution to the interaction of a plane wave on a homogeneous sphere. It also takes into account the transmission through the particle, thus the calculation requires the refractive index of both the powder and the liquid. Hence, the Mie theory is a volume based PSD technique that assumes spherical particles. This is often not the case, but the analysis will give a good impression of the PSD in the powder.[42]

2.5.4   Galvanostatic cycling

Galvanostatic cycling is a technique used to determine the capacity of the battery. When the battery is cycled galvanostatically, it means that a constant current is applied during charge and discharge to cycle the battery between a lower and an upper potential limit. When the potential limits are reached the battery is often held at a constant potential. The battery is then charged and discharged in potentiostatic mode with a constant potential until a current limit is reached.

2.5.5   Electrochemical impedance spectroscopy

Electrochemical impedance spectroscopy (EIS) is a sophisticated electrochemical characterisation technique that allows for the quantification of cell resistance of the bulk, the SEI layer, charge transfer resistance and the chemical diffusion process by one single experiment without requiring disassembly of the cell. In an EIS analysis, the resistance (R), capacitance (C) and inductance (L) is measured by applying either an alternating current (galvanostatic EIS) or voltage (potentiostatic EIS) and monitoring the response in the cell. The technique used in this thesis is potentiostatic EIS. Here, a small AC perturbation is superimposed on the potential. The impedance ($Z(\omega)$, $\omega = 2\pi f$) can be expressed as the ratio between the complex amplitudes of the voltage and the current, $V(\omega)/I(\omega)$. Thus, the impedance is the resistance that interrupts the current flow when applying an AC voltage to the circuit. The frequency-dependent impedance spectrum of a system can be represented by an equivalent electrical circuit composed of resistances, inductors, capacitances and other elements.[43]

The impedance, $Z(\omega)$ is divided into a real and an imaginary part, Z'_{real} and Z''_{im} respectively. The imaginary part is plotted vs. the real in a Nyquist plot by the use of cartesian coordinates.[43] The Nyquist plot is used to analyse the different contributions to the impedance, like the electrolyte resistance, resistance in the SEI layer, charge transfer resistance and chemical diffusion process.

2.5.6   Scanning electron microscope

A scanning electron microscope is a high resolution microscope. A focused electron beam gives information about the chemical composition and crystallinity etc., in addition to imaging the surface morphology of the electrode. The electron beam hits the surface of the sample, giving rise to secondary electrons, backscattered electrons and x-rays, which all gives different information about the sample.

Secondary electrons are generated due to the interaction between the primary electrons in

the electron beam and weakly bound valence electrons in the sample. Secondary electrons have low energy. Therefore, the probability of secondary electrons escaping the sample decreases as the penetration depth in the sample of the primary electrons increases. Hence, most of the detected secondary electrons from the sample originates from the surface, which means that secondary electrons are good for surface imaging.

Backscattered electrons are primary electrons that escapes the sample. The fraction of backscattered electrons increase with increasing atomic number of the phases in the sample. Thus, backscattered electrons can give information about the composition of the sample. Particles with higher atomic number will appear light in a matrix with lower atomic number.

X-rays are generated when the electron beam hits the sample surface. The electrons can ionize the atoms in the sample, resulting in emitting of characteristic x-rays. The characteristic x-rays are utilised in an energy-dispersive x-ray spectroscopy (EDS) analysis to identify the elements in the sample.

2.5.7 Fourier-transform infrared spectroscopy

Fourier-transform infrared spectroscopy (FTIR) is a technique used to characterise molecular bonds. Infrared (IR) radiation is passed through the sample, and the amount of absorbed radiation is dependent on the vibrations and rotations of the molecules in the sample.[44] The energy absorbed is specific depending on atomic mass and bond strength. Hence, by relating the absorbed energy to frequency by the use of Planck's law, $E = hf$, h being Planck's constant, characteristic IR frequencies are obtained for the different functional groups. By analysing the sample using FTIR, an absorbance spectrum is obtained that can determine the composition of the sample. In order to be detectable by an FTIR analysis, a change in dipole moment is necessary. Therefore, not all vibrational modes are IR active. LiF is an example of a species that is not detectable by FTIR.[45]

The IR spectra are usually given as a function of wavenumber, which is defined as the number of wavelengths (λ) per unit distance (usually cm^{-1}). The wavenumber is given by $1/\lambda$, and is related to the absorbed radiation by $E = hc/\lambda$, c being the speed of light in vacuum. FTIR is usually performed between $4000 cm^{-1}$ and $400 cm^{-1}$.[45] Some groups that can be observed are C-O bonds, which usually have wavenumbers between 1200 and 1000 cm^{-1}, OH-bonds between 3000 and 2000 cm^{-1} and Li-O bonds below 600 cm^{-1}.

There are several different ways to direct the IR light at a sample, or to detect the absorbance. Attenuated Total Reflectance (ATR) FTIR is one of them. ATR-FTIR is a technique where the IR light is directed at the interface between an internal reflection element (IRE) and the sample, which is placed on the surface of the IRE. The IRE is an IR transparent material with a high reflection index, such as a prism made of ZnSe, silicon, germanium or

diamond. The IR beam has an angle of incidence that is greater than the critical angle, thus resulting in total internal reflection.[44] This leads to an evanescent surface wave that can be analysed. The ATR-FTIR allows for faster measurements, and less sample preparation as the sample is only placed on top of the IRE. The penetration depth is typically in the range of 0.5-2μm, depending on the angle of incidence and the refractive indices of the sample and the IRE.[44,45] This makes the technique ideal for studying the surface of silicon anodes. A table showing some of the peaks that could be expected in an ATR-FTIR spectrum of cycled silicon anodes is shown in Appendix A.

3 Experimental

3.1 Chemicals

Table 3.1: Chemicals and materials used for this project, with corresponding purity, Supplier and usage.

Chemical	Purity	Supplier	Usage
RST 3-1 15-100 Si powder	99,27%	ReSiTeC	Active material in Si anodes
RST 3-1 15-59 Si powder	99,32%	ReSiTeC	Active material in Si anodes
C45 carbon black		Imerys	Additive in Si anodes for conductive network
Na-Alg		Sigma Aldrich	Binder for silicon anodes
Citric acid	99%	Sigma Aldrich	For buffer in Na-Alg binder sol.
KOH	90%	Sigma Aldrich	For buffer in Na-Alg binder sol.
LiFSI	99,9%	Solvionic	Lithium salt in electrolyte
EC	≥99%	Sigma Aldrich	Solvent in electrolyte
DMC	≥99,9%	Sigma Aldrich	Solvent in electrolyte
FEC	99%	Sigma Aldrich	Additive in electrolyte
LFP cathodes		Customcells Itzehow GmbH	Cathode in PAT-cell
Solupor 3PO7A/3PO7B (Polyethylene (PE))		Lydall	Separator for coin cells
FS-5P separator (Polypropylene (PP) fiber/PE membrane)		EL-Cell	Separator for PAT-cells

3.2   Characterisation of silicon powders

Two silicon powders, provided by ReSiTec, were used to make silicon anodes in this thesis. The silicon powder, RST 3-1, is a silicon kerf source recycled from the silicon slurry originates from the cutting process of silicon wafers for solar cells. The RST 3-1 powder has been subjected to two different post treatments done by ReSiTec to make the powder more crystalline, RST 3-1 15-59, and more amorphous, RST 3-1 15-100. For the sake of simplicity, the RST 3-1 15-59 will hereafter be referred to as crystalline silicon, and the RST 3-1 15-100 as amorphous silicon.

3.2.1   XRD

An XRD analysis was performed on the two silicon powders using Bruker D8 A25 DaVinci X-ray Diffractometer with Cu K_{α}-radiation and a θ-range of 10-90°. The raw data were plotted to create the diffractograms. The diffractograms were used to qualitatively determine whether the powders were crystalline, amorphous or semi-crystalline.

3.2.2   BET

BET analysis was performed on the two silicon powders to determine the specific surface area of the particles. The powders and empty tubes used for the analysis were weighed using a scale with 0,01 mg precision and degassed at 250°C for 860 minutes using nitrogen gas, N_2. The degassing was done using the VacPrep 061 system. The degassing is performed to remove humidity and volatile species. After degassing, the powder was weighed again and the amount of powder used was calculated and inserted into the program used for the analysis. The BET analysis was performed using the 3Flex 3500 Chemisorption analyzer with the 3Flex version 5.02 software. The analysis is performed under vacuum at approximately -193° (77K), with a filler rod and an isothermal jacket for the sample tube. The samples are cooled using liquid nitrogen (77K).

3.2.3   PSD

The Horiba - Partica LA-960 particle size analyser was used to analyse the particle size distribution of the amorphous and crystalline powders. The instrument is a laser diffraction instrument based on a volume distribution. Approximately 0,05g of powder was added to 5mL of isopropanol and degassed for 10 minutes using an ultrasonic bath. The solution was then added drop-wise to the particle size analyser until a transmittance of 90% was reached. The refractive index 3,5 was used for the silicon powder. When the particle size distribution

stabilised, four measurements were performed. PSD is a volume-based technique, assuming spherical particles with a known refractive index.

3.3   Silicon anodes

3.3.1   Na-Alg binder solution

The binder solution used for the anodes is a Sodium Alginate-based binder, mixed with a buffer solution. The buffer solution (hereafter referred to as KCA) is a mixture of potassium hydroxide ($KOH \cdot H_2O$) and citric acid ($HOC(CO_2H)(CH_2CO_2H)_2$) with a pH of 3. The buffer solution was prepared by Bjørklund (2021)[46] preceeding this thesis, by mixing approximately 4,5 g citric acid, 0,8 g KOH and 251 g of H_2O. To prepare the binder solution, KCA and Na-Alg was mixed with a 1:60 Na-Alg to KCA weight ratio. Approximately 20 g of KCA was mixed with 0,33 g of Na-Alg. Tables B.1 and B.2 in Appendix B shows the composition of the buffer and binder solutions respectively. The binder solution was mixed with 500 rpm and 60°C on a magnetic stirrer overnight.

3.3.2   Silicon slurry

The silicon anodes were made by tape casting of a silicon slurry based on one of the two different silicon powders, the crystalline and the amorphous powder. Silicon powder as the active material, C Energy C45 carbon black and Sodium Alginate binder solution with the target composition of 75:15:10 wt.% respectively, was mixed using a Retsch MM 400 mixer. Approximately 0,5527 g Si powder and 0,1105 g carbon black powder was weighed out and milled with a steel ball for 5 minutes at 15 Hz. Then approximately 2 g binder solution was added and mixed for 40 minutes at 15 Hz. Finally, approximately 0,7 g of deionized water was added and mixed for additional 5 minutes at 15 Hz to obtain the appropriate viscosity and a loading of approximately 0,4 mg/cm^2. After mixing the slurry in the Retsch MM 400 mixer with a steel ball, the slurry was degassed for at least 1 minute using an ultrasonic bath.

The silicon slurry was distributed onto a copper foil using an RK K Control coater model 101, with a fixed wet height of 60 μm using a coater bar. The casts were then dried overnight in a heating chamber with a temperature of 60°C.

3.4   Electrolytes

The electrolytes used in this work are shown in table 3.2.

Table 3.2: The composition of the electrolytes used in this work

Electrolyte	Composition
1	EC/DMC (1:1) + 1M LiFSI
2	EC/DMC (1:1) + 1M LiFSI + 10 wt.% FEC
3	EC/DMC (1:1) + 1M LiFSI + 1000 ppm H_2O
4	EC/DMC (1:1) + 1M LiFSI + 1000 ppm H_2O + 10 wt.% FEC

The electrolytes were prepared inside the glove box. The first step is to mix EC and DMC in a 1:1 weight ratio. As EC is solid at room temperature, it must be heated to the melting point at approximately 35-38°C. The mass of lithium salt LiFSI corresponding to 1M concentration was added to the EC/DMC mixture to create electrolyte 1, EC/DMC (1:1 wt.%) + 1M LiFSI.

To prepare electrolyte 2, the weight of FEC corresponding to 10 wt.% of the EC/DMC solution was added and mixed.

Electrolyte 3 was prepared by taking out some of electrolyte 1 and adding it to a vial with a septum cap. This vial was brought out of the glove box and by the use of a syringe, the weight corresponding to 1000 ppm H_2O was added through the septum cap to prevent water from entering through the atmosphere. The water level was measured using the Karl-Fischer titration method.

Electrolyte 4 was prepared in the same way as electrolyte 3. FEC corresponding to a concentration of 10 wt.% was added in the final step.

Appendix D shows the calculations of the weight of each component in the electrolytes. Table D.1, also found in Appendix D, shows the mass, weight fraction and molar fraction of the different components in the four electrolytes.

3.5   Battery cell assembly

3.5.1   Coin cells

Silicon electrode disks with a diameter of 16 mm were punched out from the tape cast and dried overnight at 120°C before being brought into the Mbraun Labmaster glove box. Coin cell parts from Hoshen Corp. were used to assemble CR2016 coin cells (20 mm diameter and 1,6 mm height). Amorphous silicon was used in combination with the three first electrolytes shown in table 3.2, and crystalline silicon was used in combination with all four electrolytes. A Solupor 3PO7B separator was used in the coin cell with 30 μL electrolyte. The half-cell

coin cells were made with lithium foil as the counter electrode with a 0,5 mm thick spacer. The cells rested for at least 12 hours before cycling to ensure proper distribution of the electrolyte. Figure 3.1a shows the assembly of a coin cell.

3.5.2 PAT-cells

Silicon and LFP electrode disks were punched out from the casts with a diameter of 18 mm and dried overnight in a binder vacuum drying furnace at 120°C before being brought into the glove box. Only anodes made from crystalline silicon powder were used in the PAT-cells. The LFP cathodes were provided by Customcells Itzehow GmbH. An insulation sleeve with a separator made of polypropylene fiber and polyethylene membrane, and a lithium reference electrode from EL-CELL®was used in the PAT-cell (EL-CELL®) to assemble a pseudo full-cell with LFP counter electrode. The lower electrode, the silicon anode, was inserted at the bottom of the insulation sleeve before inserting the lower plunger with a height of 150 mm. The insulation sleeve was then placed in the cell base. The separator was soaked in 100μL electrolyte to ensure proper contact in the cell. Then the counter electrode, LFP cathode (3,5mAh/g) was placed above the separator, and the upper plunger was inserted before the screw cap was screwed on to the cell base. The cells rested for at least 12 hours before being cycled. Figure 3.1b shows the assembly of the PAT cell.

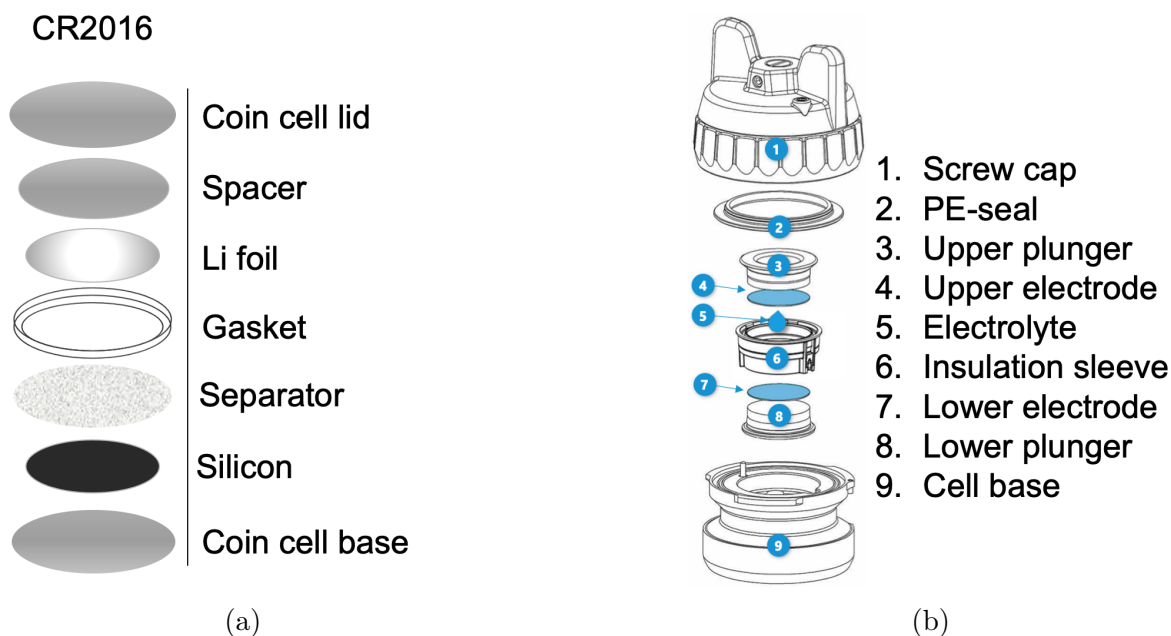|	
CR2016	
Coin cell lid	1. Screw cap
Spacer	2. PE-seal
Li foil	3. Upper plunger
Gasket	4. Upper electrode
Separator	5. Electrolyte
Silicon	6. Insulation sleeve
Coin cell base	7. Lower electrode
	8. Lower plunger
	9. Cell base

(a)   (b)

Figure 3.1: (a) Assembly of a coin cell and (b) assembly of a PAT-cell. The image of the PAT-cell assembly is taken from the EL-CELL®user manual for PAT-cells from [47]

3.6   Electrochemical testing

The coin cells were galvanostatically cycled in 25°C using BioLogic BCS-805 battery cycler with BT-lab software, between 0,05-1,05 V (vs. Li/Li$^+$). Two formation cycles were performed with a C-rate of C/20. At both the upper and lower potential limit, a potentiostatic hold step was performed until 1/2 of the current of the galvaniostatic step was reached. Two cells in each parallel were cycled for 100 cycles at a C/5 C-rate, while the third was cycled for 50 cycles before being disassembled for post mortem characterisation.

The PAT-cells were galvanostatically cycled between 3,40 and 2,40 V (vs. Li/Li$^+$), which corresponds to 0,05-1,05 V (vs. Li/Li$^+$) on the silicon anode. Two formation cycles with C-rate C/20 is performed, followed by 20 cycles with C-rate C/4. The potentiostatic hold step that was used for the coin cells did not work on the PAT-cells. Therefore, a low current step was used to replace the potentiostatic hold step for both charge and discharge. This was done by applying a current corresponding to a C-rate of C/30 for two hours with the same potential limit, after charge/discharge at C/4.

The cycling programs are described in table F.1 in Appendix F.

After 20 cycles the cell is lithiated at a low current (C/20) to a cell voltage of 3,4 V (corresponding to 0,05 V on the silicon anode) before potentiostatic electrochemical impedance spectroscopy (PEIS) was performed. The low current was used to ensure that the electrode was equilibrated before performing the EIS. The cell was scanned from 200 kHz to 5 mHz with 6 points per decade, and a sinus amplitude of 5 mV. The impedance spectra obtained were used to determine the change in total resistance in the cell.

3.7   Post mortem characterisation

3.7.1   SEM

The anodes made with crystalline silicon powder, used in both the coin cells and the PAT-cells, were characterised using an FEI APREO Scanning Electron Microscope (SEM). For the SEM images, the working distance was set to 4 mm, the accelerating voltage to 2kV and emmision current to 0,10nA. An EDS analysis was performed using an Oxford Xmax 80mm^2 EDS detector, with 10 mm working distance, 5kV accelerating voltage and 1,6nA emmision current. The anodes were exposed to air for a maximum of 5 minutes during transportation from the glove box to the vacuum chamber in the SEM.
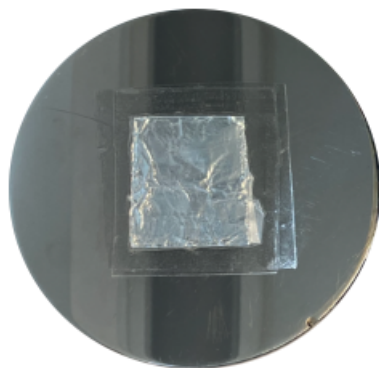
Figure 3.2: Sealing the sample on the ATR-plate to prevent contact with air

3.7.2   FTIR

The SEI composition of the anodes used in the coin cells was characterized using a Bruker Vertex 80v ATR-FTIR with a diamond crystal in vacuum. It was essential for the analysis that the anode was not exposed to air. Hence, the ATR-FTIR plate was cleaned with isopropanol and brought into the glove box. The anode was placed facing the diamond crystal and sealed with contact paper. A sheet of aluminium foil was placed on top of the contact paper and sealed with another layer of contact paper. Figure 3.2 shows how the sample was sealed on the ATR-plate for FTIR analysis. A module piston was used to obtain proper contact between the anode and the diamond. The analysis was performed under vacuum and in room temperature. A standard baseline correction was performed to better identify the peaks. In addition, the spectrum of an uncycled silicon anode was subtracted from the spectrum of the cycled cells. This ensures that the spectra constructed reflects the changes in the surface, hence the SEI layer. Furthermore, the spectrum of the anode cycled with only LiFSI in the electrolyte was subtracted with the anodes with FEC and H_2O to identify the different bond energies related to FEC and H_2O.

4 Results

4.1 Characterisation of silicon powders

4.1.1 BET

From the BET analysis of the crystalline and amorphous powder, the specific surface area of the two powders were obtained. Table 4.1 shows the results from the analysis.

Table 4.1: Results from the BET analysis showing the specific surface areas of the two silicon powders used in this thesis.

Si powder	Surface area [m^2/g]
Amorphous	29,2
Crystalline	27,8

4.1.2 PSD

A PSD analysis was performed on the powders. Figures 4.1 shows the results from the analysis. From the analysis of the amorphous powder in figure 4.1a, two peaks can be observed. This indicates that agglomerates of the powder has been formed. The graphs shows that 50 vol.% of the particles have a particle size of just below 0,95 μm in diameter or smaller. The peak at larger diameters for the amorphous powder is neglected, as it is most likely due to agglomerates.

Also for the crystalline powder in figure 4.1b, an estimate of the position of the peak indicates that 50 vol% of the particles have a particle diameter of 0,95 μm or smaller as well.

4.1.3 XRD

An XRD analysis was performed to determine the crystallinity of the powders. Figure 4.2 shows the results from the analysis. From the diffractogram it is shown that the powder that has been post treated to become crystalline, is indeed crystalline. This is evidenced by the sharp peaks. As for the amorphous powder, sharp peaks are observed in addition to the wavy baseline associated with an amorphous material. This indicates that the powder is not entirely amorphous, but semicrystalline.
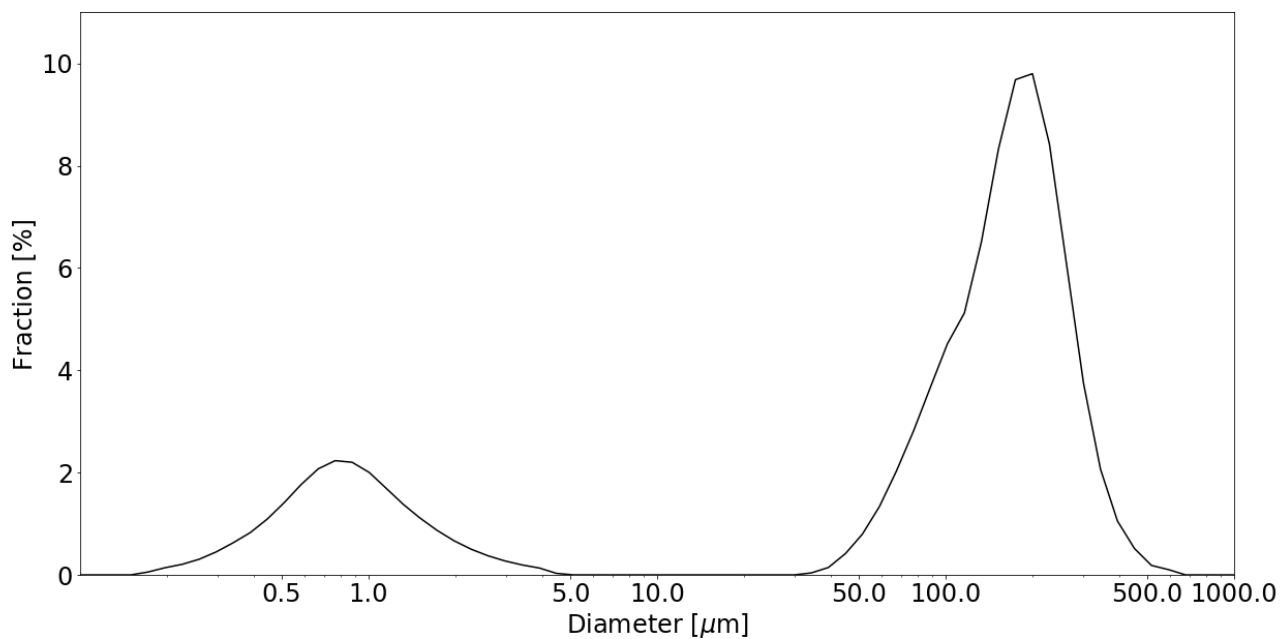
(a)
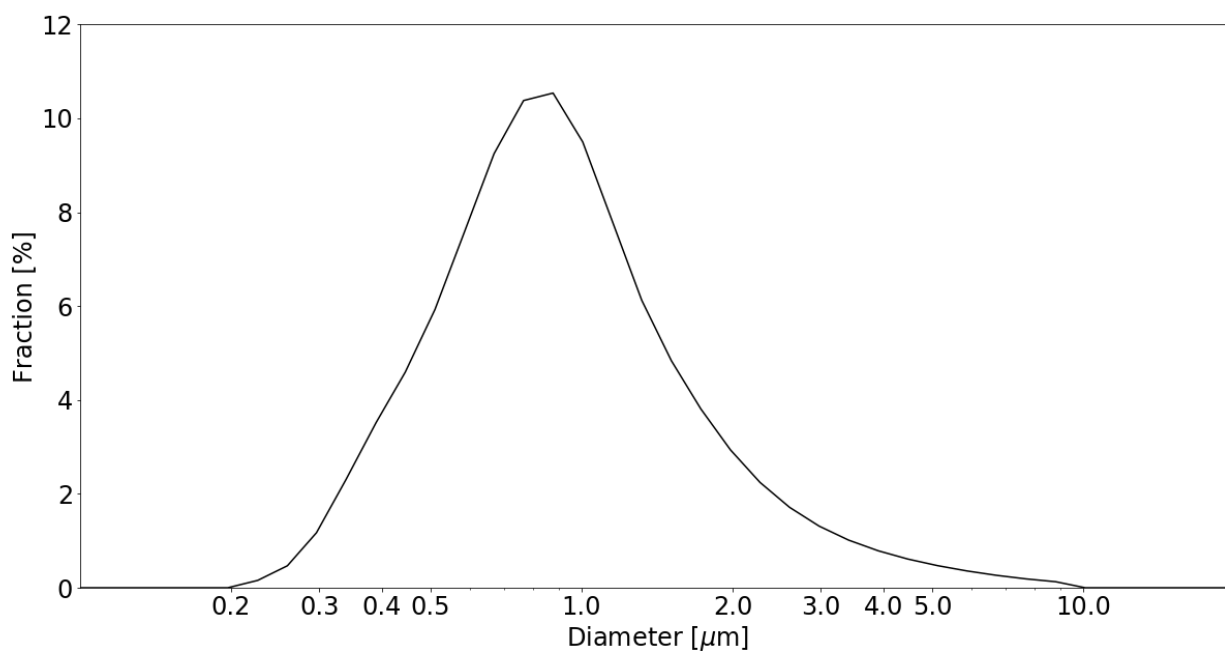
(b)

Figure 4.1: Results from the PSD analysis. Showing the distribution of particle size in the two silicon powders, (a) amorphous and (b) crystalline.
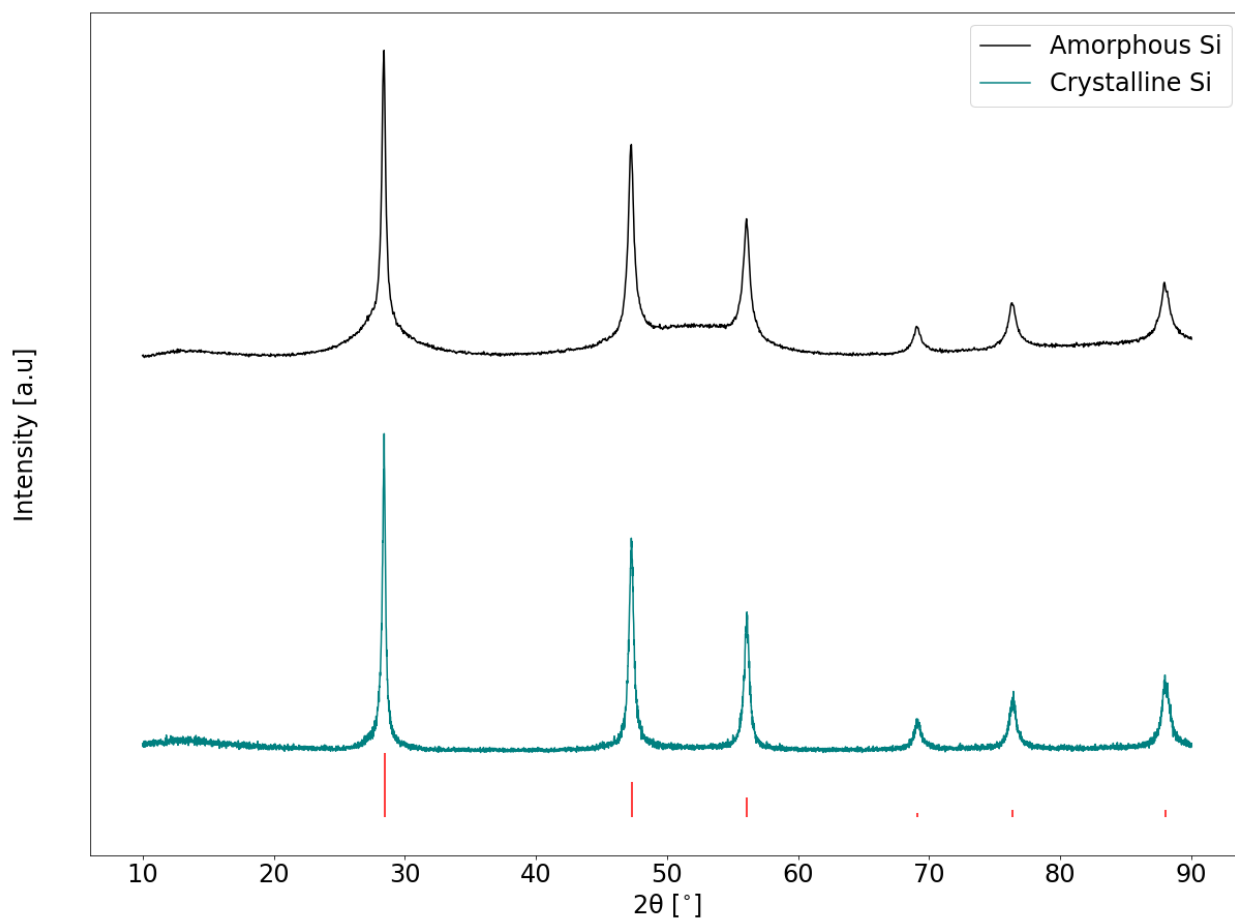
Figure 4.2: Results from the XRD analysis. The black diffractogram corresponds to the amorphous silicon powder. The teal diffractogram corresponds to the crystalline silicon powder. The red lines indicates the reference pattern of silicon with the characteristic 2θ-values of the peaks with relative intensity.

4.2   Electrochemical testing

4.2.1   Cycling performance and Coulombic efficiency

Coin cells were made in a half-cell configuration with silicon anodes and lithium as

the counter electrode. The crystalline anodes were combined with the four different electrolytes in table 3.2. The electrolytes contains (in addition to the solvents) just LiFSI salt (1), LiFSI and FEC (2), LiFSI and H_2O (3) and finally LiFSI, FEC and H_2O (4). The

amorphous anodes were only combined with electrolytes 1, 2 and 3. The cells with amorphous and crystalline silicon were cycled for 100 cycles and the specific discharge capacity and Coulombic efficiency is plotted in figure 4.3a and 4.3b respectively.

The capacity plot in figure 4.3a shows that for the amorphous silicon, the cells with FEC in the electrolyte outperforms the cells with no additives or with just water in the electrolyte. The mean initial capacities of electrolytes 1, 2 and 3 are approximately 2000, 2250, 1900 mAh/g respectively. After 100 cycles the mean capacities have decreased to 600, 1200 and 450. The error bars are especially large for the cells with electrolyte 2, with an initial capacity between approximately 2500 and 1500 mAh/g, and with capacities between 1500 and 800 mAh/g after 100 cycles. Due to time constraints, only two cells were made with the amorphous anodes and electrolyte 2.

As for the Coulombic efficiency, figure 4.3b shows that the efficiencies for cells with electrolytes 1 and 3 are quite similar up until 52 cycles, with a slightly higher efficiency for electrolyte 2 for most of the cycles. After that, the efficiency of the cells with electrolytes 1 and 3 increase slightly compared to the cells with electrolyte 2. However, all cells are quite stable above an efficiency of approximately 97%. The ICL is larger for the cells with FEC or H_2O in the electrolyte, at approximately 33% and 37% respectively, compared to the ICL for electrolyte 1 at 21%. The ICL during the second formation cycle is estimated to be around 12% for cells with electrolytes 2 and 3 and 6% for cells with electrolyte 1. Similar ICL is also observed for the third cycle (first cycle after formation cycles) for electrolytes 1 and 3 before the efficiency increases to ∼100% for all cells. The variation between the ICL of the anodes with electrolyte 1 is very large.

The capacities of the crystalline silicon anodes cycled with electrolytes 1-4 are plotted in figure 4.4a. Also for the crystalline anodes it is clear that the anodes cycled with FEC in the electrolyte, electrolytes 2 and 4, outperforms the cells cycled without FEC, electrolytes 1 and 3. The mean initial capacities of electrolytes 1, 2, 3 and 4 are approximately 2250, 2600, 2000 and 2500 mAh/g respectively. After 100 cycles, the mean capacities have decreased to around 1100, 1400, 775 and 1500 mAh/g. Thus, the crystalline anodes outperforms the amorphous anodes with higher capacity and higher stability.

The Coulombic efficiencies in figure 4.4b are quite similar for all four electrolytes. The ICLs in the first formation cycle are approximately 22%, 26%, 26% and 29% for electrolytes 1, 2, 3 and 4 respectively. The efficiencies of the cells with electrolytes 1 and 3 drops to approximately 97% after 37 cycles but is stable at 97% for the remaining cycles. The efficiency of the cell with electrolytes 2 and 4 decrease more slowly before the cell with electrolyte 2 reach 97% after 70 cycles and stabilising at approximately 96.5% for the rest of the cycles. Due to time constraints in the project, only the data from two cells were used in the data set for crystalline anodes with electrolyte 4. Figure 4.4b shows that one of the
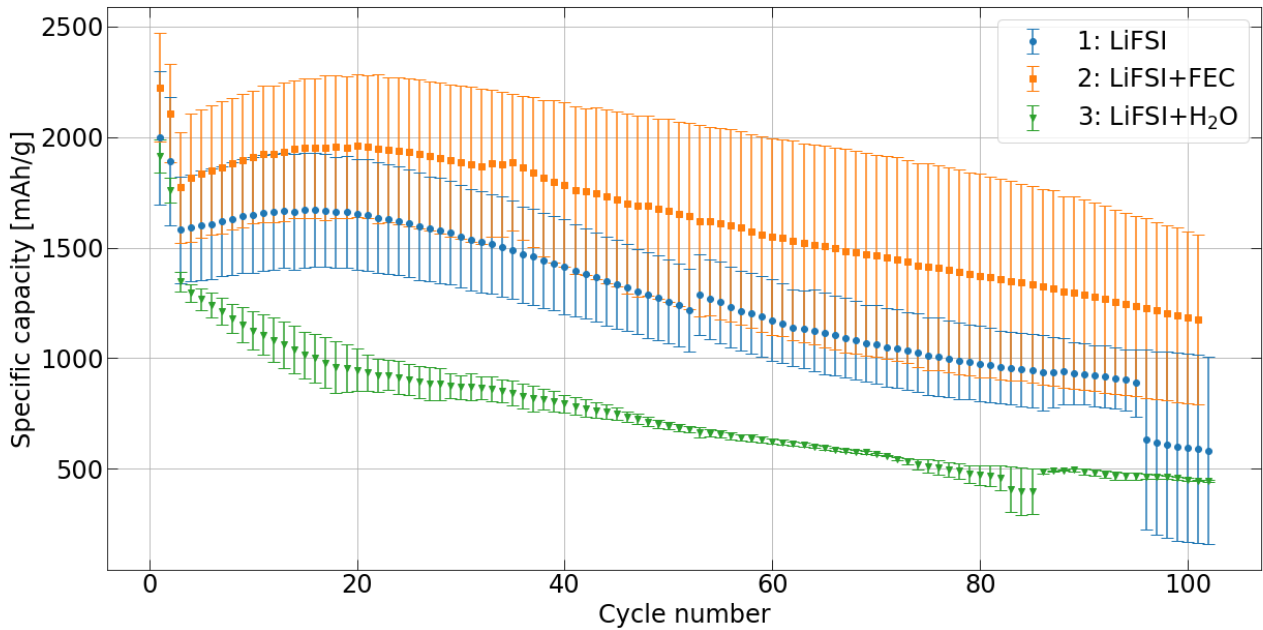
(a)
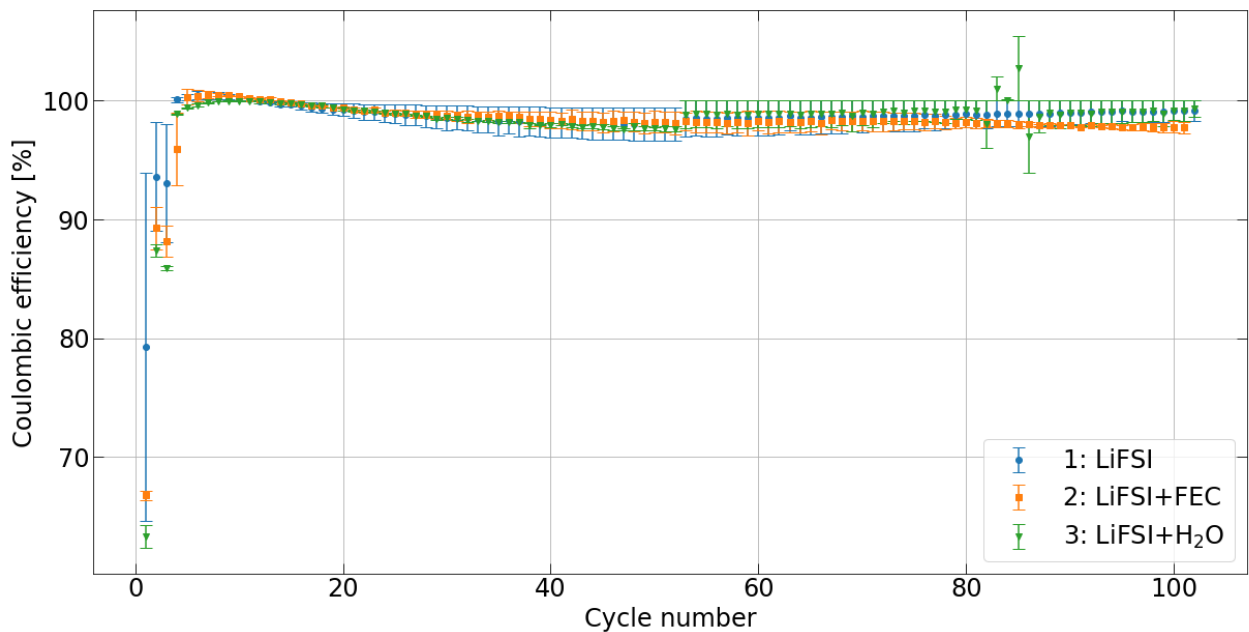
(b)

Figure 4.3: (a) The specific discharge capacity and (b) Coulombic efficiency of half cells with amorphous silicon anodes with electrolyte 1, 2 and 3 from table 3.2.

cells follows the same efficiency development as the cells cycled with electrolyte 2, while one cell reaches efficiencies well above 100%. This is probably due to trapping of lithium in
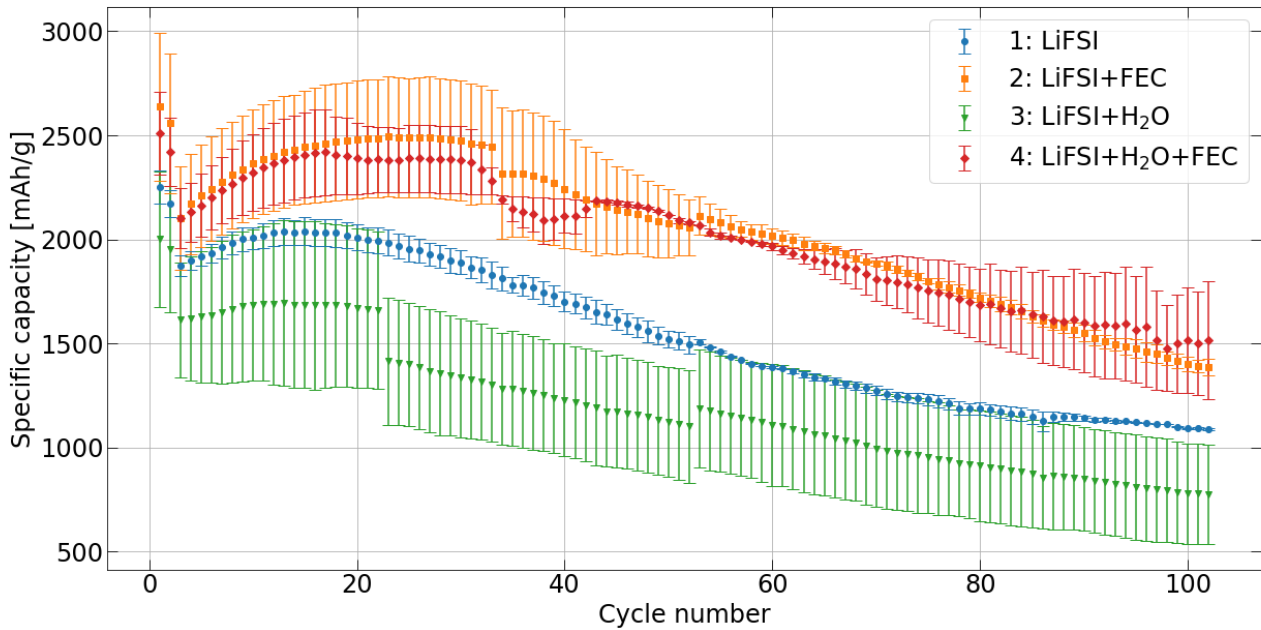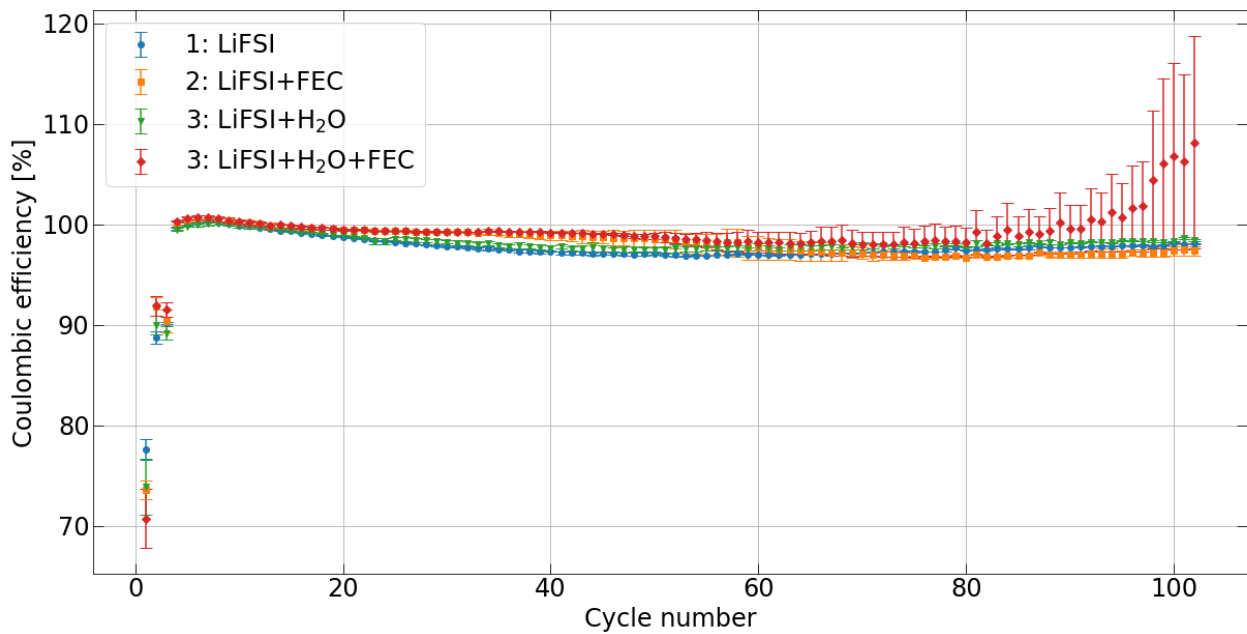
(a)

(b)

Figure 4.4: (a) The specific discharge capacity and (b) Coulombic efficiency of half cells with crystalline silicon anodes with electrolyte 1, 2, 3 and 4 from table 3.2.

the anode during earlier cycles that is released after 90 cycles, causing more charge to be released during delithiation then what was consumed during lithiation.

Si-LFP quasi full-cells were assembled in PAT-cells to prevent reactions with lithium from affecting the results. The capacities of the anodes in the four PAT-cells with the electrolytes in table 3.2 are plotted in figure 4.5. Figure 4.5 shows that the specific efficiency is higher and more stable for the cells with FEC in the electrolyte. This is the same trend as observed for the coin cells in figure 4.4a. The initial capacities for the anodes paired with electrolytes 1, 2, 3 and 4 are approximately 2500, 2800, 2300 and 2300 mAh/g respectively. After 80 cycles, the capacity decreased to approximately 340, 2400, 300 and 2200 mAh/g.

The efficiency of the PAT-cells is presented in figure G.1 in Appendix G. From the plot it seems like the cells with electrolytes 2 and 3, and partly electrolyte 1 have efficiencies above 100%.
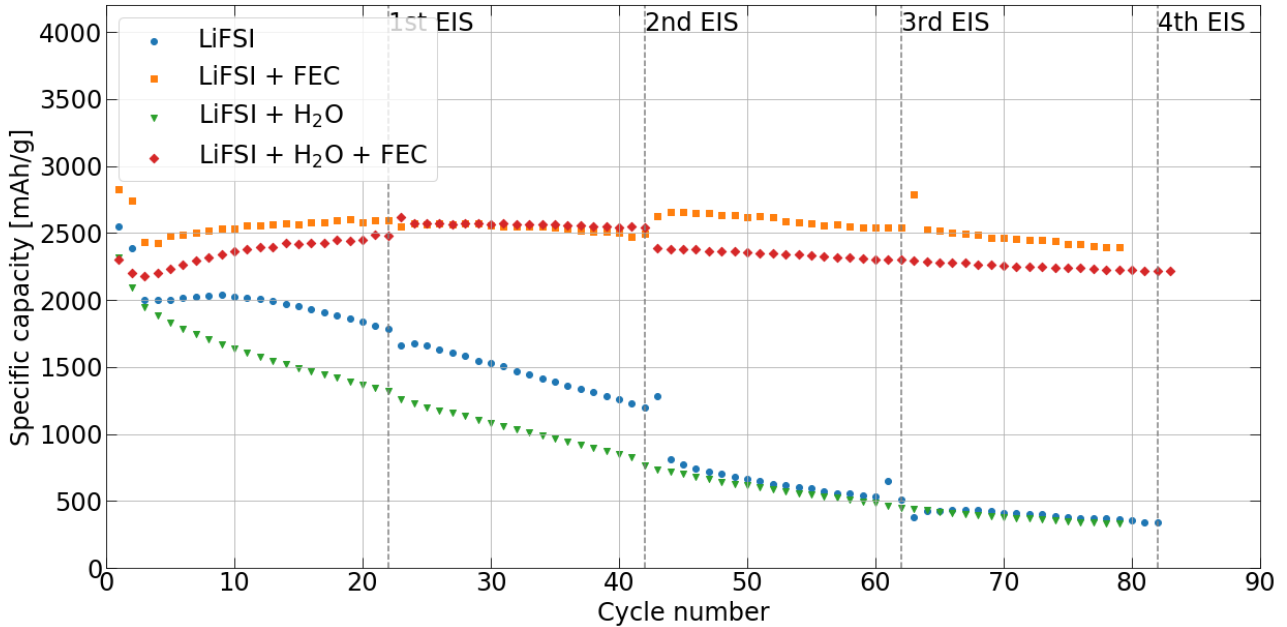
Figure 4.5: The specific discharge capacity of the anodes cycled in PAT-cells with electrolytes 1, 2, 3 and 4 from table 3.2.

4.2.2   Lithiation and delithiation potential

Differential capacity plots were used to show the lithiation and delithiation potentials of the silicon anodes with the different electrolytes. The peaks in the differential capacity plots corresponds to the plateaus observed in the potential profiles. These plateaus indicate where the lithiation and delithiation occurs. Figure 4.6 and 4.7 shows the differential capacity plots and potential profile of the amorphous and crystalline silicon anodes respectively.

For the amorphous anodes, figure 4.6a shows that the delithiation potentials for all three
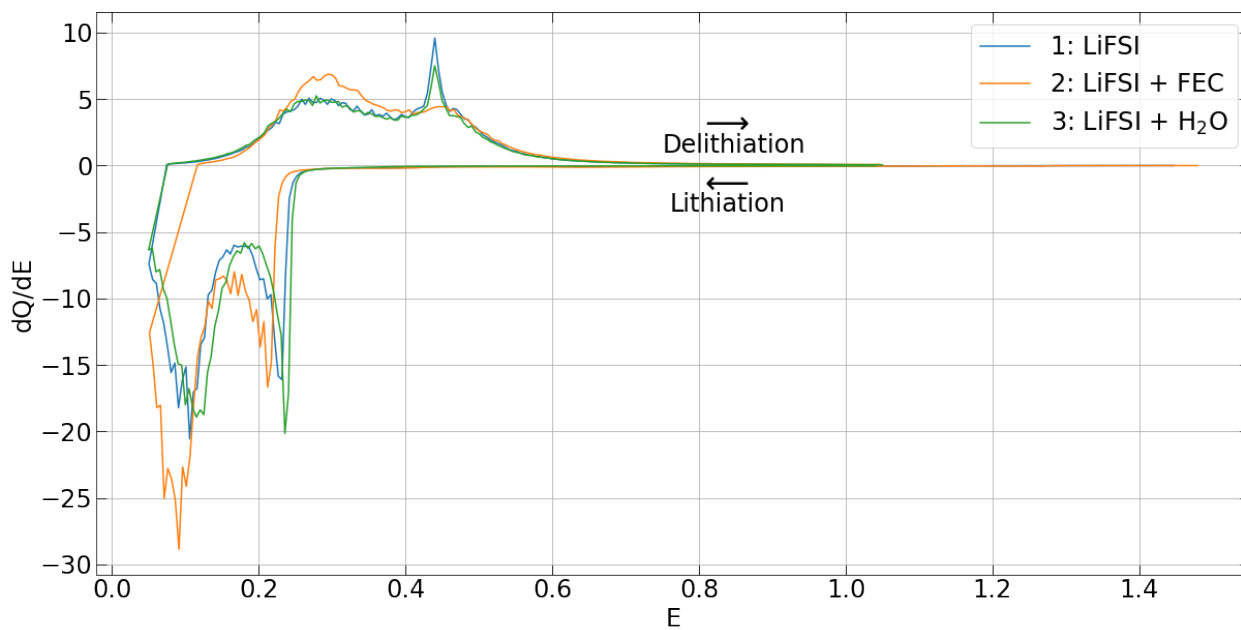
(a)
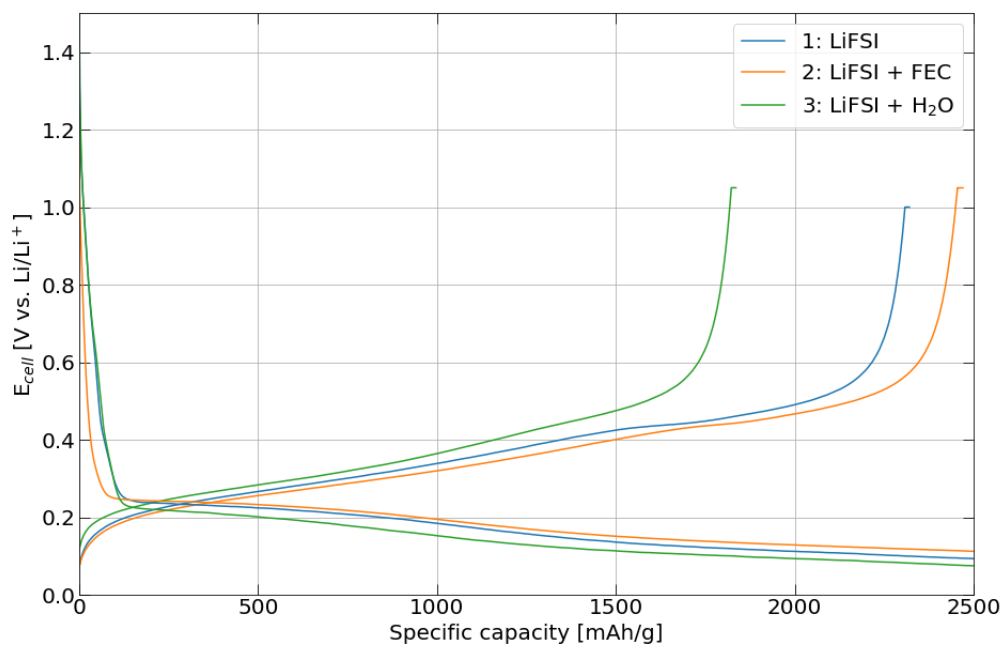
(b)

Figure 4.6: (a) Differential capacity plot and (b) corresponding potential profiles of the first formation cycle of the amorphous anodes with electrolytes 1-4.

electrolytes are quite similar. As for the lithiation, electrolyte 1 and 3 display the same lithiation potentials for the first cycle at approximately 0,23 V and 0,12 V. While the anode with electrolyte 2 is lithiated at slightly lower potentials.

As for the crystalline anodes, the lithiation and delithiation of the anodes both in the first and in the second cycle occurs at approximately the same voltages, as seen in figure 4.7a. The anode with electrolyte 3 seems to be lithiated at slightly lower potentials, but there is no significant difference compared to the other electrolytes.

The difference between the amorphous and crystalline anodes is the first cycle. The lithiation occurs only at one potential, slightly above 0,1 V for the crystalline anodes, while the lithiation occurs in two steps at approximately 0,23 V and 0,12 V for the amorphous anodes. Then, on the second cycle, shown in the subplots in figure 4.7, after the crystalline anodes have become amorphous according to reaction 2.12, the lithiation occurs at the same potentials as for the amorphous anodes.

4.2.3   Electrochemical impedance spectroscopy

The electrochemical impedance was measured on the PAT-cells with the crystalline anodes and the four different electrolytes. The results are shown in the Nyquist plots in figure 4.8. Due to inductive loops, finding an equivalent circuit to fit the spectra was very challenging. Instead, the total resistance in the cell was approximated based off of where the right end of the semicircle would intersect with -Im(Z)=0 Ω. In the case of two semicircles, the total resistance is measured at the intersection of the low frequency loop. The orign of the inductive loops is not known. A summary of the total resistances is given in table 4.2. The electrolyte resistance is described from the intersection with the left side of the semicircle.

Figure 4.8a shows the impedance spectra from the four EIS measurements performed in the cell with electrolyte 1 (LiFSI, no additive) with measurement 2 and 4 in the subplot in order to get a closer look at the spectra. The same was done for the cell with electrolyte 4 in figure 4.8d, where measurement 1 and 3 are plotted in the subplot as the overlapping of the spectra makes it difficult to read the data obtained from the graphs.

For electrolytes 2, 3 and 4 in figures 4.8b, 4.8c and 4.8d respectively, the total resistance increase with each measurement. This is not the case for electrolyte 1.
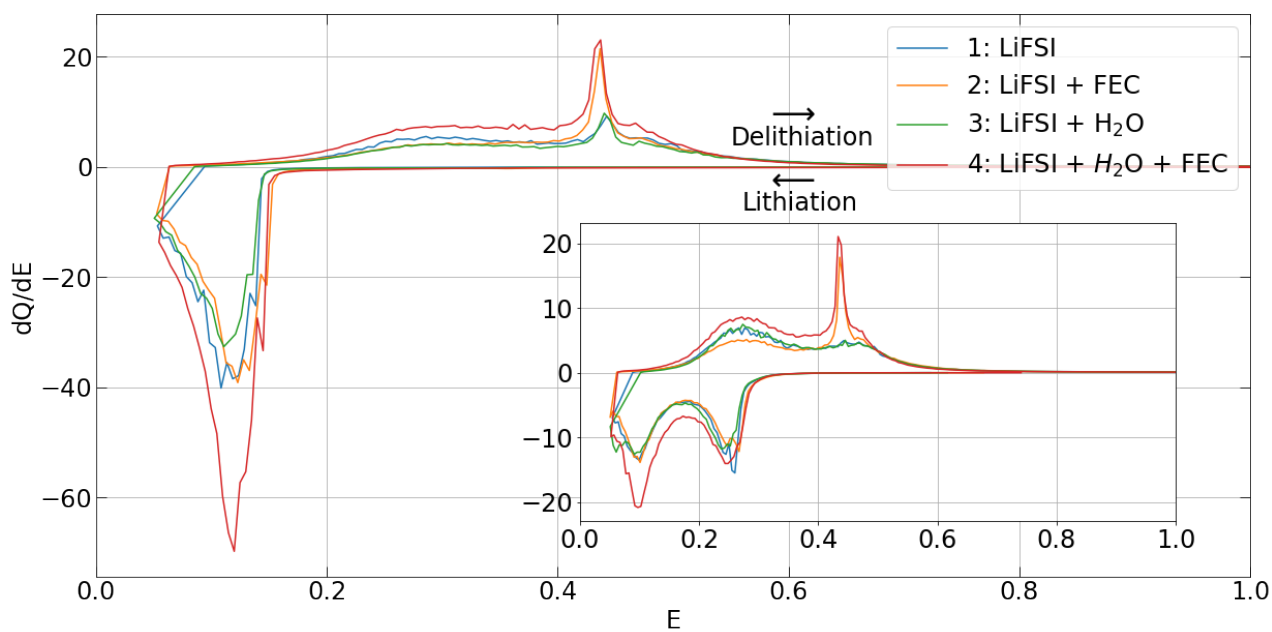
(a)
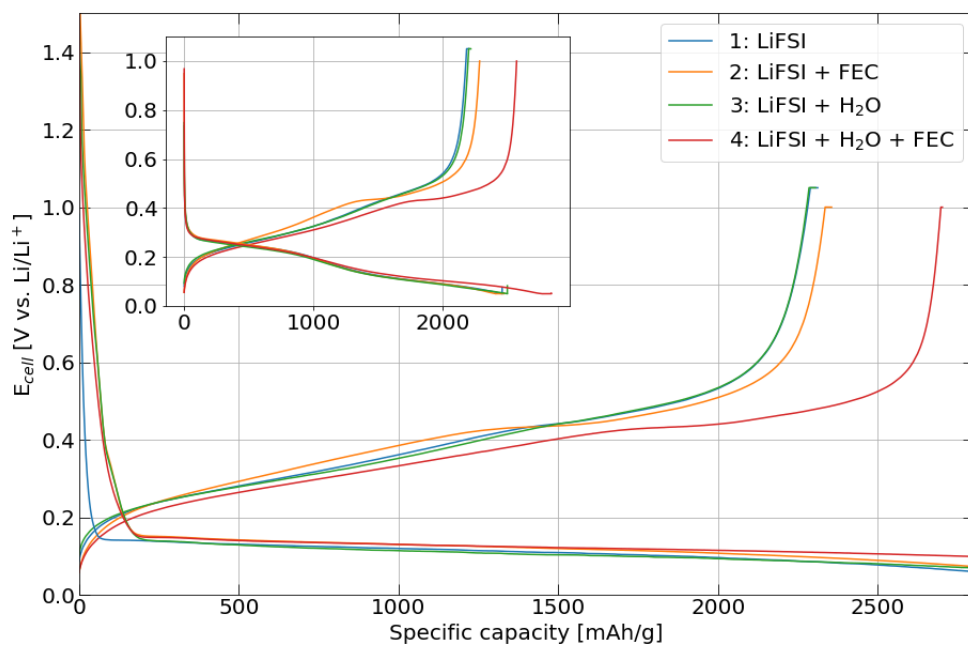
(b)

Figure 4.7: (a) Differential capacity plot and (b) corresponding potential profiles of the first and second formation cycles of the crystalline anodes with electrolytes 1-4. The second cycle is plotted in the smaller subplots.

Electrolyte	Total resistance [Ω]			
	1st EIS	2nd EIS	3rd EIS	4th EIS
1	20	9	31	8
2	7,5	9,5	11,0	13,0
3	8,2	10,6	12,1	13,2
4	7,8	8,8	9,4	10,2

Table 4.2: Approximate values of the total resistance in the cell with the four electrolytes described in table 3.2. The impedance was measured 4 times.

4.3   Post mortem characterisation

4.3.1   SEM images and EDS analysis of the SEI layers and surface of the anodes

Half cells with anodes based on the crystalline powder were cycled for 50 cycles in addition to the two formation cycles before being characterised by the use of an SEM. The anodes were cycled using the four electrolytes from table 3.2. Figure 4.9 shows the anodes at a magnification of 3500x, showing the surface of the cycled anodes, in addition to an uncycled silicon anode. The figures show the SEI layer and the cracks formed upon cycling. The scale bar on the image shows 30 μm.

Figure H.1 in Appendix H shows the anodes at a 12000x magnification. The scale bar shows 5 μm. The particles and granular SEI layer can be seen in the images. The observed SEI layer in figure H.1 is similar for all electrolytes. From figure 4.9a, it can be seen that the silicon particles are of varying size and shapes. The particles are elongated and flat, which is a result of the particles being from a kerf source originating from the cutting process of silicon wafers. A rough estimate from the scale bar in the image confirms the particle size distribution from the PSD analysis, where 50 vol% of the particles were measured to have a particle diameter of approximately 0,95 μm or smaller.

The PAT-cells were assembled as full-cells with an LFP cathode as counter electrode instead of the half-cell configuration used in the coin cells. Figure 4.10 shows the electrode surfaces of the cycled anodes.

The images show less large cracks compared to the anodes used in the coin cells in figure 4.9, despite the fact that the PAT-cells were cycled for 80 cycles (as opposed to the coin cells that were cycled for 50 cycles). The magnifications used for the anodes cycled in PAT-cells are the same as the magnifications used for the coin cells (3500x), thus the scale bars are equal.

The surface morphology of the SEI layer of the anodes cycled in PAT-cells are shown in

figure H.2 in Appendix H. The observed SEI layers have the same granular morphology as the anodes used in the coin cells in figure H.1. However, the SEI layer of the cell cycled with electrolyte 3 in figure H.2c seems to be thinner, as the Si particles are more visible in this image.

In addition, surface images at a magnification of 350x were taken of the anodes cycled in PAT-cells for 80 cycles. The images show that the cracks formed on the anode cycled with electrolyte 2 are smaller than on the other anodes in figure H.3b. The cell with electrolyte 3, in figure H.3c also seems to have less cracks, and the SEI layer is not as visible.

An EDS analysis was performed on the anode surfaces to map the relative amount of the elements in the SEI layer. Figure H.4 and H.5 in Appendix H shows the Map spectra from the anodes used in coin cells and PAT-cells respectively, with the measured weight fractions of the elements. The weight fractions of the most interesting elements, O, C, Si and F, are summarised in table 4.3. For the cell with electrolyte 3, the results from the EDS stands out from the other results, as the weight fraction of C was not listed, and the weight fraction of O was much higher than for the other cells. However, in figure H.5c, the spectrum from the analysis of the anode cycled with electrolyte 3, shows the ratio between C, Si and O, which shows a higher signal from Si than C, indicating that more Si than C is detected by the analysis.

Table 4.3: Weight fractions of the elements observed from the map spectra from the EDS analysis of the SEI layer on the crystalline anodes cycled in electrolytes 1, 2, 3 and 4.

| | Element | Electrolytes [wt.%] | | | |
		1	2	3	4
Coin cells	O	12,3	11,4	12,8	10,9
	C	6,9	9,1	6,7	6,3
	Si	3,9	5,0	3,1	1,9
	F	1,2	1,3	1,1	1,2
PAT- cells	O	10,9	7,3	84,6	8,3
	C	6,1	5,5	-	4,6
	Si	2,4	5,9	9,0	5,0
	F	1,0	4,0	6,1	1,2

Figure H.4 and table 4.3 shows that the difference in weight fractions of F for the different electrodes used in the coin cells is negligible. The weight fractions of Si and C are larger for the electrode cycled with electrolyte 2 (figure H.4b), in addition to the ratio of C and O being larger compared to the other map spectra. For the electrode cycled with electrolyte 4 in a coin cell, the weight fraction of Si is lower compared to the other spectra.

4.3.2   FTIR analysis of the SEI layers

The absorbance spectra of four anodes cycled in coin cells with the four electrolytes used in this thesis (see table 3.2), are shown in figure 4.11. The spectrum of an uncycled anode is subtracted from the spectra in order to see the peaks corresponding to the different SEI layers formed with the different electrolytes. The peaks are marked with grey, dashed lines with descriptions of possible corresponding compounds. Figure A.1 in appendix A shows the spectra of the four anodes without subtracting the uncycled anode, in addition to the spectrum of the uncycled anode. The spectrum of the anode cycled with electrode 1 (no additives, only LiFSI) is subtracted from the three other spectra in figure 4.12 to show only the peaks corresponding to FEC, H_2O, and FEC and H_2O combined. The dotted black lines show the baselines of the spectra. Negative peaks indicate that the corresponding compound is not present in the SEI layer for the respective additive, or that the intensity is larger on the anode cycled with electrolyte 1. Positive peaks indicate a higher intensity for the compound in the SEI layer for the respective additive than in the SEI layer for the anode cycled with electrolyte 1, or that the compound is not present in the SEI layer of electrolyte 1 at all. The spectra has been scaled up compared to the spectra in figure 4.11 in order to better show the peaks.

All four spectra contains peaks from $ROCO_2Li$, Li_2CO_3, polycarbonates, O_ySiH_x-deformation and solid EC and bending vibration from the EC ring.

From figure 4.12 it can be seen that the intensities of the peaks corresponding to $ROCO_2Li$ are both slightly negative and slightly positive for the spectrum of FEC, indicating that the difference in $ROCO_2Li$ content is similar for electrolytes 1 (no additive) and 2 (FEC). The same can be said for the peaks corresponding to polycarbonates. For Li_2CO_3 one of the peaks is slightly shifted towards lower wavenumbers compared to for the other electrolytes, while the other peak has a high intensity. The peaks corresponding to EC have a slightly positive intensity for the anode cycled with electrolyte 2. The spectrum from electrolyte 2 differs from the spectra from the other electrolytes as the SEI layer from electrolyte 2 does not seem to contain Li_2O. No peak is observed in figure 4.11, and a negative intensity at the corresponding wavenumber is observed in figure 4.12.

For the anode cycled with electrolyte 3 (H_2O), the spectrum is very similar to that of electrolyte 1. This can be seen in figure 4.12 as the peaks corresponding to the SEI-compounds originating from adding H_2O has low intensities. Slightly positive peaks corresponding to Li_2CO_3 and Li_2O suggest a higher amount of these molecules with H_2O present in the electrolyte. While the peaks corresponding to the polycarbonates are slightly negative. There are no peaks present in the spectrum for electrolyte 3 in figure 4.11 that are not present in any of the other spectra.

What can be observed for the spectrum of the cell cycled with electrolyte 4 is that the intensity is higher for most of the peaks compared to the other spectra. The spectrum for electrolyte 4 is similar to the spectra for electrolytes 1 and 3 with all the same peaks, only with slightly higher intensities. The peak for Li_2O is present in the spectrum for electrolyte 4, as opposed to for electrolyte 2. But from figure 4.12 is can be observed that the peak has disappeared when the spectrum for electrolyte 1 is subtracted, indicating a similar signal from Li_2O in the SEI layers from the two electrolytes.
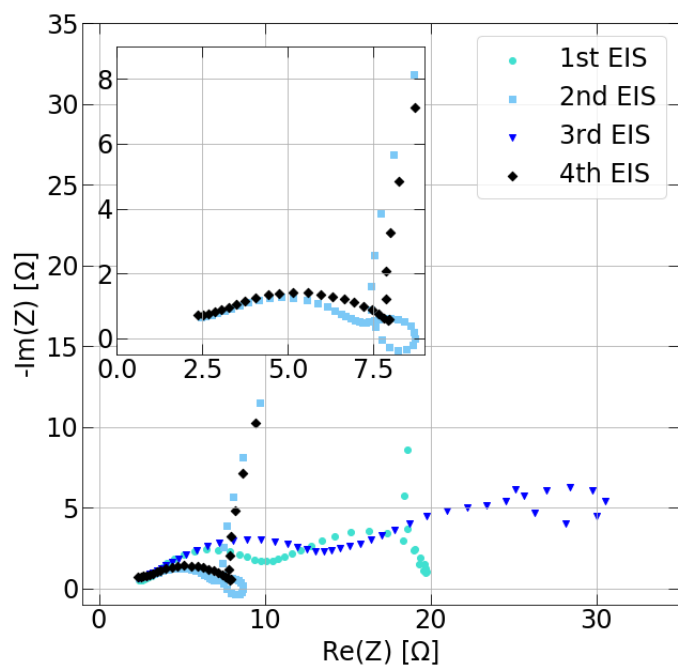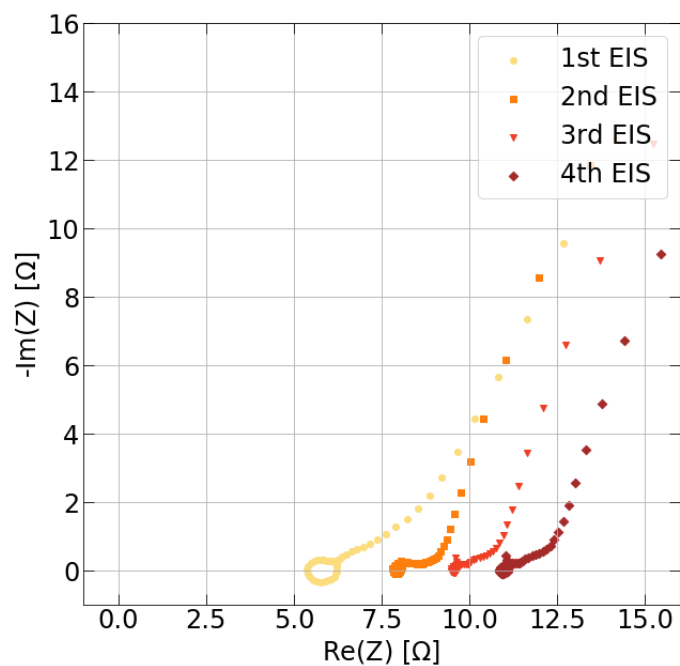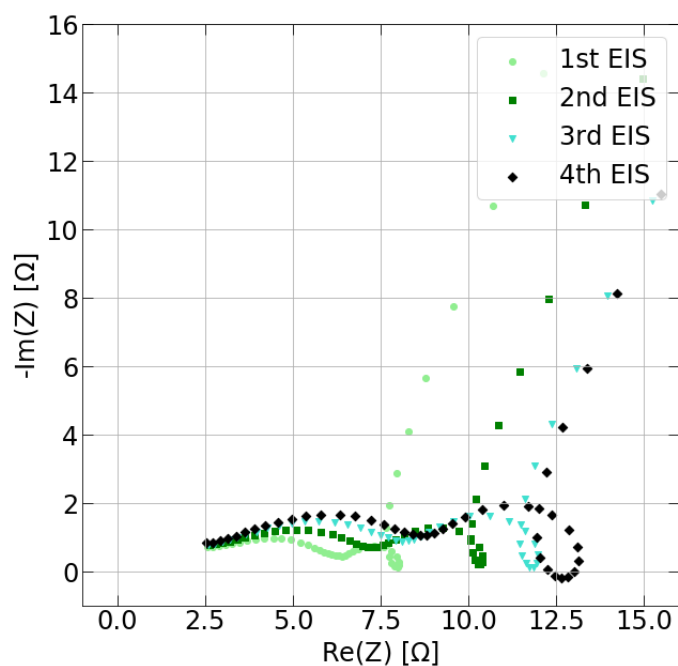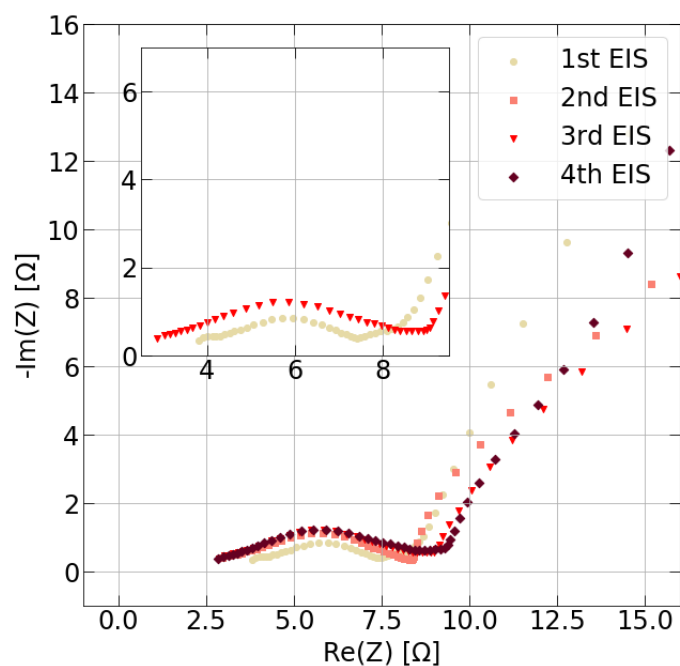
Figure 4.8: Nyquist plots showing the impedance measurements of (a) electrolyte 1 (LiFSI, no additive), (b) electrolyte 2 (LiFSI and FEC), electrolyte 3 (LiFSI and H_2O) and electrolyte 4 (LiFSI, FEC and H2O).

(a)

(b)

(c)

(d)

(e)
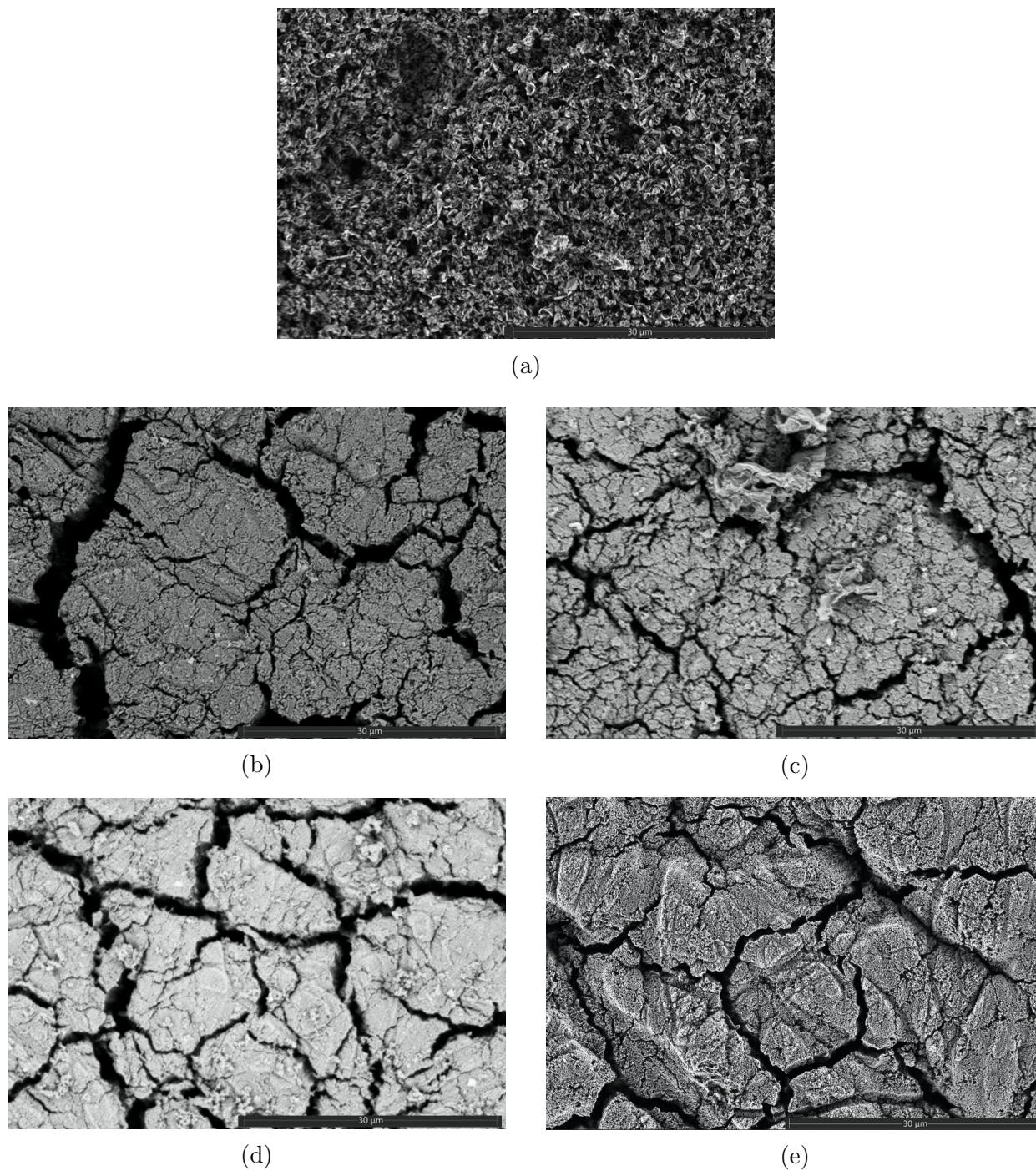
Figure 4.9: SEM images showing the surface of (a) an uncycled anode and the anodes cycled in the coin cells made using crystalline silicon powder and (b) electrolyte 1 (no additives), (c) electrolyte 2 (FEC), (d) electrolyte 3 (H_2O) and (e) electrolyte 4 (FEC and H_2O). The SEI layer and cracks formed upon cycling can be seen in all anodes.

(a)

(b)

(c)

(d)
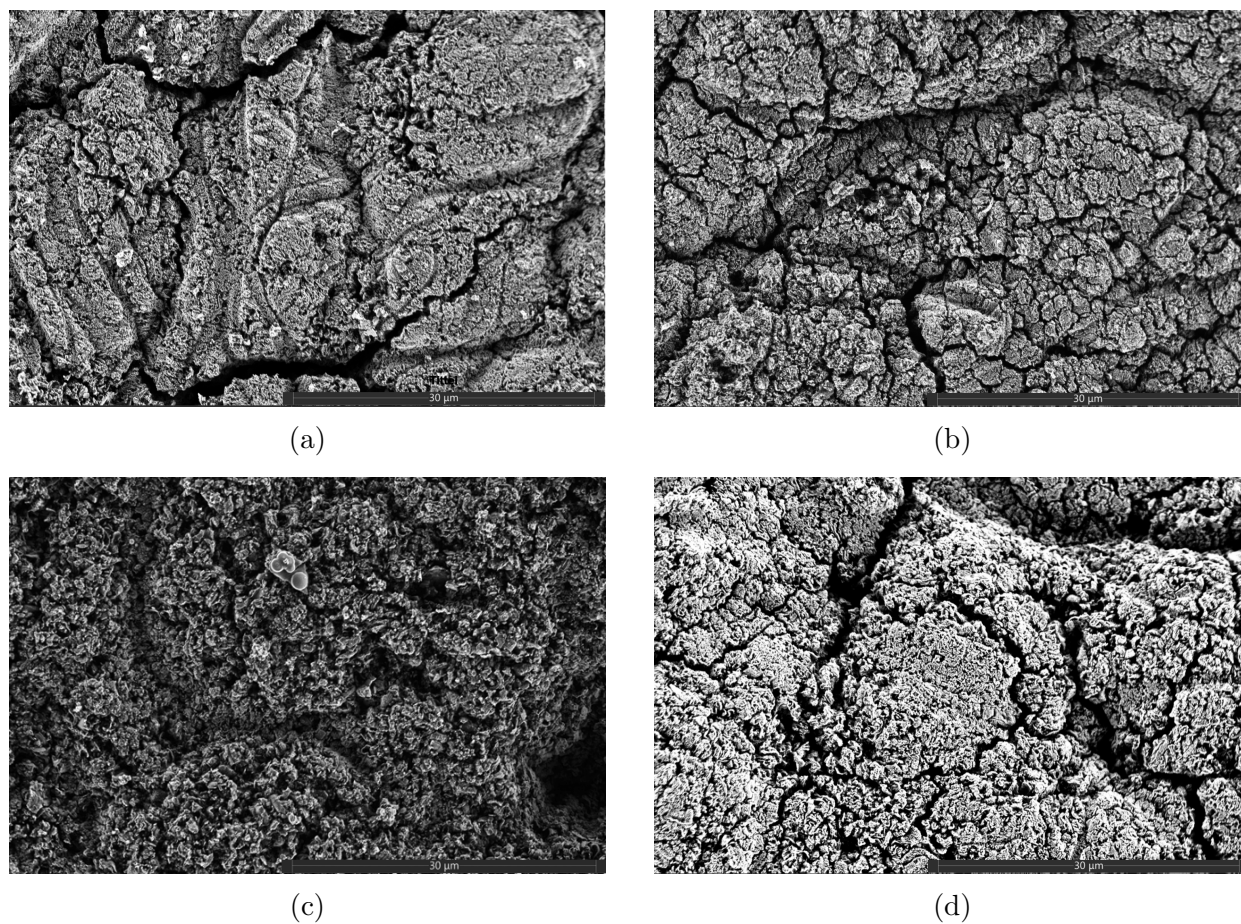
Figure 4.10: SEM images showing (a) an uncycled anode, and anodes, made with crystalline Si powder, cycled in PAT-cells with (b) electrolyte 1 (no additives), (c) electrolyte 2 (FEC), (d) electrolyte 3 (H_2O) and (e) electrolyte 4 (FEC and H_2O)
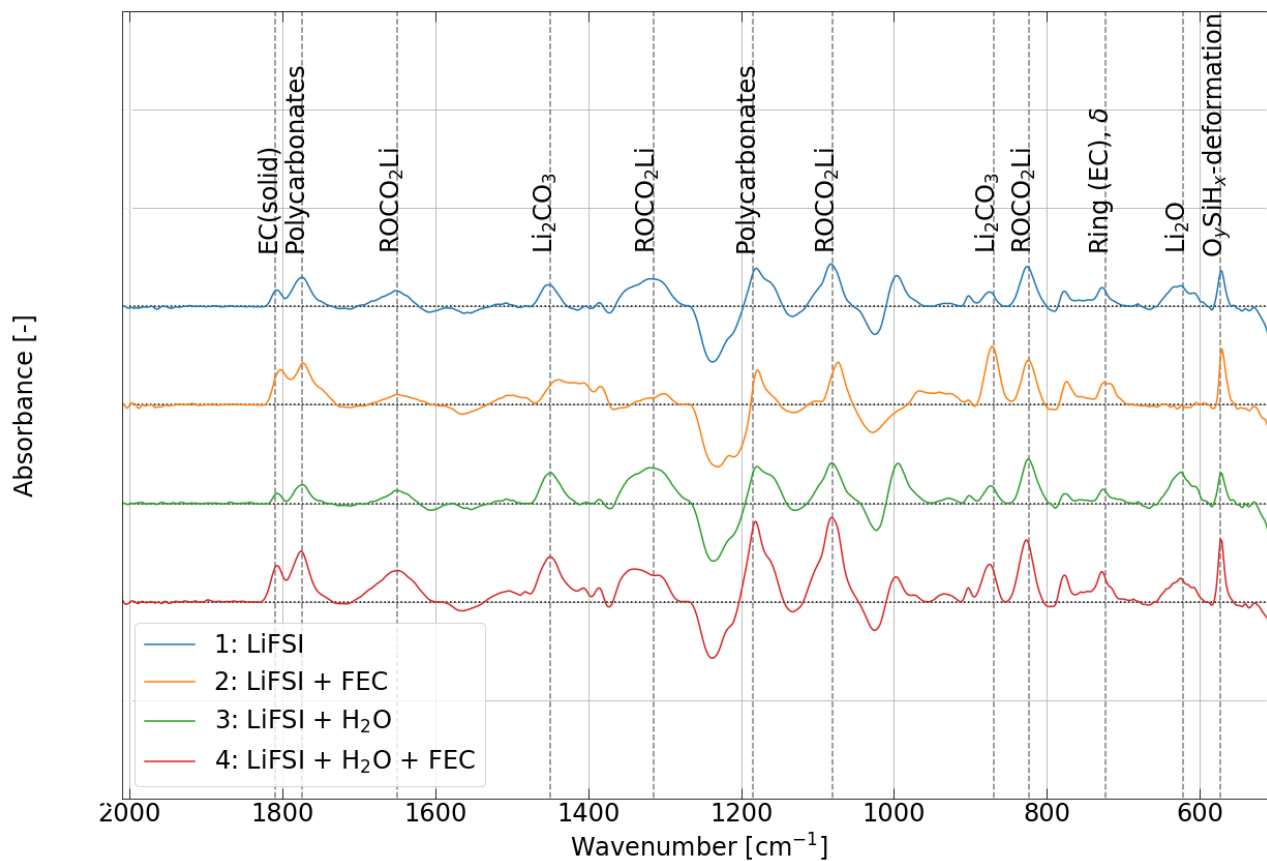
Figure 4.11: Absorbance spectra from the FTIR analysis of the SEI-layers from the four different electrolytes used in this thesis (see table 3.2). The peaks are marked with grey, dashed lines with the possible corresponding compound. The spectra from the SEI-layers are obtained by subtracting the spectrum of an uncycled pristine electrode from the spectra of the anodes.
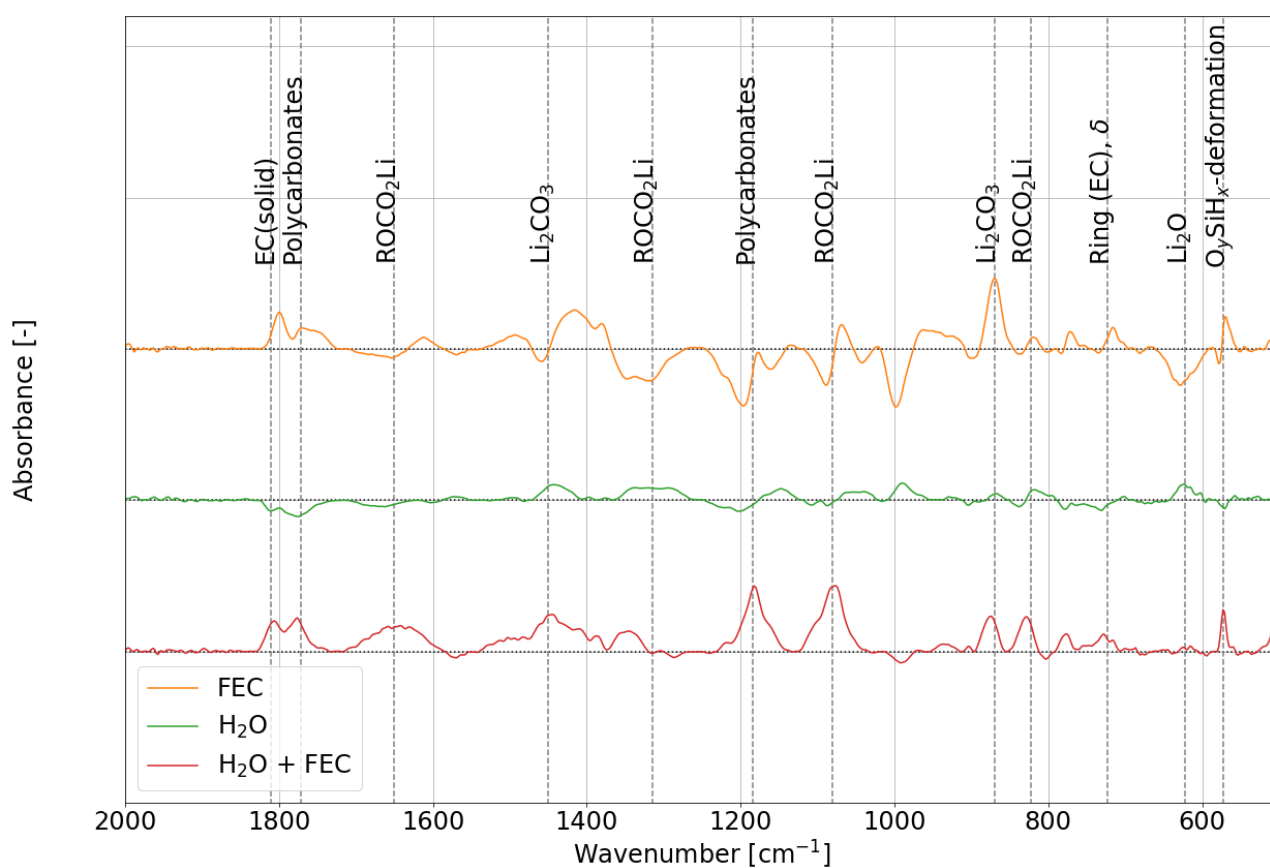
Figure 4.12: The spectrum of the anode with electrolyte 1 (no additives) was subtracted from the spectra of the anodes with the other three electrolytes, in order to obtain the spectra of the additives FEC and H_2O and of FEC and H_2O together.

5 Discussion

5.1 Amorphous vs. crystalline silicon powder

The capacities of the anodes made from amorphous and crystalline silicon powder are shown in figures 4.3a and 4.4a respectively, with large variation in performance for several measurements, possibly due to agglomeration of the Si particles or varying loading on the anodes. The variation in performance is large for almost all Si powder and electrolyte combinations. One explanation could be differences in loading of active material on the anodes. The target loading was 0,4 mg/cm^2, but the loading of the anodes varied from approximately 0,32-0,46 mg/cm^2. Higher loading gives a thicker anode, thus the diffusion length for Li$^+$ is longer which results in a lower capacity. For instance, for the amorphous anodes cycled with electrolyte 2, the anode with the lower loading gave a higher capacity compared to the other anode. Only two cells were used to determine the mean capacity of the cells with electrolyte 2 and amorphous anodes due to time constrains. Another reason can be uneven distribution of silicon in the anodes. The PSD of the amorphous Si powder in figure 4.1a shows that the powder is prone to agglomeration. And although figure 4.1b indicates no agglomeration for the crystalline Si powder, it is possible that the mixing program of the silicon slurry is not sufficient to break agglomerates for either of the powders. Agglomeration in the silicon anodes could lead to uneven distribution of the silicon, thus causing varying capacity and conductivity of the anode.

Figures 4.3a and 4.4a shows that the anodes made with crystalline silicon powder outperforms the anodes made with amorphous silicon powder, both with respect to the capacity and stability. Thus, the crystalline anodes were further used to study the effect of FEC and H$_2$O as additives.

The anodes cycled with electrolytes 2 and 4 showed a higher stability, compared to the anodes used by Asheim et al.[25] and Rogstad et al.,[16] due to lower initial capacity, thus smaller volume changes. As mentioned in section 2.4.2, Asheim et al.,[25] reported an initial capacity of 2700 mAh/g with a 45% capacity decrease after 100 cycles with anodes with 60 wt.% Si. While Rogstad et al.[16] reported an initial capacity of 3000 mAh/g with a 75% reduction after 100 cycles with 73,2 wt.% Si. An increased Si amount could increase the capacity, but high initial capacity reduce the stability as it allows for more extensive cracking. The electrolytes used in this project that are most comparable to the electrolytes used by Asheim[25] and Rogstad[16] is electrolyte 2 with FEC, and electrolyte 4 with FEC and H$_2$O. The capacities of the anodes used in this thesis were lower than those obtained by Asheim[25] and Rogstad.[16] However, with a capacity reduction of 46% and 40% for the crystalline anodes with electrolyte 2 and 4 respectively, the stability of the anodes made

with 75 wt.% silicon powder from ReSiTec was better compared to the anodes used by Asheim[25] and Rogstad.[16] The increased stability of the anodes used in this thesis compared to those of Asheim[25] and Rogstad[16] can be explained by the lower initial capacity, which again cause less extensive volume changes.

5.2   The effect of FEC

5.2.1   Electrochemical measurements

From figure 4.4a it is clear that the cycling performance of the anodes cycled as half-cells, is drastically improved by the addition of FEC in the electrolyte, with higher capacity for all cycles compared to the electrolyte with no additives. The capacity of the anodes with electrolyte 2 decreased with approximately 48% as opposed to 52% for the anodes cycled with electrolyte 1. The difference in stability is small after 100 cycles, but a slight improvement by the addition of FEC is observed.

The results from the anodes cycled in PAT-cells showed an improved cycling performance upon the addition of FEC. Silicon anodes and LFP cathodes were assembled in PAT-cells. LFP cathodes were used to avoid the influence of lithium metal as counter electrode. The cell with electrolyte 2 displayed higher capacities than the cell with electrolyte 1. The capacity reduction of the anode with electrolyte was just 15%, as opposed to 87% for the anode with electrolyte 1. The difference in stability was much larger then what was observed for the half cells. This could be due to the unstable nature of the lithium metal used as counter electrode in coin cells, or that FEC might react differently with lithium metal than with LFP. The results from the PAT-cells only stems from one cell with each electrolyte, which is insufficient data to draw any conclusions. But the plot clearly shows the same trend as for the coin cells, which is that FEC is essential to improve the cycling performance of silicon anodes with a LiFSI-based electrolyte.

Schroder et al.[33] and Jauman et al.[23] tested the effect of 10 wt.% FEC in a LiPF$_6$-based electrolyte with amorphous nano-silicon anodes and composites made of nanostructured silicon/carbon respectively. Etacheri et al.[32] tested the effect of 3 wt.% FEC in a LiPF$_6$-based electrolyte with micro-silicon anodes. For all three cases, FEC increased the stability of the anodes. The results obtained with Schroder,[33] Jauman[23] and Etacheri[32] shows the same trend as observed in this thesis, namely increased stability with the addition of FEC in the electrolyte. Thus, the results demonstrate that FEC creates a passivating SEI layer that increase the stability of silicon anodes regardless of the type of silicon particles used and with another lithium salt in the electrolyte.

The efficiency of the anodes with electrolyte 1 decreased rapidly before stabilising, but the

efficiency of the anodes with electrolyte 2 continued to decrease below electrolyte 1 after 50 cycles, possibly due to the higher capacity causing larger volume expansions and electrolyte consumption. Figure 4.4b shows that the mean efficiency obtained with electrolyte 2 was higher compared to for the anodes cycled with electrolyte 1 for approximately the first 50 cycles. The efficiency of the anodes with electrolyte 2 continued to decrease slowly for the remaining cycles before stabilising at a slightly lower value than for electrolyte 1. One explanation for the continued efficiency decrease could be the higher capacity of the anodes with electrolyte 2 compared to with electrolyte 1. This cause larger volume expansions, thus more cracking and electrolyte consumption for the anodes with electrolyte 2 at higher cycle numbers, resulting in a slightly lower efficiency.

It should be mentioned that a half-cell configuration is not sufficient to properly study the effect of the electrolyte on the Coulombic efficiency, as lithium is continuously provided by the lithium counter electrode. Hence, it would be imperative to study the effect of additives on the Coulombic efficiency using coin cells in a full-cell configuration.

The impedance was measured in PAT-cells with silicon anodes, LFP counter electrodes and the four different electrolytes. The Nyquist plots from the measurements are shown in figure 4.8 and the total resistances are summarised in table 4.2. The EIS measurements performed on the cell with electrolyte 1, in figure 4.8a, showed an unexpected trend. One would expect increasing resistance in the cell with increasing amounts of cycles, but this is not observed for the cell with electrolyte 1. The reason for this behaviour could be an instrument artifact or the measurements could have been performed at different states of charge.

The impedance measurements of the PAT-cell with electrolyte 2 showed that the addition of FEC caused a lower total electrode resistance. The total resistance increased after increasing amounts of charge/discharge cycles. The loops observed for all four measurements in figure 4.8b resembles the loops observed in the Nyquist plots of cells with electrolytes 1 and 3. Hence, the observed loops at the higher frequency range for the measurements with electrolyte 2 could be representing parts of a semicircle. There is an indication of a second semicircle past the loops in the EIS spectra from the anode with electrolyte 2. These semicircles were used as the basis of the total resistance. However, if the loops represent the end of the semicircles, as seen for electrolytes 1 and 3, the total resistance would be slightly lower then what is reported in table 4.2.

Regarding the lithiation and delithiation potential, a marginally lower lithiation potential was observed with electrolyte 1 compared to electrolyte 2, indicating that electrolyte 1 requires a higher overpotential. However, the difference is insignificant and it seems like the lithiation and delithiation potentials are controlled by the lithium salt, LiFSI.

5.2.2   Characterisation of SEI layers formed with FEC as an additive using SEM

By comparing the uncycled anode to the cycled anodes in figure H.1 in Appendix H, it is clear that a granular SEI layer has formed on all four anodes. The granular morphology of the SEI layer was also observed in the SEM-images used in Karina Asheim's doctoral thesis.[12] No significant difference is observed in the surface morphology of the SEI formed by addition of FEC in the electrolyte, in figure H.1c, compared to the SEI formed with no additives in the electrolyte.

The improved cycling performance of the anodes cycled with FEC in the electrolyte might be due to the thinner SEI layer with smaller cracks in the anode surface seen in figure 4.9c, as opposed to the larger cracks observed for electrolyte 1. The reason for this could be that a thinner SEI layer is formed with FEC in the electrolyte, as the SEI layer from the other electrolytes appears to be slightly more continuous.

Less cracks were detected on the anodes cycled in PAT-cells, but the same trend with smaller cracks on the anode with electrolyte 2 was observed, indicating a thinner SEI. The anodes used in PAT-cells were examined by the use of an SEM to investigate if an LFP counter electrode affects the anodes differently compared to lithium foil as counter electrode. From figure H.2 in Appendix H, the SEI layer formed in the PAT-cells seems to be similar to the SEI formed in the coin cells. By comparing figures 4.9 and 4.10, which shows the surfaces of the coin cells and PAT-cells respectively, the cracking of the anode surface is less prominent for the PAT-cells. This might also be local variations of the surfaces. Figure 4.10b shows the same trend in the PAT-cell as in the coin cell, with smaller cracks for the cell with electrolyte 2. This is especially clear in figure H.3 where the surfaces of the PAT-cells were imaged at lower magnifications. The cracks in the surface of the cell cycled with electrolyte 2 are smaller than the cracks in the other cells. This could explain the high stability with FEC in the electrolyte.

The EDS analysis implied a thinner SEI layer and higher F content in the SEI, which indicates higher LiF levels, on the anodes cycled in PAT-cells with electrolyte 2. From the EDS analysis, the relative amounts of the different elements on the surface of the anode were observed and summarised in table 4.3. The EDS spectra for the PAT-cells are shown in figure H.5 in Appendix H. The difference in F content is more significant for the PAT-cells as opposed to for the coin cells. Table 4.3 shows that higher amounts of F is observed for the cell cycled with electrolyte 2 compared to the other electrolytes. The higher F content stems from the fluoride in FEC, and can indicate a higher LiF level in the SEI. The Si content is higher for electrolyte 2 compared to electrolyte 1, indicating a thinner SEI layer when FEC is added to the electrolyte. Thinner SEI layers imply a more flexible and passivating layer, thus explains the improved cycling performance.

5.2.3   Characterisation of SEI layers formed with FEC as an additive using ATR-FTIR

The ATR-FTIR analysis of the anodes showed similar spectra for the SEI layers, but Li_2O was not detected in the SEI layer formed by electrolyte 2, possibly due to surface passivation caused by FEC before Li_2O was formed. According to Wang's theory on reduced ductility with Li_2O,[30] the increased effect on cycling performance from FEC might be due to the absence of Li_2O. There is no clear reason as to why no Li_2O is formed with FEC as an additive, but it might be due to other reactions preventing the formation of Li_2O. According to the reactions in equation 2.15,[26] SO_2 formed from the reduction of LiFSI, reacts with Li^+ and forms $Li_2S_2O_4$ that further reacts with Li^+ to form Li_2O. Thus, the formation of Li_2O occurs in two steps. As FEC is reduced at higher potentials, it could be that the reduction products from FEC passivates the surface before Li_2O can be formed. Another explanation could be that FEC reacts with trace amounts of H_2O in the electrolyte and forms HF. Philippe et al.[34] showed that HF will etch away species in the SEI layer, including Li_2O. Hence, it might be that the absence of Li_2O is due to HF formed with FEC and H_2O. LiF is not IR active and cannot be detected by an FTIR analysis. But it has been proposed that adding FEC to the electrolyte will cause formation of a LiF-rich SEI layer. Hence, the lack of Li_2O in the SEI formed by electrolyte 2 may indicate that Li_xSi is bound to LiF instead of Li_2O, causing a more ductile SEI that improves the cycling performance of the cells. However, the research done by Wang was entirely theoretic and based on an ideal system, so the effect on Li_2O in a real system is not clear.

Larger amounts of polycarbonates and Li_2CO_3 were observed in the SEI upon addition of FEC, which can explain the enhanced cycling performance. Figure 4.12 shows that one of the peaks of Li_2CO_3 in the spectrum corresponding to FEC at approximately 1470 cm^{-1} is slightly shifted towards lower wavenumbers compared to for the other additives, but overall, an increased amount of Li_2CO_3 is observed with FEC. The same goes for one of the peaks for polycarbonates at approximately 1180 cm^{-1}. FEC has shown to form more polycarbonates in the SEI layer with passivating properties. The intensity of one of the peaks for polycarbonates was positive for the spectrum corresponding to FEC in figure 4.12, thus the addition of FEC has resulted in slightly larger amounts of polycarbonates. The increased amounts of polycarbonates that forms a passivating SEI explains the enhanced cycling performance. An increased amount of Li_2CO_3 could, together with LiF, form conductive paths at the grain boundaries, which is also a theory used to explain the increased performance of silicon anodes with FEC as an additive.

5.3   The effect of water

5.3.1   Electrochemical measurements

Figure 4.4a shows that both the capacity and stability of the silicon anodes decreased with 1000 ppm H_2O as an additive in the electrolyte, compared to for the anodes cycled with no additive in the electrolyte. The anodes with electrolyte 3 experienced a capacity reduction of approximately 61%, while the capacity of the anodes with electrolyte 1 decreased approximately 52%. Although, from figure 4.4a it is clear that at there is a large variance in performance for the cells with electrolyte 3, and of the cells did perform similarly to the cells with electrolyte 1, but the mean capacity illustrate that adding H_2O to the electrolyte will reduce the cycling performance.

As for the PAT-cells, figure 4.5 shows that the anode paired with electrolyte 1 displayed a higher capacity than the anode with electrolyte 3 for the first 40 cycles. Then, after the second impedance measurement, the anodes with electrolytes 1 and 3 obtained the same capacity for the remaining cycles. The capacity reduction of the anodes were 87% and 86% for electrolytes 1 and 3 respectively, which is a large reduction in capacity, but the difference between the two electrolytes is insignificant.

Young et al.[3] claimed that the addition of 1000 ppm H_2O in a $LiPF_6$-based electrolyte would cause continuous formation of CO_2, which would have enhancing properties on the cycling performance of silicon anodes. However, the results obtained in this thesis shows the opposite results. Young used the lithium salt $LiPF_6$, which has shown to hydrolyse and form HF which cause detrimental side reactions on the silicon anode.[24] While LiFSI does not hydrolyse, thus does not form HF.[35] Hence, one would assume that adding water to a $LiPF_6$-based electrolyte would reduce the performance of the silicon anode and that a LiFSI-based electrolyte would tolerate the water addition better. However, it might be that in a LiFSI-based electrolyte the water reacts differently inside the cell compared to with a $LiPF_6$-based electrolyte, forming other species rather than CO_2, therefore not obtaining the enhanced effect on the cycling properties.

As for the Coulombic efficiency shown in figure 4.4b the efficiencies obtained with electrolytes 1 and 3 are similar for all cycles, although after approximately 25 cycles, the mean efficiency is marginally higher for the anodes with water in the electrolyte. The anodes cycled with electrolyte 1 showed higher capacity than the anodes cycled with electrolyte 3, indicating that the volume expansions would be larger for the anodes with electrolyte 1, which cause more cracking of the SEI layer, thus lower efficiency.

The charge used for splitting of the H_2O molecules was calculated to be 8 and 19 mAh per gram of active material in the anodes used in coin cells and PAT-cells respectively, for

electrolyte 3. The calculations are shown in Appendix E. The amounts of charge used for water splitting is insignificant compared to the charge stored in the anodes, thus the water splitting should not affect the efficiency to a noticeable extent.

The total resistance in the cell is shown in table 4.2. A higher resistance was obtained with water in the electrolyte for the 2nd and 4th impedance measurement, compared to for the cells with electrolyte 1, and the resistances obtained are larger compared to the anode cycled with electrolyte 2, but the difference is small for the forth measurement. Hence, the results implies that addition of water slightly increase the resistance.

The electrolyte resistance seems to be quite similar for the four EIS measurements for electrolyte 3. The resistance in the electrolyte can be read from the Nyquist plot as the intersection between the semi circle at the highest frequencies (lower Re(Z) values) and -Im(Z)=0. From the Nyquist plot of the EIS measurements, in figure 4.8, it seems like the cell obtain the same electrolyte resistance for each measurement, indicating that the electrolyte resistance and the resistance through the separator remains unchanged. Thus, the increase in total resistance originate from changes in the SEI layer and available surface area.

The lithiation and delithiation potentials of the anodes cycled with electrolytes 1 and 3 are identical for the first two cycles, which can be seen in figure 4.7. The peaks in the differential capacity plot in figure 4.7a are situated at the same potentials and the corresponding potential profiles in figure 4.7b are close to identical. Thus, it seems like water in the electrolyte has no effect on the lithiation and delithiation potentials of silicon anodes.

5.3.2 Characterisation of SEI layers formed with H_2O as an additive using SEM

Figure 4.9 shows the SEM images of the surface of the anodes cycled in coin cells. By comparing the image of the anode cycled with electrolyte 1 in figure 4.9b with the anode cycled with electrolyte 3 in figure 4.9d, it seems like more cracks are observed on the anode cycled with electrolyte 3, while larger cracks are observed in the anode cycled with electrolyte 1. However, the difference is not distinct and could also be a result of local variations on the sample surface. No clear difference can be observed in figure H.1 in Appendix H either. Although, possible agglomerates of SEI layer might be observed in figure H.1d which would imply an uneven SEI formation.

For the anodes cycled in PAT-cells, the images of the anode cycled with electrolyte 3 differs from the other anodes. The SEM image of the SEI layer on the anode paired with electrolyte 3 in figure H.2c, and the image of the surface in figure 4.10c indicates that a thinner SEI layer has been formed with this electrolyte, as the Si particles are more visible for these images. In

addition, figure H.3c shows that less cracking has occurred. The same agglomerates might be observed in figure H.2c as for the anode cycled in a coin cell in figure H.1d, however, the agglomerates could also be carbon black covered with an SEI layer.

The weight fractions of the different elements detected by the EDS analysis, on the surface of the anodes cycled in coin cells and PAT-cells are shown in table 4.3 and in figures H.4 and H.5. The weight fraction of Si is similar for the anodes cycled in coin cells with electrolytes 1 and 3, implying that the SEI layers are of approximately the same thickness. While for the anodes cycled in a PAT-cells, the difference is more significant. However, the values for the weight fractions of the elements observed on the anode paired with electrolyte 3 stands out from the other cells, especially with the high weight fraction of oxygen. This might be due to different settings on the EDS software, as the measurements were performed on different days. Nevertheless, figure H.4c shows the spectrum of the anode obtained from the EDS analysis, and the signal ratio between silicon and oxygen is larger for the anode cycled with electrolyte 3 compared to with electrolyte 1 in figure H.4a. This possibly implies that more Si was detected from the anode cycled with electrolyte 3, which means that a thinner SEI layer was formed. This corresponds to the SEI layers observed in the SEM images. One would assume that a thinner SEI layer would cause a better cycling performance, but this is not the case here. The reason for the thin SEI layer could be that the lithium reference electrode used in the PAT-cell was unstable, or that the SEI layer is unevenly distributed on the anode as a result of addition of water. Poor passivation of the anode surface would explain the reduced cycling performance.

5.3.3   Characterisation of SEI layers formed with H_2O as an additive using ATR-FTIR

Figure 4.11 shows that a peak corresponding to Li_2O was observed in the SEI layers formed by electrolytes 1 and 3. According to reaction 2.20 and 2.21, an increased amount of Li_2O would be expected with water in the electrolyte. This is confirmed in figure 4.12 where more Li_2O is detected in electrolyte 3 compared to electrolyte 1. The reduced cycling performance of the anodes paired with electrolyte 3 could be explained by the increased amount of Li_2O causing a less ductile SEI, if the DFT calculations done by Wang et al.[30] also applies to a non-ideal system.

An increased amount of Li_2CO_3 and $ROCO_2Li$ was observed in the SEI layer from electrolyte 3, but less polycarbonates were formed, which might imply that a less passivating SEI layer has been formed, explaining the reduced cycling property of electrolyte 3. Figure 4.12 shows that the SEI-layer from electrolyte 3 contains more Li_2CO_3 than the SEI-layer from electrolyte 1. The signal from EC in figure 4.12 is lower for electrolyte 3 than electrolyte 1, which indicates more EC decomposition in electrolyte 3 compared to electrolyte 1. As

claimed by Young et al. OH^-, which is a product from the water splitting occurring in the cell, will react with EC and form CO_2 and polycarbonates, according to equation 2.18. CO_2 reacts further to form Li_2CO_3 according to reaction 2.19. However, the results form the FTIR analysis of electrolyte 3 does not seem to confirm that more polycarbonates has been formed with H_2O. An increased amount of Li_2CO_3 in the SEI could form conductive paths if LiF is present as well. But without FEC, less LiF will be formed due to less F in the electrolyte. Hence, the effect of more Li_2CO_3 in the SEI layer is not clear. The inner inorganic layer is not as passivating as the flexible organic outer layer of the SEI, thus if less polycarbonates are formed in the outer layer, a less passivating SEI might have been formed with electrolyte 3 which explains the poor cycling performance.

5.4 The effect of FEC and water

5.4.1 Electrochemical measurements

Figure 4.4a shows that the same enhanced cycling performance of silicon cells were observed with the addition of both FEC and 1000 ppm H_2O, as for the anodes with just FEC in the electrolyte. The same trend is observed in figure 4.5, for the anodes cycled in PAT-cells. This suggests that FEC improves the cycling performance of silicon anodes and is required to form a passivating SEI, but that the anode tolerates H_2O in the electrolyte, both in half-cell and full-cell configurations, due to the non hydrolysing properties of LiFSI. However, a detail worth mentioning regarding electrolyte 4 is that a distinct change in color from transparent to dark brown was observed in the electrolyte after a few months. This indicates that FEC might react with H_2O, possibly forming HF. Hence, the stable nature of cells made with electrolyte 4 observed in this thesis might change over time if the remaining FEC in the electrolyte reacts with trace amounts of H_2O.

The capacity reduction of the anodes cycled with the electrolyte with just LiFSI and no additives were, as mentioned, 52% and 87% for the anodes used in half-cell and full-cell configurations, respectively. While the anodes cycled with electrolyte 4 experienced just 40% and 4% capacity reduction, respectively. Thus, the addition of FEC increase the stability of the silicon anode, also with water in the electrolyte.

The Coulombic efficiency is shown in figure 4.4b. The mean efficiency of the anodes is higher compared to the other cells for all cycles. This indicates that a good surface passivation occurred in the initial cycles, causing less electrolyte decomposition for the remaining cycles. The anodes with electrolyte 4 follows the same trend as for electrolyte 2 regarding the efficiency. However, after 88 cycles, the mean efficiency increase to values above 100%. An explanation is that instrumental artifacts has affected the measurements, or that lithium ions have been continuously trapped in the anode for several cycles, while after 80 cycles,

the trapped lithium is released, causing more charges to be released during discharge than what is consumed during charge. The error bars are large, indicating that this behaviour only occurred for one of the two cells. The lower values of the error bars implies that the other cell follows the same trend as for electrolyte 2. Thus, it is possible that if the lithium trapping does not occur, the cells with electrolyte 4 would behave like the cells with electrolyte 2 regarding the Coulombic efficiency. For the first 50 cycles, approximately, the anodes cycled with electrolyte 4 follows the same trend as for electrolyte 2, with higher efficiency compared to the anodes with electrolyte 1. However, the mean efficiency for electrolyte 4 is higher than for the other electrolytes for all cycle numbers, but one of the cells follows the same trend as for electrolyte 2, where the efficiency decrease to values below those obtained with electrolyte 1, which can be explained by higher capacity. However, the other cell experience higher efficiencies for all cycles, thus outperforming the other electrolyte combinations, before obtaining efficiencies above 100%.

The water in electrolyte 4 will split according to equation 2.16, and the required charge for the water splitting is approximately 7 and 17 mAh per gram of active material in the anodes cycled in coin cells and PAT-cells respectively. The calculations are shown in Appendix E. Again, the charge used for water splitting has an insignificant effect on the efficiency.

The impedance measurements of the anodes cycled in a PAT-cell with electrolyte 4 stands out from the measurements with just FEC or just H_2O as additives. The total resistance is comparatively lower for electrolyte 4 for the 2nd, 3rd and 4th EIS measurements. Jauman et al.[23] suggested that reduced impedance could be explained by conductive pats formed at the grain boundaries between LiF and Li_2CO_3 in the SEI layer.[23] Increased amounts of LiF is formed with the addition of FEC due to the larger amount of F in the electrolyte. Young et al.[3] claimed that water in the electrolyte would cause CO_2 formation, which again reacts with the lithium ions according to equation 2.19 to form increasing amounts of Li_2CO_3. Thus, the lower total resistance observed with electrolyte 4 could be explained by more conductive paths formed in the SEI layer, as a result of larger amounts of LiF and Li_2CO_3 formed with the additives FEC and H_2O. The electrolyte resistance seems to be unchanged for the four EIS measurements for the cell with electrolyte 4 as well, indicating that the change in resistance originates from the formation of the SEI layer and available surface area. As the increase in total resistance is smaller for electrolyte 4 compared to for the other electrolytes, a stable, passivating and flexible SEI might have been formed in the initial cycles, possible due to a flexible passivating layer of polycarbonates, which reduce the continuous SEI formation for the following cycles.

It should be mentioned that the PAT-cells with electrolytes 1, 2 and 3 were cycled in a temperature regulated room at 25°C. While the PAT-cell with electrolyte 4 was, for practical reasons, cycled in another lab with no temperature regulations. A significantly higher temperature may cause lower resistances in the cell. However, as the temperature differ-

ences presumably were insignificant, the measurements should be comparable. However, for further work, all cells should be cycled at the same temperature ensuring proper basis for comparison.

The lithiation and delithiation potentials have not been affected by the addition of FEC and H_2O in the electrolyte either, implying that the potentials are controlled by the lithium salt.

5.4.2   Characterisation of SEI layers formed with FEC and H_2O as additives using SEM

From figure 4.9, the anode cycled with electrolyte 4 seems to have less cracking than the anode cycled with electrolyte 1, which correlates with the higher efficiency observed for electrolyte 4. Due to time constraints, only two cells were cycled with electrolyte 4. Therefore, the cell used for post mortem characterisation was cycled for 100 cycles as opposed to the other cells that were cycled for 50 cycles. From table 4.3 the small weight fraction of Si implies a thicker SEI layer. Hence, it is possible that the surface of the anode in figure 4.9e would have been similar to the anode cycled with electrolyte 2, in figure 4.9c, if the characterisation was performed after the same amount of cycles. But no conclusive effect from FEC and H_2O is observed from the SEM images.

Figure 4.10 shows the surface of the anodes cycled in PAT-cells. Larger cracks are observed for electrolyte 4, but to a smaller extent than for electrolyte 1. The anode surface seems to be more continuous for the anode cycled with electrolyte 4 compared to for electrolyte 1. In figure H.3, the surface of the anodes in PAT-cells are imaged at a lower magnification. Again, fewer cracks were observed than for electrolyte 1. Hence, less cracks in the surface could explain the increased cycling performance observed with the anodes cycled with electrolyte 4.

The EDS analysis performed on the anode cycled in a PAT-cell shows that more Si was detected on the anode with electrolyte 4 than with electrolyte 1, implying a thinner SEI. The Si signal is similar to that obtained with electrolyte 2, thus it indicates that a thin and passivating SEI has been formed with electrolyte 4 as well.

5.4.3   Characterisation of SEI layers formed with FEC and H_2O as additives using ATR-FTIR

Figure 4.12 also shows that increased amounts of Li_2CO_3 is formed from electrolyte 4 compared to from electrolyte 1, which strengthens the hypothesis of increased cycling performance and reduced total resistance due to conductive paths formed on the grain boundaries

with LiF in the SEI layer. The good cycling performance of the anodes with electrolyte 4 is also explained by the increades amount of polycarbonates. The FTIR analysis showed that a larger amount of polycarbonates were formed with FEC and water as additives, resulting in a passivating and flexible outer layer of the SEI, thus an enhanced cycling performance of the silicon anodes.

In figure 4.12 similar amounts of Li_2O is observed in the SEI formed by electrolytes 1 and 4 despite the H_2O addition. With the same amount of H_2O as for electrolyte 3, one could expect larger amounts of Li_2O from electrolyte 4 compared to electrolyte 1, or as the same amount of FEC as for electrolyte 2 is added, one could expect that FEC would prevent the formation of Li_2O. One explanation could be that the H_2O in the electrolyte has caused the formation of some Li_2O, but the formation has been restricted due to the FEC. The cyclability of the anodes with electrolyte 4 was similar to electrolyte 2. Hence, given that Wang's calculations apply also for a non-ideal system, one would assume that FEC forms more LiF that bonds to Li_xSi instead of Li_2O, forming the same ductile SEI as for electrolyte 2.

6   Conclusion

The aim of this thesis was to investigate if H_2O can replace FEC as an additive in a LiFSI-based electrolyte with a silicon anode, with respect to the cycling performance, Coulombic efficiency, lithiation/delithiation potential and the total electrode resistance.

The capacity plots in figures 4.3a and 4.4a showed that the crystalline Si powder outperformed the amorphous with respect to the capacity and stability of the anodes, hence, the crystalline powder was used further in the thesis.

The addition of FEC in the electrolyte drastically enhanced the cycling performance of the anodes, compared to no additives, possibly due to the increased amount of polycarbonates or the absence of Li_2O, resulting in a more stable, ductile and passivating SEI layer. A lower total resistance was observed in the cell, which can be explained by a thinner SEI and possibly by the increased amount of LiF and Li_2CO_3 which has been suggested to form conductive paths for Li^+ at the grain boundaries. The efficiency decreased to lower values with the electrolyte with FEC compared to the electrolyte without additives after 100 cycles, possibly due to higher capacity obtained with FEC, thus larger volume expansions and electrolyte consumption.

The addition of H_2O resulted in lower capacities compared to the electrolyte without additives, which was explained by less polycarbonates and increased amounts of Li_2O, probably resulting in a less passivating and ductile SEI layer. The Coulombic efficiency followed the same trend as for the anodes without additives in the electrolyte, with marginally higher values for the anodes with H_2O added to the electrolyte after 25 cycles, possibly due to slightly lower capacity, thus smaller volume expansions. No significant difference from the addition of H_2O was observed from the SEM images or EDS analysis. The EIS measurements showed that an increasing resistance was observed with water in the electrolyte compared to no additives.

The addition of both FEC and H_2O resulted in similar enhancement of the capacity and stability as observed with only additions of FEC to the electrolyte, probably due to increased amounts of polycarbonates in the SEI layer. The cycling performance and Coulombic efficiency of the electrolyte with FEC and H_2O was similar to the anodes cycled with the electrolyte with FEC as the only additive. Thus, indicating that the silicon anodes tolerate water in the electrolyte due to the non hydrolysing properties of LiFSI, and the presence of FEC results in formation of a stable SEI. The impedance measurements showed that the cell with FEC and H_2O in the electrolyte displayed lower total resistance compared to the other electrolytes, possibly due to the increased amount of Li_2CO_3 and LiF from the additives, forming conductive paths along the grain boundaries.

Lastly, no significant difference was observed on the lithiation and delithiation potentials for any of the additives, implying that the lithiation and delithiation potentials are controlled by the lithium salt alone.

To conclude, the poor cycling performance of the silicon anodes with only additions of H_2O in the electrolyte illustrates that H_2O can not replace FEC as an additive in a LiFSI-based electrolyte.

7 Further work

The LiFSI salts ability to enhance the cycling performance of silicon anodes, and to tolerate humidity to a larger extent than for instance $LiPF_6$, opens up the possibilities for better LIBs with higher capacity and for less energy consuming production methods. However, there is still a lot of research to be done.

Regarding the Coulombic efficiency, one suggestion would be to use LFP cathodes as counter electrodes instead of lithium metal, as the stable operating potential allows for better control of the monitoring of the reactions on the anode. LFP cathodes are highly pressure sensitive, hence it is imperative to ensure the right pressure when assembling the cell. The assembly of full-cells in a CR2016 coin cell was attempted in this thesis, but due to insufficient pressure inside the cell, no results were obtained. However, CR2032 coin cells allows for better pressure regulation as a spring is introduced in the cell. Hence, CR2032 coin cells with LFP cathodes should be assembled to investigate the effect of water in an LiFSI-based electrolyte on the Coulombic efficiency of silicon anodes.

The results of this thesis showed that H_2O can not replace FEC as an additive entirely, but the silicon anode will tolerate 1000 ppm of H_2O in the electrolyte if 10 wt.% FEC is present to form a stable SEI. A subject for further work would be to find the lower threshold for the amount of FEC required before the performance of the battery is significantly reduced, as FEC is an expensive additive. Similarly, an upper threshold for the amount of water the cell can tolerate could reduce the cost related to drying. By combining a lower threshold for the FEC content and an upper threshold for the H_2O content, the cost and energy consumption related to high capacity LIBs can be reduced.

The effect of additives in an electrolyte with higher LiFSI concentration would be interesting to investigate. If the cycling performance of silicon anodes is indeed enhanced with conductive paths along the grain boundaries of LiF and Li_2CO_3, a higher concentration of LiFSI could increase the amount of LiF and the FTIR analysis showed an increased amount of Li_2CO_3 with the addition of H_2O. Thus, the ionic conductivity through the SEI layer could be improved.

Micron-sized silicon particles were used as active material in this thesis. Hence, a subject for further research could be to investigate the effect of LiFSI-based electrolytes with moisture on nano-silicon powder. In addition, the effect of LiFSI-based electrolytes with moisture on silicon-graphite composites is interesting to investigate as a silicon-graphite composite is proposed as a promising anode material due to the suppression of volume changes in the silicon.

References

[1] Jinasena, A., Stokke Burheim, O. & Hammer Strømman, A. (2021). A Flexible Model for Benchmarking the Energy Usage of Automotive Lithium-Ion Battery Cell Manufacturing. *Batteries.* https://doi.org/10.3390/batteries

[2] Zhang, H., Yang, Y., Ren, D., Wang, L. & He, X. (2021). Graphite as anode materials: Fundamental mechanism, recent progress and advances. *Energy Storage Materials*, *36*, 147–170. https://doi.org/10.1016/j.ensm.2020.12.027

[3] Young, R. S., Yu, H. & Obrovac, M. N. (2021). Enhancing NMC/silicon alloy full cell cycling by adding water to the electrolyte. *Journal of Applied Electrochemistry*, *51*(10), 1501–1507. https://doi.org/10.1007/s10800-021-01594-6

[4] Bergmann, C. P., Veit, H. M., Moura, A. & Editors, B. (2015). *Topics in Mining, Metallurgy and Materials Engineering Series Editor: Electronic Waste Recycling Techniques.* http://www.springer.com/series/11054

[5] Wenzl, H. BATTERIES AND FUEL CELLS — Lifetime. In: *Encyclopedia of electrochemical power sources.* Elsevier, 2009, pp. 552–558. https://doi.org/10.1016/B978-044452745-5.00048-4.

[6] Lamb, J. J. & Burheim, O. S. (2021). Lithium-ion capacitors: A review of design and active materials. *Energies*, *14*(4). https://doi.org/10.3390/en14040979

[7] Borah, R., Hughson, F. R., Johnston, J. & Nann, T. (2020). On battery materials and methods. *Materials Today Advances*, *6*. https://doi.org/10.1016/j.mtadv.2019.100046

[8] Nitta, N., Wu, F., Lee, J. T. & Yushin, G. (2015). Li-ion battery materials: Present and future. *Materials Today*, *18*(5), 252–264. https://doi.org/10.1016/j.mattod.2014.10.040

[9] Whittingham, M. S. (2021). Lithium titanium disulfide cathodes. *Nature Energy*, *6*(2), 214. https://doi.org/10.1038/s41560-020-00765-7

[10] Mizushima, K., Jones, P., Wiseman, P. & Goodenough, J. (1980). LixCoO2: A new cathode material for batteries of high energy density. *Materials Research Bulletin*, *15*(6), 783–789. https://doi.org/10.1016/0025-5408(80)90012-4

[11] Nzereogu, P., Omah, A., Ezema, F., Iwuoha, E. & Nwanya, A. (2022). Anode materials for lithium-ion batteries: A review. *Applied Surface Science Advances*, *9*, 100233. https://doi.org/10.1016/j.apsadv.2022.100233

[12] Asheim, K. (2021). *Lithium bis (fluorosulfonyl) imide as electrolyte salt for high-content silicon-based anodes for Li-ion batteries* (Doctoral dissertation). Norwegian University of Science and Technology.

[13] Asenbauer, J., Eisenmann, T., Kuenzel, M., Kazzazi, A., Chen, Z. & Bresser, D. (2020). The success story of graphite as a lithium-ion anode material-fundamentals, remaining challenges, and recent developments including silicon (oxide) composites. *Sustainable Energy and Fuels*, *4*(11), 5387–5416. https://doi.org/10.1039/d0se00175a

[14] Puthusseri, D., Wahid, M. & Ogale, S. (2018). Conversion-type Anode Materials for Alkali-Ion Batteries: State of the Art and Possible Research Directions. *ACS Omega*, *3*(4), 4591–4601. https://doi.org/10.1021/acsomega.8b00188

[15] Obrovac, M. N. (2018). Si-alloy negative electrodes for Li-ion batteries. *Current Opinion in Electrochemistry*, *9*, 8–17. https://doi.org/10.1016/j.coelec.2018.02.002

[16] Rogstad, D. T., Einarsrud, M.-A. & Svensson, A. M. (2021). Evaluation of Selected Ionic Liquids as Electrolytes for Silicon Anodes in Li-Ion Batteries. *Journal of The Electrochemical Society*, *168*(11), 110506. https://doi.org/10.1149/1945-7111/ac330f

[17] Hatchard, T. D. & Dahn, J. R. (2004). In Situ XRD and Electrochemical Study of the Reaction of Lithium with Amorphous Silicon. *Journal of The Electrochemical Society*, *151*(6), A838. https://doi.org/10.1149/1.1739217

[18] Li, Q., Chen, J., Fan, L., Kong, X. & Lu, Y. (2016). Progress in electrolytes for rechargeable Li-based batteries and beyond. *Green Energy and Environment*, *1*(1), 18–42. https://doi.org/10.1016/j.gee.2016.04.006

[19] Goodenough, J. B. & Park, K. S. (2013). The Li-ion rechargeable battery: A perspective. *Journal of the American Chemical Society*, *135*(4), 1167–1176. https://doi.org/10.1021/ja3091438

[20] Xu, K. (2004). Nonaqueous liquid electrolytes for lithium-based rechargeable batteries. *Chemical Reviews*, *104*(10), 4303–4417. https://doi.org/10.1021/cr030203g

[21] Younesi, R., Veith, G. M., Johansson, P., Edström, K. & Vegge, T. (2015). Lithium salts for advanced lithium batteries: Li-metal, Li-O2, and Li-S. *Energy and Environmental Science*, *8*(7), 1905–1922. https://doi.org/10.1039/c5ee01215e

[22] Haregewoin, A. M., Wotango, A. S. & Hwang, B. J. (2016). Electrolyte additives for lithium ion battery electrodes: Progress and perspectives. *Energy and Environmental Science*, *9*(6), 1955–1988. https://doi.org/10.1039/c6ee00123h

[23] Jaumann, T., Balach, J., Langklotz, U., Sauchuk, V., Fritsch, M., Michaelis, A., Teltevskij, V., Mikhailova, D., Oswald, S., Klose, M., Stephani, G., Hauser, R., Eckert, J. & Giebeler, L. (2017). Lifetime vs. rate capability: Understanding the role of FEC and VC in high-energy Li-ion batteries with nano-silicon anodes. *Energy Storage Materials*, *6*, 26–35. https://doi.org/10.1016/j.ensm.2016.08.002

[24] Ha, Y., Stetson, C., Harvey, S. P., Teeter, G., Tremolet De Villers, B. J., Jiang, C. S., Schnabel, M., Stradins, P., Burrell, A. & Han, S. D. (2020). Effect of Water Concentration in LiPF6-Based Electrolytes on the Formation, Evolution, and Properties of the Solid Electrolyte Interphase on Si Anodes. *ACS Applied Materials and Interfaces*, *12*(44), 49563–49573. https://doi.org/10.1021/acsami.0c12884

[25] Asheim, K., Vullum, P. E., Wagner, N. P., Andersen, H. F., Mæhlen, J. P. & Svensson, A. M. (2022). Improved electrochemical performance and solid electrolyte interphase properties of electrolytes based on lithium bis(fluorosulfonyl)imide for high

content silicon anodes. *RSC Advances*, *12*(20), 12517–12530. https://doi.org/10.1039/D2RA01233B

[26] Jafta, C. J., Sun, X. G., Lyu, H., Chen, H., Thapaliya, B. P., Heller, W. T., Cuneo, M. J., Mayes, R. T., Paranthaman, M. P., Dai, S. & Bridges, C. A. (2021). Insight into the Solid Electrolyte Interphase Formation in Bis(fluorosulfonyl)Imide Based Ionic Liquid Electrolytes. *Advanced Functional Materials*, *31*(23). https://doi.org/10.1002/adfm.202008708

[27] Tezel, A. O., Streich, D. K., Guéguen, A., Hahlin, M., Sunde, S., Edström, K., Novák, P. & Svensson, A. M. (2020). Solid Electrolyte Interphase (SEI) Formation on the Graphite Anode in Electrolytes Containing the Anion Receptor Tris(hexafluoroisopropyl)borate (THFIPB). *Journal of The Electrochemical Society*, *167*(13), 130504. https://doi.org/10.1149/1945-7111/abb567

[28] Eshetu, G. G., Diemant, T., Grugeon, S., Behm, R. J., Laruelle, S., Armand, M. & Passerini, S. (2016). In-Depth Interfacial Chemistry and Reactivity Focused Investigation of Lithium-Imide- and Lithium-Imidazole-Based Electrolytes. *ACS Applied Materials and Interfaces*, *8*(25), 16087–16100. https://doi.org/10.1021/acsami.6b04406

[29] Uchida, S., Yamagata, M. & Ishikawa, M. (2015). Effect of Electrolyte Additives on Non-Nano-Si Negative Electrodes Prepared with Polyimide Binder. *Journal of The Electrochemical Society*, *162*(3), A406–A412. https://doi.org/10.1149/2.0581503jes

[30] Wang, H. & Chew, H. B. (2017). Nanoscale Mechanics of the Solid Electrolyte Interphase on Lithiated-Silicon Electrodes. *ACS Applied Materials and Interfaces*, *9*(31), 25662–25667. https://doi.org/10.1021/acsami.7b07626

[31] Shkrob, I. A., Wishart, J. F. & Abraham, D. P. (2015). What Makes Fluoroethylene Carbonate Different? *Journal of Physical Chemistry C*, *119*(27), 14954–14964. https://doi.org/10.1021/acs.jpcc.5b03591

[32] Etacheri, V., Haik, O., Goffer, Y., Roberts, G. A., Stefan, I. C., Fasching, R. & Aurbach, D. (2012). Effect of Fluoroethylene Carbonate (FEC) on the Performance and Surface Chemistry of Si-Nanowire Li-Ion Battery Anodes. *Langmuir*, *28*(1), 965–976. https://doi.org/10.1021/la203712s

[33] Schroder, K., Alvarado, J., Yersak, T. A., Li, J., Dudney, N., Webb, L. J., Meng, Y. S. & Stevenson, K. J. (2015). The Effect of Fluoroethylene Carbonate as an Additive on the Solid Electrolyte Interphase on Silicon Lithium-Ion Electrodes. *Chemistry of Materials*, *27*(16), 5531–5542. https://doi.org/10.1021/acs.chemmater.5b01627

[34] Philippe, B., Dedryvèire, R., Gorgoi, M., Rensmo, H., Gonbeau, D. & Edström, K. (2013). Improved performances of nanosilicon electrodes using the salt LiFSI: A photoelectron spectroscopy study. *Journal of the American Chemical Society*, *135*(26), 9829–9842. https://doi.org/10.1021/ja403082s

[35] Han, H. B., Zhou, S. S., Zhang, D. J., Feng, S. W., Li, L. F., Liu, K., Feng, W. F., Nie, J., Li, H., Huang, X. J., Armand, M. & Zhou, Z. B. (2011). Lithium bis(fluorosulfonyl)imide

(LiFSI) as conducting salt for nonaqueous liquid electrolytes for lithium-ion batteries: Physicochemical and electrochemical properties. *Journal of Power Sources*, *196*(7), 3623–3632. https://doi.org/10.1016/j.jpowsour.2010.12.040

[36] Xu, W., Wang, J., Ding, F., Chen, X., Nasybulin, E., Zhang, Y. & Zhang, J. G. (2014). Lithium metal anodes for rechargeable batteries. *Energy and Environmental Science*, *7*(2), 513–537. https://doi.org/10.1039/c3ee40795k

[37] Jung, R., Metzger, M., Maglia, F., Stinner, C. & Gasteiger, H. A. (2017). Oxygen Release and Its Effect on the Cycling Stability of LiNixMnyCozO2 (NMC) Cathode Materials for Li-Ion Batteries. *Journal of The Electrochemical Society*, *164*(7), A1361–A1377. https://doi.org/10.1149/2.0021707jes

[38] Chauhan, A. (2014). Powder XRD Technique and its Applications in Science and Technology. *Journal of Analytical & Bioanalytical Techniques*, *5*(6). https://doi.org/10.4172/2155-9872.1000212

[39] Artioli, G. (2017). *Encyclopedia of Geoarchaeology* (A. S. Gilbert, Ed.). Springer Netherlands. https://doi.org/10.1007/978-1-4020-4409-0

[40] Walton, K. S. & Snurr, R. Q. (2007). Applicability of the BET method for determining surface areas of microporous metal-organic frameworks. *Journal of the American Chemical Society*, *129*(27), 8552–8556. https://doi.org/10.1021/ja071174k

[41] Dollimore, D, Spooner, P & Turner, A. (1976). *The BET method of analysis of gas adsorption data and its relevance to the calculation of surface areas* (tech. rep.). Elsevier Sequoia S.A.

[42] Eshel, G., Levy, G. J., Mingelgrin, U. & Singer, M. J. (2004). Critical Evaluation of the Use of Laser Diffraction for Particle-Size Distribution Analysis. *Soil Science Society of America Journal*, *68*(3), 736–743. https://doi.org/10.2136/sssaj2004.7360

[43] Choi, W., Shin, H. C., Kim, J. M., Choi, J. Y. & Yoon, W. S. (2020). Modeling and applications of electrochemical impedance spectroscopy (Eis) for lithium-ion batteries. *Journal of Electrochemical Science and Technology*, *11*(1), 1–13. https://doi.org/10.33961/jecst.2019.00528

[44] Glassford, S. E., Byrne, B. & Kazarian, S. G. (2013). Recent applications of ATR FTIR spectroscopy and imaging to proteins. *Biochimica et Biophysica Acta - Proteins and Proteomics*, *1834*(12), 2849–2858. https://doi.org/10.1016/j.bbapap.2013.07.015

[45] Mulder, N. R. (2018). *The Effect of LiFSI Salt Concentration and Electrolyte Additives on the Performance of Silicon Anodes for Lithium-Ion Batteries* (tech. rep.).

[46] Bjørklund, J. S. (2021). *Effect of binders chemistry on the performance of silicon anodes in Li-ion batteries prepared from micron sized silicon* (tech. rep.).

[47] EL-CELL. (n.d.). PAT-Cell User Manual. https://el-cell.com//wp-content/uploads/downloads/manuals/Manual_PAT-Cell_Release_2.52.pdf

[48]   Kaland, H. (2017). *On the Cycling Performance and Stability of Silicon-Based Anodes in Lithium-Ion Batteries Revealing Challenges and Failure Mechanisms Using Post Mortem Analyses* (tech. rep.).

Appendix

A   FTIR

Table A.1 shows the wavenumber of some of the peaks that could be present for silicon anodes cycled in LiFSI-based electrolytes. The table is partly rewritten from the master thesis of Kaland 2017.[48]

The spectra of an uncycled pristine anode and anodes cycled with the four electrolytes (see table 3.2) used in this thesis are shown in figure A.1.
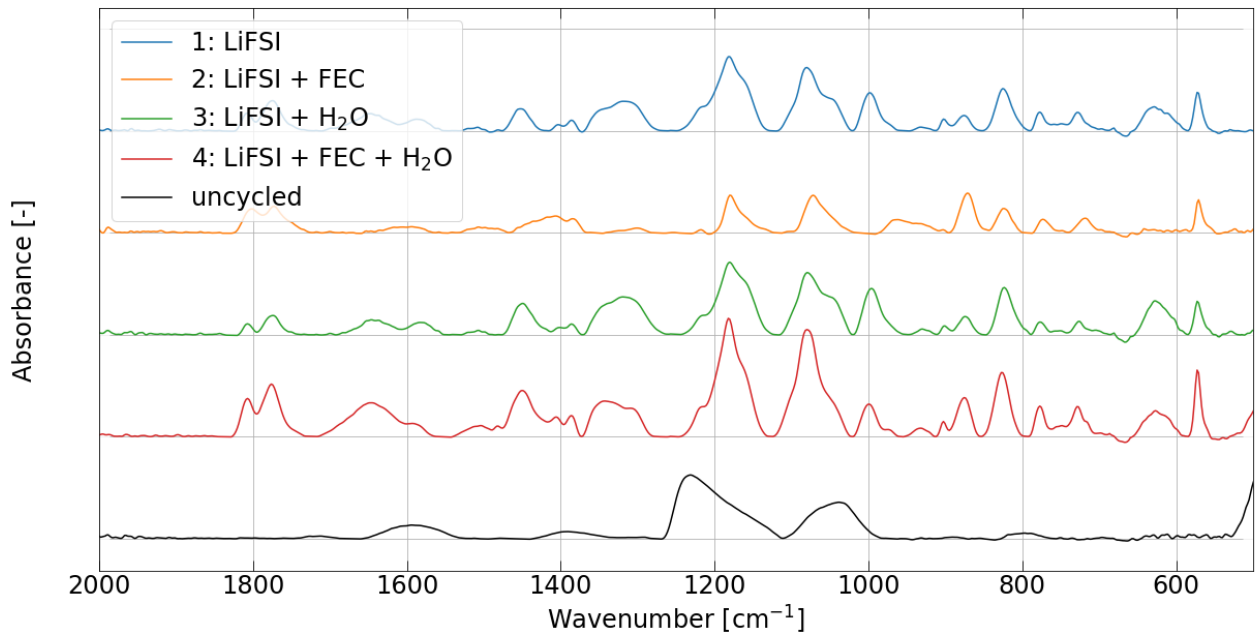

Figure A.1: Spectra of an uncycled pristine anode, and anodes cycled with the four electrolytes (see table 3.2) used in this thesis.

Table A.1: Wavenumber of some of the peaks that could be observed in the spectrum obtained from silicon anodes cycled in LiFSI-based electrolytes. υ: stretching vibrations, υ_a: asymmetric stretching vibrations, δ: bending vibration, δ_a: asymmetic bending vibration, δ_s: symmetric bending vibrations

Peak [cm^{-1}]	Possible component
3700-3500	O-H$_{\text{free}}$, υ
3500-3100	O-H$_{\text{bonded}}$, υ
2900	ROCO$_2$Li
2400-2300	CO$_2$
1870	EC (liquid)
1810	EC (solid)
1800-1750	Ring carbonyl
1782	Solvated EC
1765	Polycarbonates from EC/DMC polymerisation
1650	ROCO$_2$Li
1642	C=O, υ_a
1553	EC
1481	CH$_2$ (EC), δ
1454	CH$_3$ (DMC), δ_a
1435	Li$_2$CO$_3$
1433	CH$_3$ (DMC), δ_s
1391	CH$_2$ (EC), δ
1300	ROCO$_2$Li
1196	Polycarbonates from EC/DMC polymerisation
1163-1160	Ring (EC), υ_a
1090	ROCO$_2$Li
1069	C-O, υ_s
965	SiO in an a-Si:H network
857	Li$_2$CO$_3$
820	ROCO$_2$Li
717	Ring (EC), δ
609	Li$_2$O
472	O-Si-O bond deformation

B   Slurry composition

The binder solution used for the silicon slurry consists of a Na-Alginate binder mixed with a KCA-buffer solution. The composition of the KCA-buffer solution is shown in table B.1. The binder solution was made with a 1/60 ratio of Na-Alginate to KCA-buffer.

Table B.1: Composition of 250 mL citric acid - KOH buffer solution prepared by Bjørklund 2021[46]

Component	Mass [g]	Concentration [wt.%]
Citric acid	4,53	1,77
KOH	0,79	0,31
H_2O	251,01	97,92

Table B.2: Composition of Na-Alg binder solution based on 20 g of KCA buffer used for silicon anodes

Component	Mass [g]	Concentration [wt.%]
Citric acid	0,35	1,71
KOH	0,06	0,30
H_2O	19,58	94,72
Na-Alg	0,33	1,64

The target composition of the silicon slurry with masses corresponding to one tape cast is given in table B.3

Table B.3: Composition of silicon slurry for silicon anodes. The mass values corresponds to one tape cast.

Component	Mass [g]	Concentration [wt.%]
Si powder	0,5476	75,00
Carbon black	0,1095	15,00
Na-Alg	0,0328	4,49
Citric acid	0,0342	4,69
KOH	0,0060	0,83

C   Mixing program for silicon slurry

The mixing program for the slurry for the silicon anodes is given in table C.1. The mixing was done by the use of a Retsch MM 400 mixer with a steel ball at 15 Hz.

Table C.1: Mixing program used for fabrication of silicon slurry for silicon anodes. 15 Hz was used for the mixing at all steps of the program.

Compound added	Duration of mixer/ultrasonic bath
Si powder + Carbon black	Mixed for 5 min
Na-Alg binder solution	Mixed for 40 min
Deionized water	Mixed for 5 min
	Degassed for at least 1 min

D   Calculations for electrolyte composition

Four different electrolytes were prepared for this thesis. The electrolytes are described in table 3.2. This appendix shows the calculations used for the preparation of the electrolytes.

EC/DMC (1:1) + 1M LiFSI

10 g of EC and DMC was weighted out and mixed (20 g in total).

The volume of the EC/DMC mixture is calculated using the densities of EC and DMC, ρ_{EC} = 1,32 g/cm^3, ρ_{DMC} = 1,07 g/cm^3

$$V_{\text{EC/DMC}} = \frac{m_{\text{EC}}}{\rho_{\text{EC}}} + \frac{m_{\text{DMC}}}{\rho_{\text{DMC}}} = 16,93 \text{ cm}^3 \tag{D.1}$$

$V_{\text{EC/DMC}}$ and M_{LiFSI} = 187,09g/mol is used to calculate the required mass of LiFSI to obtain a concentration of 1M LiFSI.

$$m_{\text{LiFSI}} = c_{\text{LiFSI}} \cdot V_{\text{EC/DMC}} \cdot M_{\text{LiFSI}} = 3,17 \text{ g} \tag{D.2}$$

EC/DMC (1:1) + 1M LiFSI + 10wt.% FEC

The mass of FEC was calculated using the mass of EC/DMC and LiFSI. With 20 g of EC/DMC solution, the required mass of FEC to obtain a concentration of 10 wt.% will be

$$\begin{aligned} m_{\text{FEC}} &= 0,1 \cdot (m_{\text{EC/DMC}} + m_{\text{LiFSI}} + m_{\text{FEC}}) \\ &= \frac{m_{\text{EC/DMC}} + m_{\text{LiFSI}}}{9} \\ &= 2,57 \text{ g} \end{aligned} \tag{D.3}$$

EC/DMC (1:1) + 1M LiFSI + 1000ppm H$_2$O

The mass of H$_2$O required to obtain a concentration of 1000ppm H$_2$O was calculated using the mass of the EC/DMC solution and the LiFSI. With 20 g of EC/DMC solution, the required mass of water is given by

$$m_{\text{H}_2\text{O}} = \frac{1000}{10^6} \cdot (m_{\text{EC/DMC}} + m_{\text{H}_2\text{O}}) = 0,023 \text{ g} \tag{D.4}$$

EC/DMC (1:1) + 1M LiFSI + 1000ppm H$_2$O + 10wt.% FEC

The water required is calculated by the use of the mass of the EC/DMC solution and LiFSI like what was done for the electrolyte with H$_2$O without FEC. The amount of FEC required is then calculated based on the mass of EC/DMC, LiFSI and H$_2$O. The mass of FEC required based on 20 g of EC/DMC solution is given by

$$m_{\text{FEC}} = 0,1 \cdot (m_{\text{EC/DMC}} + m_{\text{LiFSI}} + m_{\text{H}_2\text{O}} + m_{\text{FEC}})$$
$$= \frac{m_{\text{EC/DMC}} + m_{\text{LiFSI}} + m_{\text{H}_2\text{O}}}{9} \tag{D.5}$$
$$= 2,58 \text{ g}$$

Table D.1 shows the mass (based on 20 g solvent mixture), weight fraction and molar fraction of each component in each of the four electrolytes.

Table D.1: Mass, weight fraction and molar fraction of the components in the four different electrolytes used in this thesis.

Electrolyte	Chemical	Mass [g]	Weight frac. [%]	Molar frac. [%]
EC/DMC + LiFSI	EC	10,0	43,2	47,0
	DMC	10,0	43,2	46,0
	LiFSI	3,17	13,7	7,0
EC/DMC + LiFSI + FEC	EC	10,0	38,9	42,7
	DMC	10,0	38,9	41,8
	LiFSI	3,17	12,3	6,4
	FEC	2,57	10,0	9,1
EC/DMC + LiFSI + H$_2$O	EC	10,0	43,1	46,8
	DMC	10,0	43,1	45,7
	LiFSI	3,17	13,7	7,0
	H$_2$O	0,023	0,1	0,5
EC/DMC + LiFSI + H$_2$O + FEC	EC	10,0	38,8	42,5
	DMC	10,0	38,8	41,6
	LiFSI	3,17	12,3	6,3
	H$_2$O	0,023	0,1	0,5
	FEC	2,58	10,0	9,1

E   Calculations for charge used for water splitting

EC/DMC (1:1) + 1M LiFSI + 1000 ppm H$_2$O

Approximately 0,45 mL of the electrolyte was measured to weigh 0,6449 g. This is used to calculate the density of the electrolyte.

$$\rho = \frac{m}{V} = 1,43 \text{ g/mL} \tag{E.1}$$

In one coin cell, the amount of electrolyte used is 30 µL and 100 µL electrolyte was used in a PAT-cell, which corresponds to the masses

$$m_{coin} = \rho \cdot V = 0,043 \text{ g}$$
$$m_{PAT} = \rho \cdot V = 0,143 \text{ g} \tag{E.2}$$

The weight percent of the electrolyte is given in table D.1, and is used to calculate the amount of moles of H$_2$O in the cell.

$$n_{coin} = \frac{m_{coin} \cdot wt.\% \text{H}_2\text{O}}{M_{\text{H}_2\text{O}}} = 2,38 \cdot 10^{-4} \text{ mol}$$
$$n_{PAT} = \frac{m_{PAT} \cdot wt.\% \text{H}_2\text{O}}{M_{\text{H}_2\text{O}}} = 7,94 \cdot 10^{-4} \text{ mol} \tag{E.3}$$

The charge required to split $2,38 \cdot 10^{-4}$ moles of H$_2$O is given by

$$Q_{coin} = n_{coin}F = 6,4 \text{ mAh}$$
$$Q_{PAT} = n_{PAT}F = 21,3 \text{ mAh} \tag{E.4}$$

The active mass of silicon in one anode is approximately 0,8g at the target loading of 0,4mg/cm^2 for a coin cell and approximately 1,1g for the PAT-cells. Thus, the charge used for water splitting in the cells expressed per mass of active material is

$$\frac{6,4\text{mAh}}{0,8\text{g}} = 8,0 \text{ mAh/g}$$
$$\frac{21,3\text{mAh}}{1,1\text{g}} = 19,4 \text{ mAh/g} \tag{E.5}$$

For coin cells and PAT-cells respectively.

EC/DMC (1:1) + 1M LiFSI + 1000 ppm H$_2$O + 10wt.% FEC

The same calculations can be done for electrolyte 4. Approximately 0,45 mL of the electro-

lyte was measured to weigh 0,5476 g. The calculations will be as followed

$$\rho = \frac{m}{V} = 1,22 \text{ g/mL} \tag{E.6}$$

$$m_{coin} = 0,037 \text{ g}$$
$$m_{PAT} = 0,122 \text{ g} \tag{E.7}$$

$$n_{coin} = \frac{m_{coin} \cdot wt.\%\text{H}_2\text{O}}{M_{\text{H}_2\text{O}}} = 2,05 \cdot 10^{-4} \text{ mol}$$
$$n_{PAT} = \frac{m_{coin} \cdot wt.\%\text{H}_2\text{O}}{M_{\text{H}_2\text{O}}} = 6,77 \cdot 10^{-4} \text{ mol} \tag{E.8}$$

$$Q_{coin} = n_{coin}F = 5,5 \text{ mAh}$$
$$Q_{PAT} = n_{PAT}F = 18,1 \text{ mAh} \tag{E.9}$$

Expressed per mass of active material, the charge used is

$$\frac{5,5\text{mAh}}{0,8 \text{ g}} = 6,9 \text{ mAh/g}$$
$$\frac{18,1\text{mAh}}{1,1 \text{ g}} = 16,5 \text{ mAh/g} \tag{E.10}$$

For coin cells and PAT-cells respectively.

Compared to the charge used for lithiation and delithiation of the anodes, the charge used for water splitting is very small.

F   Cycling programs

Table F.1: Cycling programs for the coin cells and PAT-cells

	C-rate during charge and discharge	Number of cycles
Coin cells	C/20 (formation)	2
	C/5	100 (50)
PAT-cells	C/20 (formation)	2
	C/4	20
	(EIS)	
	C/4	20
	(EIS)	
	C/4	20
	(EIS)	
	C/4	20
	(EIS)	
	C/4	20

G   Coulombic efficiency of anodes in PAT-cells

The Coulombic efficiency of the anodes cycled in PAT-cells are shown in figure G.1.
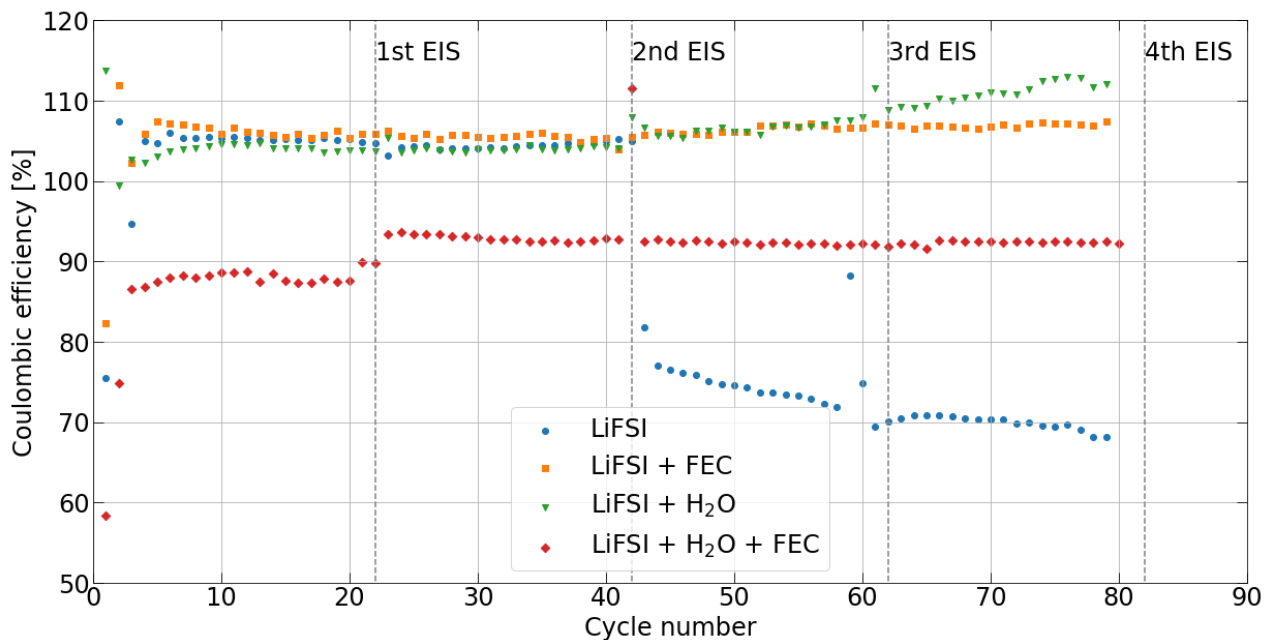
Figure G.1: The Coulombic efficiency of the anodes cycled in PAT-cells with electrolytes 1-4 from table 3.2.
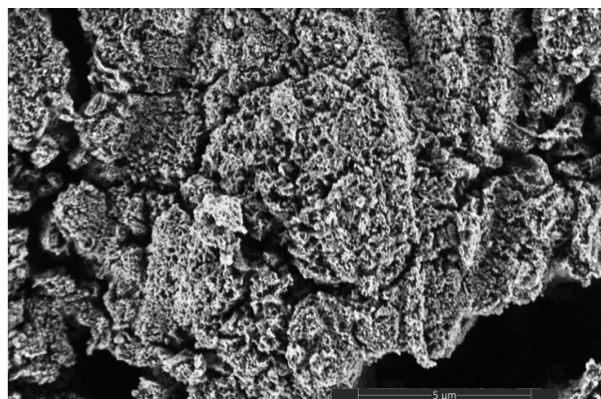
The efficiencies of the cells with electrolytes 2 and 3 and partly 1 obtained values above 100% for reasons unknown.
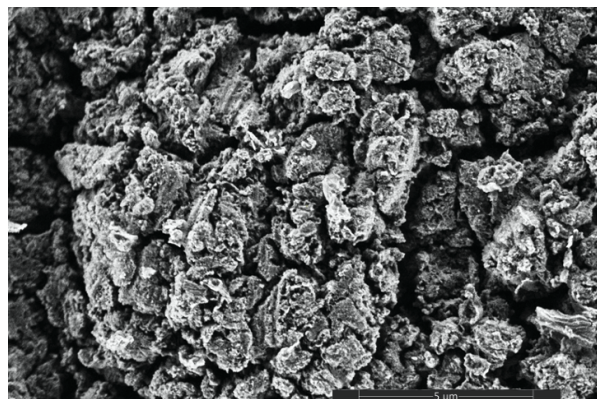
H SEM

The SEM images of the SEI layers of the cycled anodes in the coin cells, and the particles in an uncycled anode are shown in figure H.1.
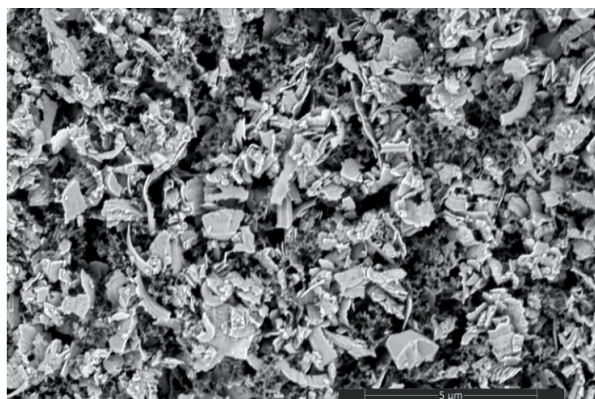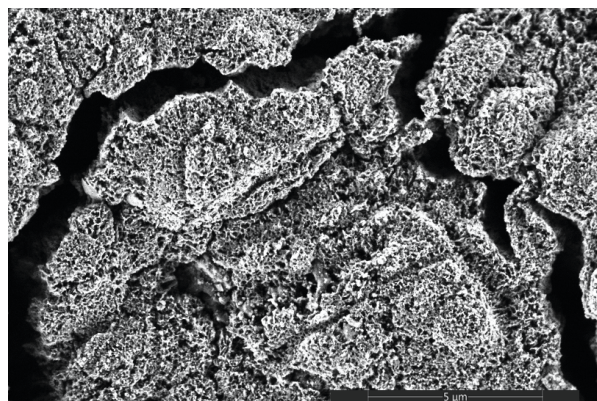

(a)

(b)

(c)
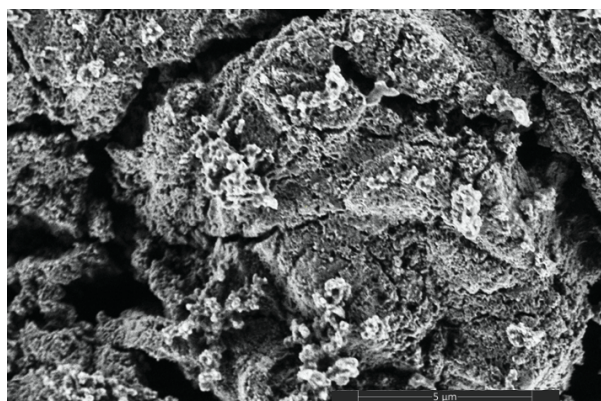
(d)

(e)

Figure H.1: SEM images showing (a) an uncycled anode, and the cycled anodes made using crystalline silicon powder and (b) electrolyte 1, (c) electrolyte 2, (d) electrolyte 3 and (e) electrolyte 4.

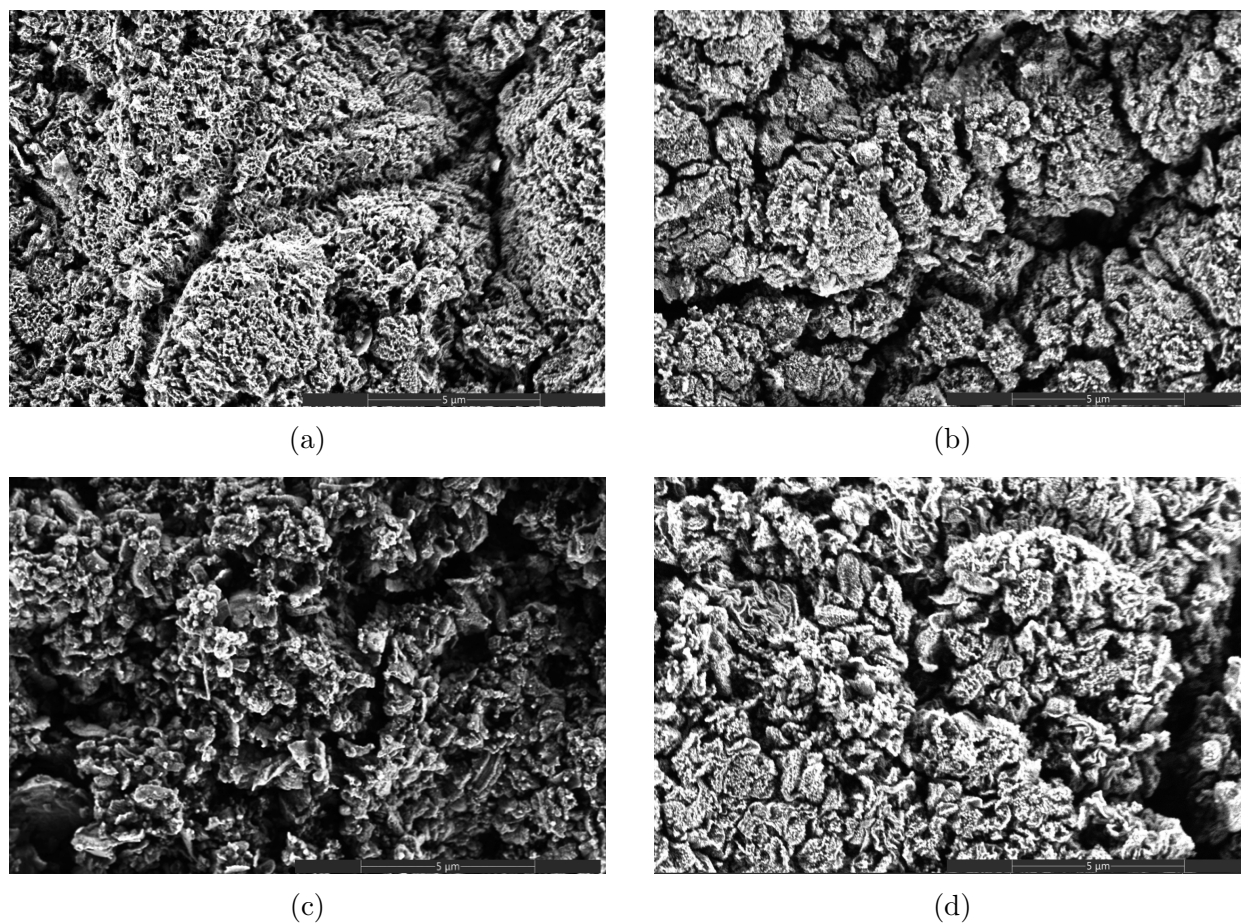The SEM images of the anodes cycled in PAT-cells are shown in figure H.2.

(a)

(b)

(c)

(d)

Figure H.2: SEM images showing (a) an uncycled anode, and the cycled anodes made using crystalline silicon powder and (b) electrolyte 1, (c) electrolyte 2, (d) electrolyte 3 and (e) electrolyte 4.
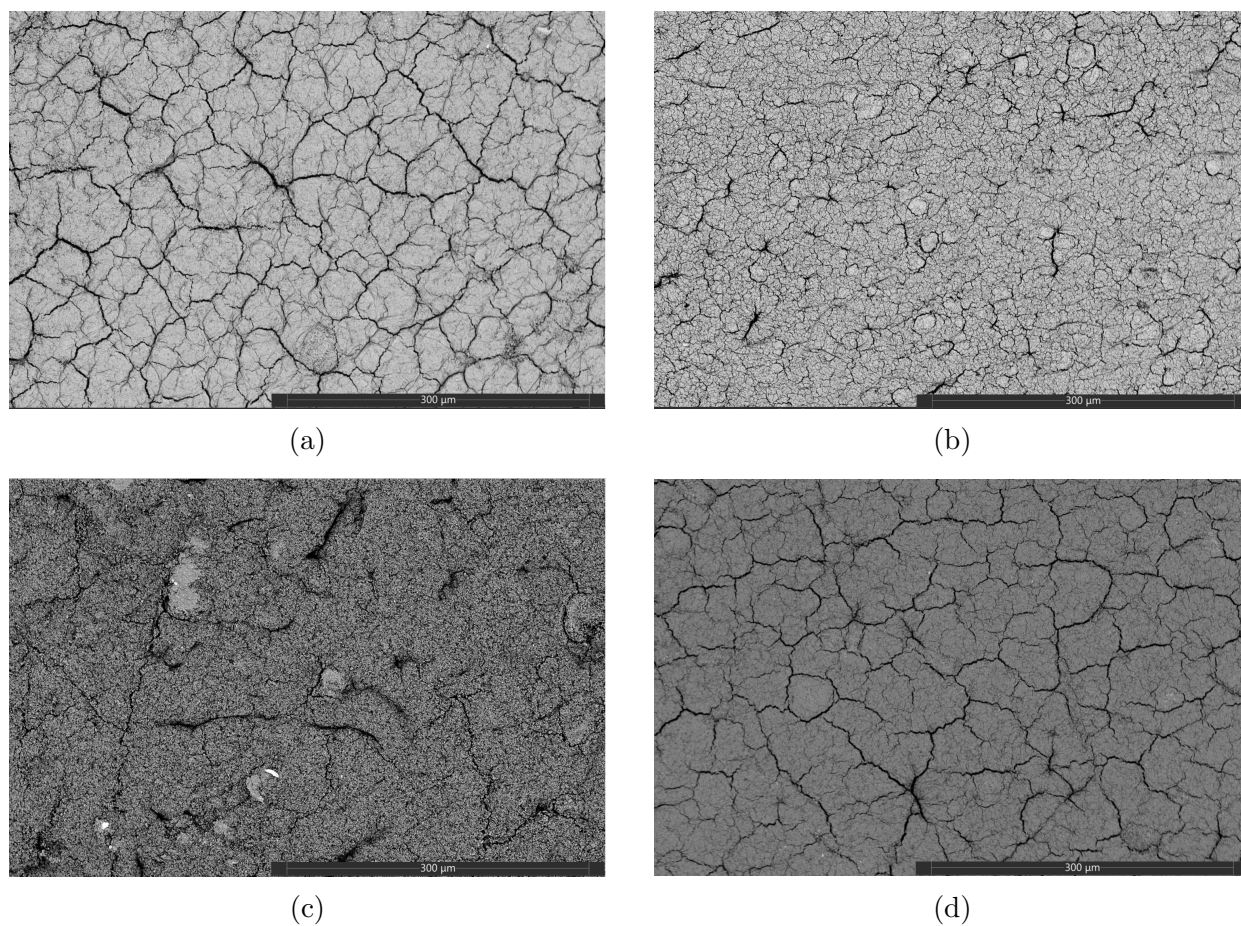
(a)

(b)

(c)

(d)

Figure H.3: SEM images showing (a) an uncycled anode, and the cycled anodes made using crystalline silicon powder and (b) electrolyte 1, (c) electrolyte 2, (d) electrolyte 3 and (e) electrolyte 4.
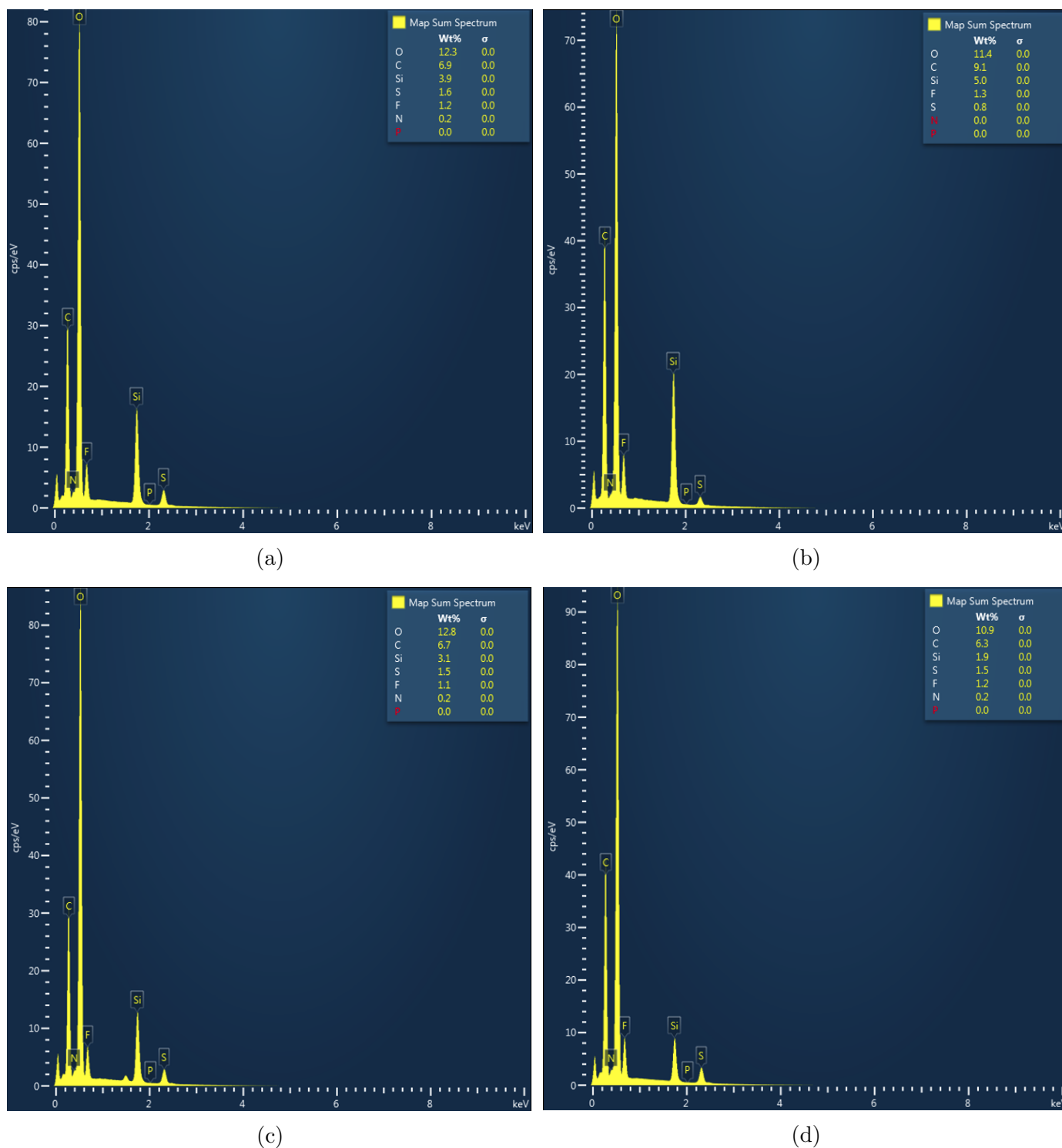
Figure H.4: Map spectra from the EDS analysis showing the relative amount of elements in the SEI layer of the anodes made using crystalline silicon powder cycled in coin cells with electrolyte 1, 2, 3 and 4 from table 3.2.
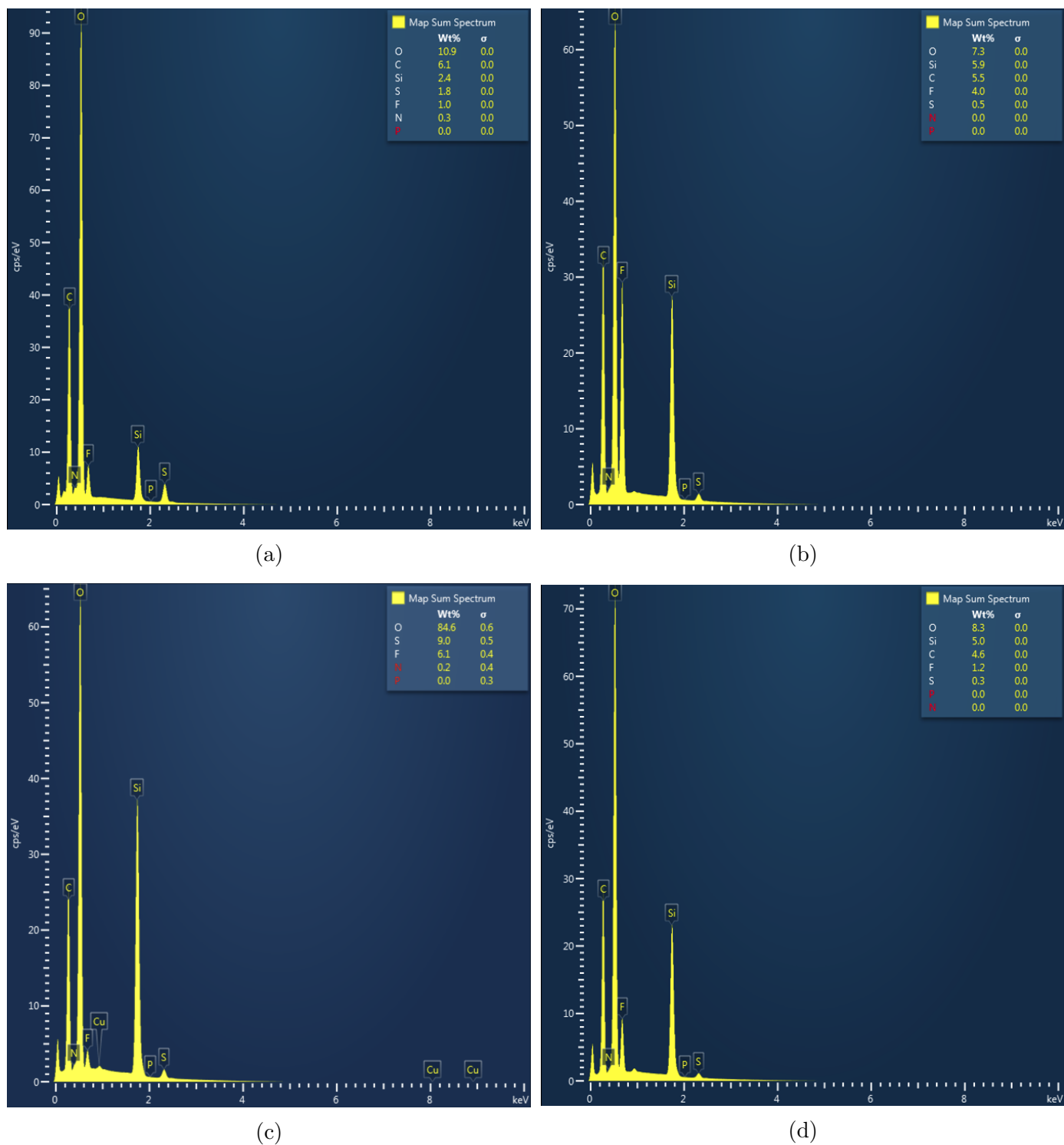
Figure H.5: Map spectra from the EDS analysis showing the relative amount of elements in the SEI layer of the cycled anodes made using crystalline silicon powder cycled in PAT-cells electrolyte 1, 2, 3 and 4 from table 3.2.

Ragnhild Akre Reite

FEC and H_2O as additives in LiFSI-based electrolytes with silicon anodes

NTNU
Norwegian University of
Science and Technology